Inaugural dissertation

for

obtaining the doctoral degree

of the

Combined Faculty of Mathematics, Engineering and Natural Sciences

of the

Ruprecht – Karls – University

Heidelberg

Presented by

M. Sc. Julia Maria Meßmer

born in: Villingen-Schwenningen, Germany

Oral examination: September 20th, 2022

Dynamic intravital imaging reveals a T lymphocyte recruitment mechanism to melanoma brain tumors

Referees:

Prof. Dr. Frank Winkler

Prof. Dr. Viktor Umansky

Acknowledgements

First, I would like to express my sincere gratitude to Prof. Frank Winkler and Dr. Matthia Karreman for giving me the opportunity to conduct my PhD research in the Winkler Lab and for supervising my project. Many thanks for the great scientific discussions in person or during many virtual meetings.

I would like to thank Prof. Iris Helfrich and Prof. Dirk Schadendorf for kindly sharing the cell line Ret CM TyrKO (CM TyrKO #43) with me and Prof. Jennifer Landsberg and Prof. Thomas Tüting for the HCmel12 cell lines and Prof. Cyrus M. Ghajar for the E0771 cell line. I would also like to thank Daniel Hinze and Prof. Michael Hölzel for performing the Tyrosinase KO for the HCmel12 and Ret CM cell lines. Many thanks also go to Prof. Michael Platten and his group for sharing animals of the pmel-1 mouse line for our own pmel-1 breeding and for gifting us the GL261 gp100 over-expressing cell line. I would also like to thank Dr. Darjus Tschaharganeh and Prof. Ana Martin-Villalba for sharing mice to start the breedings of the mouse lines LCK-Cre x LSL-TdTomato and CD4-Cre x LSL-tdTomato.

I am grateful for previous work on establishing experimental procedures by Dr. Anna S. Berghoff and Manuel Piechutta, and for Manuel's help with T cell tracking.

A big thank you to all the members of AG Winkler for making our time in the lab fun. I enjoyed working with you a lot. Special thanks to Dani and Yvonne for your friendship and for our "Anetto" times within and outside of the lab. Thanks again to Matthia, for energizing every room and every meeting with your cheerfulness and laughter, which could even be transported via zoom. Many thanks also go to Christina as my companion in the struggles with MoVi and other breeding-related issues; solving these problems together made them much less annoying. I am also very grateful for the technical and organizational support from Chanté Mayer, Katharina Frey, Susann Wendler and Cathrin Löb, and for the support with image processing and quantification by Varun Venkataramani.

I would also like to acknowledge the support of the DKFZ Flow Cytometry Core facility and the DKFZ Light Microscopy core facility for providing devices, resources and support for FACS sorting of cells and imaging of tissue. I would also like to acknowledge the support of my colleagues from the DKFZ animal housing facilities with animal breeding and housing.

I am very thankful for the funding for my PhD research and would like to thank the Deutsche Forschungsgemeinschaft and the Research Training Group 2099 "Hallmarks of Skin Cancer" and the HBIGS graduate school for providing a structured PhD program offering various opportunities for personal and professional growth as a scientist.

Acknowledgements

I would also like to thank my thesis advisory committee members Prof. Viktor Umansky and Prof. Michael Platten for taking their time to give me feedback and input on the progress of my PhD research.

Many thanks go to my wonderful family, especially to my parents for their tremendous support throughout the years and their generous trust in all my decisions. A very special thank you goes to my partner Patrick. Thank you for your love and support, for enduring my long working hours, inflexibilities due to running experiments, and my mood swings, that were highly dependent on the amount of red or green dots I was seeing at the microscope. Thank you for the many hours you had to spend travelling on trains so we could synchronize our lives for parts of the week. I am beyond thankful to have you in my life.

Annalena, you are the best reminder for me that all my efforts to be a good scientist do matter.

I am very thankful, and I sincerely honor every single animal who gave their life for this research. I highly respect each individual animal life and I always tried to keep the suffering involved in this research at a minimum.

Zusammenfassung

Das kutane maligne Melanom ist eine seltene, sehr aggressive Form des Hautkrebses, die häufig ins Hirn metastasiert. Da die Behandlungsoptionen für Patienten, die an Hirn-Metastasen leiden, sehr begrenzt sind, geht die Diagnose der Hirnmetastasen mit einer schlechten Prognose einher. Allerdings wecken jüngste präklinische und klinische Erkenntnisse Hoffnung, dass Hirnmetastasen-Patienten von immuntherapeutischen Ansätzen profitieren könnten. Ein intrakranielles Ansprechen auf Immuncheckpoint Inhibition (ICI) ist möglich, jedoch sehr stark von einer effizienten T Zell-Rekrutierung ins Gehirn abhängig. Das Gehirn wurde lange als immun-privilegiertes Organ angesehen, doch aktuelle Studien deuten darauf hin, dass spezielle meningeale lymphatische Gefäße eine Immun-Überwachung des Hirngewebes ermöglichen. Allerdings wird der Mechanismus der T Zell-Rekrutierung im Kontext von Hirntumoren sowie dessen Beeinflussung durch ICI weiterhin nur unzureichend verstanden. Um anatomische und molekulare Mechanismen der T Zell-Rekrutierung zu Hirntumoren aufzuklären, habe ich neue Intravital-Mikroskopie-Methoden etabliert, die es erlauben Interaktionen zwischen T Zellen und Tumorzellen in Echtzeit und über einen Zeitraum von zwei Wochen in zwei verschiedenen syngenen Mausmodellen für Melanom-Hirntumore zu verfolgen. Damit konnte ich die Dynamik der T Zell-Rekrutierung zum Gehirn während der Tumorentwicklung visualisieren. Dadurch habe ich eine neue Route durch bestimmte anatomische Strukturen entdeckt, nämlich peritumorale venöse Blutgefäße (PVVs), die von zirkulierenden T Zellen genutzt werden, um in den Hirntumor einzuwandern. Die Nutzung dieser PVVs für die T Zell-Rekrutierung zu intrakraniellen Tumoren wurde durch ICI-Behandlung verstärkt. Ich konnte nachweisen, dass PVVs Stellen aufweisen, an denen zirkulierende T Zellen bevorzugt arretieren und extravasieren. Andere Strukturen, wie Hirn-Kapillaren, intratumorale Blutgefäße und parasagittale Regionen, konnten als alternative Routen der T Zell-Rekrutierung zum intrakraniellen Melanom ausgeschlossen werden. Außerdem konnte an PVVs eine besonders hohe T Zell-Anzahl und T Zell-Motilität nachgewiesen werden. Zudem wiesen PVVs eine hohe luminale Expression des endothelialen Adhäsionsmoleküls Intercellular adhesion molecule 1 (ICAM-1) auf. Tatsächlich konnte nach funktionaler ICAM-1 Blockade *in vivo* ein Trend zur Minderung der ICI-vermittelten T-Zell-Infiltration sowie der Inhibition des intrakraniellen Tumorwachstums festgestellt werden. Die ICI-Behandlung verstärkte die T Zell-Motilität im Gehirn, wodurch der Weg der T-Zellen vom PVV zum Tumor erleichtert wurde, was zur Inhibition des intrakraniellen Tumorwachstums führte. Diese Erkenntnisse beschreiben einen bestimmten Mechanismus, durch den zelluläre Komponenten des adaptiven Immunsystems in Hirntumore eintreten können, um deren Wachstum zu überwachen. Die molekularen und zellulären Merkmale der PVVs sowie die spezifischen Effekte der ICI auf die Funktionalität der T Zellen im Gehirn *in vivo* wurden hier zum ersten Mal beschrieben und bilden ein Fundament für die Verbesserung von Immuntherapien gegen Hirntumore.

Abstract

Cutaneous malignant melanoma is a rare, but very aggressive type of skin cancer, that frequently metastasizes to the brain. As treatment options for patients suffering from brain metastases are very limited, the diagnosis of brain metastasis is associated with a poor prognosis. However, recent preclinical and clinical findings raise hope that immunotherapeutic approaches could benefit brain metastasis patients. Intracranial anti-tumor response to immune checkpoint inhibition (ICI) is possible but strongly depends on efficient T cell recruitment to the brain. While the brain has long been considered an immune privileged organ, recent studies have suggested that special meningeal lymphatic vessels facilitate immune surveillance of brain tissue. However, in the context of brain tumors, the mechanism of T cell recruitment to the brain, and how this is affected by ICI, is still poorly understood. To elucidate anatomical and molecular mechanisms of T cell homing to brain tumors, I established novel intravital microscopy methods that allow to track T cell and tumor cell interactions in real-time over two weeks in two different syngeneic mouse models for melanoma brain tumors. With this, I was able to visualize the dynamics of T cell recruitment to the brain during tumor development, and I discovered a new route for circulating T cells to access brain tumors via distinct anatomical structures, namely peritumoral venous vessels (PVVs). Exploitation of PVVs for T cell homing to intracranial tumors was enhanced by ICI treatment. I could demonstrate that PVVs are the sites where circulating T cells preferably arrest and extravasate. Other structures, such as brain capillaries, intratumoral blood vessels, and parasagittal regions could be excluded as alternative T cell routes to intracranial melanoma. Moreover, at PVVs, a particularly high T cell motility and number was observed, and PPVs were characterized by high luminal expression of the endothelial intercellular adhesion molecule 1 (ICAM-1). Indeed, a trend of mitigation of ICI-mediated T cell infiltration and intracranial tumor growth control could be detected following functional blocking of ICAM-1 *in vivo*. ICI treatment increased T cell motility in the brain, facilitating the route from the PVV to the tumor, which resulted in intracranial tumor growth inhibition. These findings describe a distinct mechanism by which cellular components of the adaptive immune system can access and control brain tumors, and potentially other brain pathologies. The molecular and cellular features of PVVs, and also the specific effects of ICIs on T cell functionality in the brain *in vivo,* which is described for the first time, provide a fundament which will help to further improve immunotherapies against brain tumors.

Content

List of abbreviations

ACK lysing buffer	ammonium-chloride-potassium lysing buffer
ACT	adoptive cell transfer
ANOVA	analysis of variance
APC	antigen presenting cell
BBB	blood-brain barrier
BCSFB	blood-cerebrospinal-fluid barrier
BRAF	B-Raf proto-oncogene, serine/threonine kinase
CAR T cell	chimeric antigen receptor T cell
CCL	CC chemokine ligand
CD	cluster of differentiation
CDKN2A	Cyclin dependent kinase inhibitor 2A
CIR	crude incidence rate
CMFDA	5-chloromethylfluorescein diacetate
CNS	central nervous system
Cre	cyclization recombinase
CRISPR/Cas9	clustered regularly interspaced short palindromic repeats/CRISPR associated protein 9
CSF	cerebrospinal fluid
CTLA-4	Cytotoxic T-lymphocyte associated protein 4
CXCL	CXC chemokine ligand
CXCR	CXC chemokine receptor
DAPI	4’,6-Diamidino-2-phenyl-indol -dihydrochlorid
DC	dendritic cell
DMEM	Dulbecco's Modified Eagle Medium
DPBS	Dulbecco’s phosphate-buffered saline
EAE	experimental autoimmune encephalomyelitis
FACS	fluorescence activated cell sorting
FBS	fetal bovine serum
FDA	Food and Drug Administration
FITC	fluorescein isothiocyanate
gp100	glycoprotein 100
HEPES	4-(2-hydroxyethyl)-1-piperazineethanesulfonic acid
HEV	high endothelial venule
$hgp100_{25-33}$	human glycoprotein 100 peptide 25-33
HRP	horseradish peroxidase
i.p.	intraperitoneal
i.v.	intravenous
ICAM-1	Intercellular adhesion molecule 1
ICI	immune checkpoint inhibition
IDO	Indoleamine-pyrrole 2,3-dioxygenase
IFN	interferon
IL	interleukin
ISF	interstitial fluid

Iso	isotype
IVM	*in vivo* two-photon microscopy
LAG-3	Lymphocyte activation gene 3
LCK	lymphocyte protein tyrosine kinase
LFA-1	Lymphocyte function-associated antigen 1
LN	lymph node
LSL	lox-stop-lox
MAPK	Mitogen activated protein kinase
MDSCs	Myeloid derived suppressor cells
MHC	major histocompatibility complex
MIP	maximum intensity projection
MMP	matrix metalloproteinase
MS	multiple sclerosis
NK cell	natural killer cell
NRAS	NRAS proto-oncogene GTPase
PBS	phosphate-buffered saline
PD-1	Programmed cell death protein 1
PD-L1	Programmed death ligand 1
Pmel-1	premelanosome protein 1
PNAd	peripheral lymph node adressin
PVV	peritumoral venous vessels
RPMI 1640 medium	Roswell Park Memorial Institute 1640 Medium
s.c.	subcutaneous
SDS	sodium dodecyl sulfate
s	seconds
SEM	standard error of the mean
TBS	Tris-buffered saline
TCR	T cell receptor
tdTom	tdTomato
TGF-β	Transforming growth factor β
Th	T helper
TI	tumor injection
TIM-3	T cell immunoglobulin and mucin domain-containing protein 3
TME	tumor microenvironment
TP53	Tumor protein p53
TRITC	tetramethylrhodaminisothiocyanat
Tyr	Tyrosinase
TyrKO	Tyrosinase knock out
VCAM-1	Vascular cell adhesion molecule 1
VEGFR2	vascular endothelial growth factor receptor 2
VLA-4	Very late antigen 4

List of figures

List of tables

1 Introduction

1.1 Anti-tumor immunity

Cancer is a disease caused by cell transformation leading to malignant neoplastic growth. The transformation process involves mutagenesis and epigenetic dysregulation (Vogelstein et al., 2013), resulting in molecular characteristics differentiating tumor cells from healthy cells. This causes many tumor types to express tumor-specific antigens, that in principle allow tumor recognition by the immune system of the host (Jhunjhunwala et al., 2021). Many of the current strategies aim to use the immune system as a tool to fight cancer by enhancing or inducing anti-tumor immunity with cellular or molecular therapies (Waldman et al., 2020). To elicit an effective immune response against tumor cells, a complex cascade of events has to occur, which was described as the cancer immunity cycle (Chen & Mellman, 2013). This cycle includes the release of tumor antigens, their recognition by antigen-presenting cells, subsequent priming and activation of other immune cells in secondary lymphoid organs, especially lymphocytes, the trafficking of activated immune cells to the tumor lesion via blood vessels, effective extravasation from the blood and infiltration into the tumor which finally results in tumor cell killing (Figure 1).

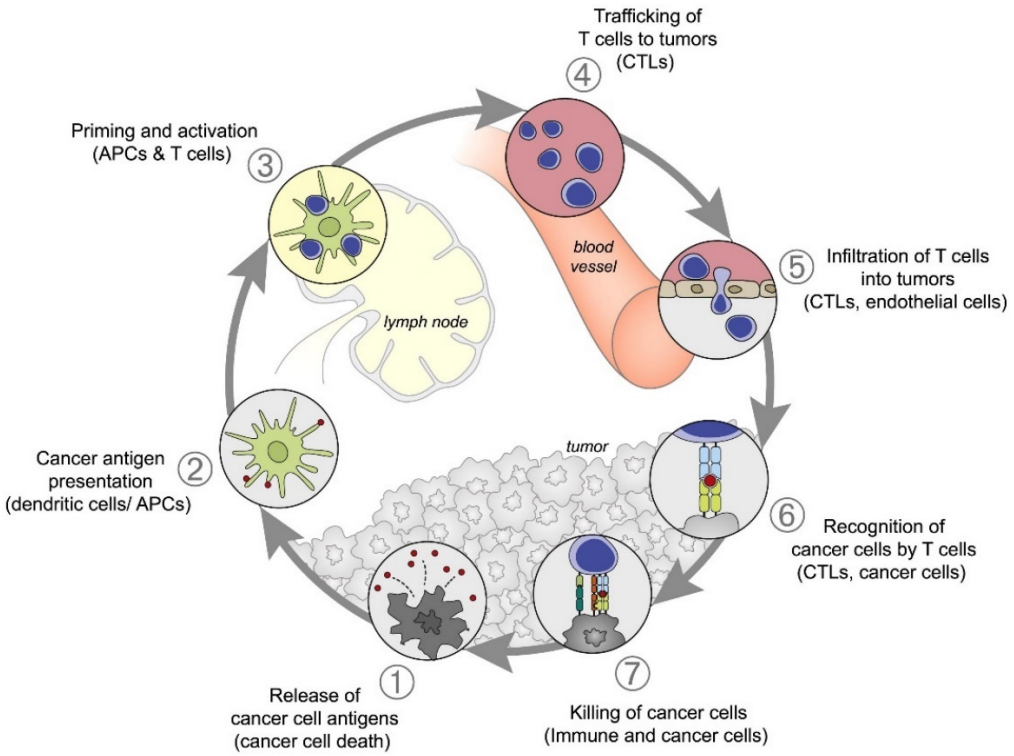

Figure 1: Schematic depiction of the cancer immunity cycle

Image taken from Chen and Mellman 2013 (Chen & Mellman, 2013).

Introduction

For an effective anti-tumor immune response, all of the steps of the cancer immunity cycle have to be functionally well balanced. Solid tumors, including malignant melanoma can apply several strategies targeting different steps of the cycle to escape from immunity (Chen & Mellman, 2013; Kalaora et al., 2022; Motz & Coukos, 2013). This can be achieved e.g. by downregulating of major histocompatibility complex (MHC) class I and preventing antigen-presentation (Cornel et al., 2020; Restifo et al., 1996; Sucker et al., 2014), or by creating an immunosuppressive tumor microenvironment (TME) (Anderson et al., 2017; Falcone et al., 2020). The latter can be induced by the secretion of immunosuppressive cytokines and chemokines, such as Interleukin 10 (IL-10) (Yaguchi et al., 2012), Transforming growth factor β (TGF-ß) (Fedorenko et al., 2015), IL-4 (Kobayashi et al., 1998), so that immunosuppressive cell types namely regulatory T cells (Ascierto et al., 2010; Baumgartner et al., 2007) and myeloid derived suppressor cells (MDSCs) (Huber et al., 2018; Umansky et al., 2014) are recruited to or induced in the TME. Other mechanisms of immunosuppression in the TME are metabolite depletion by expression of e.g. amino acid depleting enzymes arginase (Lowe et al., 2019) and Indoleamine-2,3-dioxygenase (IDO) (Brody et al., 2009; Lee et al., 2005). Immune responses against pathogens need to be limited and terminated after some time to avoid excessive tissue damage by an ongoing response, and to maintain peripheral tolerance. For a balanced immune response immune-stimulating and immune-inhibitory signaling must be tightly regulated (ElTanbouly & Noelle, 2021). The expression of immune checkpoint molecules and their ligands such as Programmed cell death protein 1 (PD-1), Programmed death ligand 1 (PD-L1) , Cytotoxic T-lymphocyte associated protein 4 (CTLA-4), T cell immunoglobulin and mucin domain-containing protein 3 (TIM-3), and Lymphocyte activation gene 3 (LAG-3) induce immune inhibitory signaling, dampening an immune response (Pardoll, 2012). Tumors can exploit these mechanisms to achieve immune resistance (Zou & Chen, 2008). They often express immune-inhibitory receptors or induce their expression in the TME, which is associated with lymphocyte anergy and exhaustion (Barber et al., 2006; Waldman et al., 2020).

1.1.1 Molecular concept of immune checkpoint inhibition

Immune checkpoint inhibition exploits the concept of taking away the immuno-suppressive “brakes” from an ongoing immune response against cancer. Immunotherapeutic anti-cancer treatment mostly targets the immune checkpoints PD-1/PD-L1 and CTLA-4, as monotherapies or in combination of both pathways (Figure 2). CTLA-4 is an inhibitory surface receptor expressed on T lymphocytes, that counteracts the co-stimulatory signaling of cluster of differentiation (CD)28, by binding to their common ligands B7.1 (CD80) and B7.2 (CD86) and outcompeting CD28-B7.1 binding (Freeman et al., 1993; Tivol et al., 1995; Waterhouse et al., 1995). CTLA-4 therefore regulates the early stages of T cell activation by antigen presenting cells (APCs) through contact of antigen presented on MHC molecules and the T cell receptor (TCR) (Pardoll, 2012) (Figure 2a).

The mechanism of immune-inhibition by PD-1/PD-L1 signaling is distinctly different from CTLA-4 signaling, as PD-1 limits the inflammatory reaction and suppresses T cell effector functions in the peripheral tissue (Blank et al., 2004) (Figure 2b). PD-1 expression on T cells is induced after successful activation. Its ligands PD-L1 and PD-L2 are expressed on other immune cells, such as antigen presenting cells in the tumor microenvironment, or they can be directly expressed on tumor cells (Zou & Chen, 2008). TCR signaling is suppressed by PD-1 signaling, and T cells become anergic, exhausted, or even apoptotic (Ahmadzadeh et al., 2009; Barber et al., 2006; Dong et al., 2002).

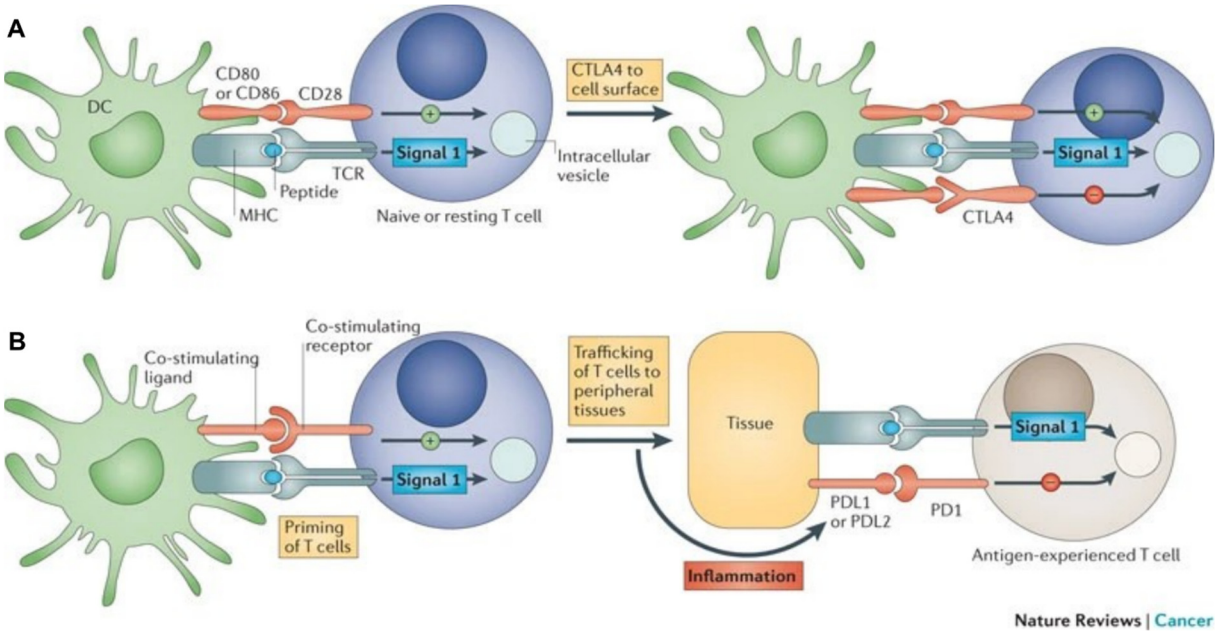

Figure 2: Schematic depiction of immune checkpoint molecules CTLA-4 (A) and PD-1 (B)

Image taken from Pardoll 2012 (Pardoll, 2012)

(**A**) CTLA-4 signaling on T cells counteracts the co-stimulatory signaling conferred by binding of CD28 on T cells to its receptors CD80 and CD86 expressed on dendritic cells (DCs), thus inhibiting T cell activation during contact of the TCR with peptide presented on DC MHC molecules

(**B**) Upon activation, antigen-experienced T cells upregulate PD-1 expression. Binding of its ligands PD-L1 or PD-L2 expressed on other cells in peripheral tissue induces immune-inhibitory signaling, counteracting TCR-mediated signaling.

1.2 Immune cell recruitment to extracranial solid tumors

A prerequisite for anti-tumor immunity is the availability of immune recognition of one or more distinct, tumor specific neoantigens. Melanoma is a tumor entity with a high mutational burden, and thus is a strongly immunogenic cancer, with a comparatively high chance to respond to immunotherapy (Chan et al., 2019; Lawrence et al., 2013). The nature and quality of antigens have an impact on the elicited immune response against the tumor (Achar et al., 2022; Łuksza et al., 2022;

McGranahan & Swanton, 2019). The variety of tumor antigens, and the discovery of neoantigens and their corresponding T cell receptors are subject of many other research projects (Bassani-Sternberg et al., 2016; De Mattos-Arruda et al., 2020; Gupta et al., 2021; Ott et al., 2017) heavily relying on next generation sequencing technologies, and will not be covered in this study.

Successfully activated T lymphocytes primed for their cognate tumor antigen, strongly rely on active migratory functions for an effective trafficking to their tumor targets. Activated lymphocytes need to be able to leave the secondary lymphoid organ, enter the blood circulation and extravasate from the blood at the right site and migrate within the tissue towards the tumor. This requires spatiotemporally tightly regulated, complex interactions between immune cells and endothelium (Carman & Martinelli, 2015; von Andrian & Mackay, 2000). Outside of the brain immune cells extravasate from the blood at post-capillary venules (Thurston et al., 2000; von Andrian & Mackay, 2000), which is a multi-step process (Figure 3). The endothelial cells of these vessels can respond to inflammatory stimuli by luminally expressing adhesion molecules that allow to induce lymphocyte tethering, rolling, firm adhesion and subsequently transmigration through the blood vessel wall (Carman & Martinelli, 2015; Thurston et al., 2000; von Andrian & Mackay, 2000). Early tethering contacts are established by binding of selectins, such as L-selectin on leukocytes and P- and E-selectin expressed on endothelial cells, to their oligosaccharide ligands. These contacts allow to induce leukocyte rolling at the vascular wall. By integration of chemokine signaling, other integrins expressed on the rolling leukocytes, such as Lymphocyte function-associated antigen type 1 (LFA-1)(Kelly et al., 1999) and Very late antigen 4 (VLA-4), can be activated. Integrin activation initiates stronger adhesion to their respective endothelial receptors, such as intercellular adhesion molecules (ICAMs), and vascular-cell adhesion molecule 1 (VCAM-1) (Alon et al., 1995). Subsequently, leukocytes undergo polarization and migrate along the luminal vasculature to find a permissive site of the endothelium for extravasation (Phillipson et al., 2006; Schenkel et al., 2004) either by paracellular or transcellular diapedesis (Muller, 2011; Sage & Carman, 2009). The organotropism of T cell homing to the correct location is orchestrated by interactions between distinct sets of certain chemokines, vascular addressins and leukocyte homing receptors (Fu et al., 2016). During priming of T cells with their cognate antigen in secondary lymphoid organs, a unique profile of homing receptor and adhesion molecule expression is induced (Haddad et al., 2003; Ley & Kansas, 2004; Picker et al., 1990). Upon inflammation endothelium of different organs express a distinct combination of adhesion molecules, addressins and chemokines, representing counterparts to the lymphocytic molecular profile (Fu et al., 2016). This mechanism acts like a complex postal code system, allowing selective recruitment of distinct lymphocyte subtypes.

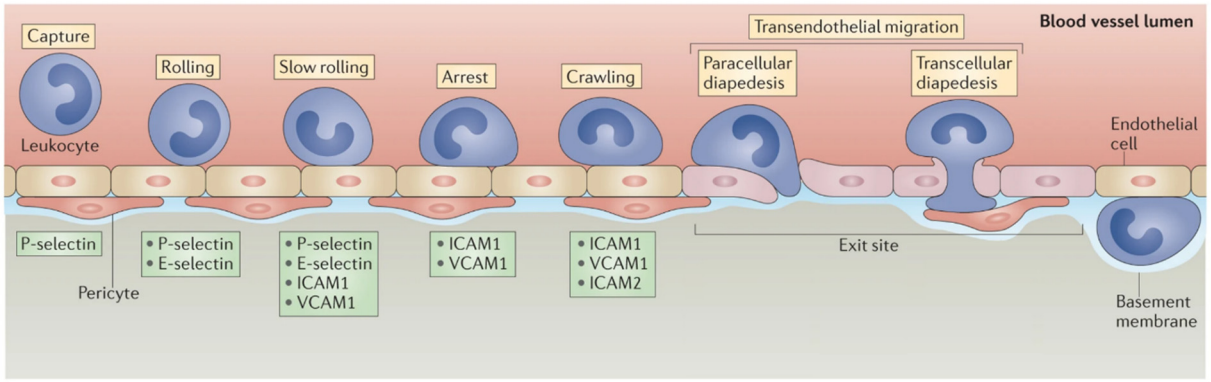

Figure 3: Schematic representation of the leukocyte extravasation cascade

Leukocyte transmigration is initiated by tethering to selectin molecules expressed on the endothelium, which induces rolling, leukocyte arrest and crawling, followed by paracellular or transcellular diapedesis. Adapted from Vestweber, 2015. (Vestweber, 2015)

Upon extravasation, lymphocytes need to migrate through the tissue driven by cytokine stimulation and chemokine gradients to find their targets (Fu et al., 2016; van der Woude et al., 2017). Skin homing of T cells, for example, depends on the chemokines CC chemokine ligand (CCL)-17 and CCL27 produced by dendritic cells, endothelial cells, keratinocytes, and fibroblasts, and binding to their receptors CCR4 and CCR10, respectively (Jiang et al., 2010; Morales et al., 1999; Reiss et al., 2001). Another important T cell attractant to various solid extracranial tumors is the CXC chemokine receptor (CXCR)3-CXC chemokine ligand (CXCL)9/10/11 axis (Dangaj et al., 2019; Kohli et al., 2022), which is induced by type-1 interferons (IFN) and interferon γ (IFNγ) (Farber, 1997; Ohmori et al., 1993). In addition to these chemokines, in melanoma the expression of CCL2, CCL3, CCL4, and CCL5 was associated with the presence of lymphocytes (Harlin et al., 2009).

1.3 Cutaneous malignant melanoma

Cutaneous malignant melanoma is the rarest, but also the most aggressive form of skin cancer. It is characterized by neoplastic growth of melanocytes in the skin. The major risk factor for melanoma development is sun exposure (Arnold et al., 2018; Garibyan & Fisher, 2010). Solar UV light can cause DNA mutations through pyrimidine dimer formation (Pfeifer et al., 2005), which leads to a mutation signature typical for melanoma, that is characterized by cytidine to thymidine transitions (Alexandrov et al., 2013; Lawrence et al., 2013). These somatic mutations can alter the function of their gene products resulting in oncogenic driver formation. In melanoma oncogenic mutations in *B-Raf proto-oncogene, serine/threonine kinase (BRAF)*, *NRAS proto-oncogene GTPase (NRAS)*, *Cyclin dependent kinase inhibitor 2A (CDKN2A)*, *Tumor protein p53 (TP53)*, and other genes associated with cell cycle

progression or cell cycle control, proliferation and apoptosis are commonly found (Hayward et al., 2017).

For decades, the crude incidence rate (CIR) of cutaneous melanoma has been rising in Germany, with an average increase of 3.9% to 4.8% per year between 1999 and 2012, resulting in a CIR of 26.5/100 000/year in males and 25.3/100 000/year in females in 2012 and crude mortality rates of 4.1/100 000 in males and 3.0/100 000 in females (Garbe et al., 2019). Melanoma is an aggressive disease with fast dissemination and metastatic spread and is often only diagnosed at an advanced stage. Until 2011 the standard of care treatment for advanced or metastatic melanoma was surgical resection and chemotherapy, which was not sufficient to improve patient outcome substantially, leading to a median survival time of 6.2 months (Korn et al., 2008). The identification of the BRAF mutations commonly found in cutaneous melanoma, drove the development of small molecule inhibitors targeting the mitogen-activated protein kinase (MAPK) pathway (Tanda et al., 2020). The first small molecule BRAF inhibitor Vemurafenib was Food and Drug Administration (FDA) approved in 2011 for the treatment of unresectable, $BRAF^{V600E}$ mutant, metastatic melanoma (Chapman et al., 2011; Sanchez et al., 2018), which improved the overall survival rate at 6 months to 84% compared to 64% in the control group (Chapman et al., 2011). However, primary and acquired resistance to targeted therapy impose challenges for the treatment of metastatic melanoma patients and prevent durable response to therapy (Robert et al., 2019). A crucial breakthrough in treatment of advanced melanoma was the development of immunotherapy, particularly the immune checkpoint inhibitor antibodies targeting PD-1 and CTLA-4 in 2015. Combination treatment of Nivolumab (anti-PD-1) and Ipilimumab (anti-CTLA-4) improved median progression-free survival of patients to 11.5 months (Larkin et al., 2015), and 5-year progression free survival was reached in 36% of patients treated with the combination, while overall 5-year survival was 52% (Larkin et al., 2019). Due to the high frequency of somatic mutations found in melanoma tumors as compared to other tumor entities (Lawrence et al., 2013), the frequency of neoantigens, which can be recognized by the immune system, is also relatively high in melanoma. A high tumor mutational burden could be associated with improved prognosis and better response to immunotherapy in melanoma (Kang et al., 2020) and other cancer entities (Chan et al., 2019; Rizvi et al., 2015). Because of these features melanoma represents an interesting target for the development of novel immunotherapeutic approaches.

1.4 Melanoma brain metastases – clinical features

A very serious complication of malignant melanoma is its metastatic spread to the brain, which is associated with poor prognosis (Davies et al., 2011; Fife et al., 2004). Approximately 10-20% of patients already suffer from brain metastases (BrM) at the diagnosis of advanced melanoma, and up to 50-75%

of advanced melanoma patients develop BrM during the course of the disease (Davies et al., 2011; Fife et al., 2004; Sampson et al., 1998). Tumors in the brain can be inoperable and systemic treatments often cannot reach the brain parenchyma due to the integrity of the blood-brain barrier (BBB). Despite the tremendous advances in the systemic treatment of advanced melanoma, treatment of patients suffering from brain metastasis remains difficult. Before the era of targeted and immunotherapies, the median overall survival of melanoma brain metastasis patients treated with chemotherapy, surgical resection, whole-brain radiation, or radiosurgery was 4-6 months (Davies et al., 2011; Eigentler et al., 2011; Vosoughi et al., 2018). Due to their poor prognosis, advanced melanoma patients suffering from brain metastases had been excluded from clinical trials for a long time. In 2018, the first results were published of clinical trials on immunotherapy for advanced melanoma treatment that included brain metastasis patients (Long et al., 2018; Tawbi et al., 2018). With the combination treatment of anti-PD1 and anti-CTLA-4 an intracranial response rate of 46% (Long et al., 2018) and 57% (Tawbi et al., 2018) was reached, which is even comparable to the rate of extracranial benefit. However, this response was often not durable and eventually patients relapsed (Long et al., 2018). These clinical findings highlight the potential of immunotherapeutic approaches for the treatment of melanoma brain metastasis patients and possibly of other cancer entities, but they also show their limitations. However, immunotherapeutic options for brain metastasis treatment have to be improved so that more patients can benefit in the future. For this, it is crucial to improve the understanding of the underlying cellular and molecular mechanisms, that allow immune cell recruitment to the brain.

1.5 Immune surveillance of the healthy brain

1.5.1 The brain immune microenvironment

To improve immunotherapy for brain metastasis patients, it is important to understand and take into consideration the peculiar characteristic of the brain in respect of its immune surveillance. For a long time, the healthy brain was considered completely devoid of infiltration of circulating immune cells. Experimental animal studies showed that, unlike at extracranial sites, tissue was not rejected when implanted into the central nervous system (CNS) (Mason et al., 1986; Medawar, 1948), which supported the dogma of the CNS being an immune-privileged site. However, this paradigm has been changing due to recent discoveries, which will be addressed later in this work. The microenvironment of the brain indeed is distinctly different from other tissues, when it comes to accessibility for the immune system (Sampson et al., 2020). The only brain-resident immune cell type are microglia cells – the macrophages of the brain (Li & Barres, 2018). Microglia actively monitor the brain parenchyma by extending and retracting their cellular protrusions (Nimmerjahn et al., 2005) and they play an important role in tissue maintenance and protection (Frost & Schafer, 2016; Ueno et al., 2013). Like

other myeloid cells, microglia express pattern recognition receptors (Schetters et al., 2018; Wang et al., 2015), can phagocytose brain foreign and damaged molecules, and can present antigen on MHC class II molecules, of which the expression is upregulated upon microglia activation (Dalpke et al., 2002; Dutta et al., 2003; Schetters et al., 2018). However, microglia have not been observed to recirculate to secondary lymphoid organs outside of the brain, where activation of naïve T cells usually takes place (Schetters et al., 2018). Additionally, during neurodegeneration or in primary brain tumors, microglia express a gene set associated with immunosuppression (Schetters et al., 2018). Among these genes are PD-1 (Ren et al., 2011), C-type lectin dectin-1 (Bode et al., 2019; Dillon et al., 2006; Shah et al., 2008), and ILT3 (Kim-Schulze et al., 2006; Schetters et al., 2018). Microglial antigen presentation to T cells does not always efficiently activate T cells and can even have immunosuppressive effects (Ford et al., 1996; Unger et al., 2018).

Another important aspect contributing to the distinctiveness of the brain immune microenvironment is the BBB. The integrity of the BBB not only prevents access of pathogens and toxins to the brain parenchyma, but also represents a strong hurdle to overcome for the immune cells to home to the CNS. The BBB is located at the brain capillary walls and venules, and is composed of distinct molecular and cellular features (Galea, 2021), such as a negatively charged glycocalyx (Yuan et al., 2010), an unfenestrated endothelial cell layer connected by tight junctions (Nitta et al., 2003; Vorbrodt & Dobrogowska, 2003) and a basement membrane, a pericytic sheathing around the endothelial layer (Armulik et al., 2010) and astrocytic end-feet (glia limitans) covering any remaining gaps (Mathiisen et al., 2010). However, evidence has accumulated showing that there is immune surveillance of the healthy brain. Recent studies have shown that following viral infections, memory T cells can be induced even peripherally, and can reside in the brain to protect the tissue by preventing recurring infections (Steinbach et al., 2016; Urban et al., 2020). Combined, these distinct features impact the immune microenvironment of the brain to protect the delicate brain tissue against damaging (auto-) immune responses. Immune-related tissue destruction can lead to detrimental defects in the CNS, as for example by destruction of neurons during the progression of multiple sclerosis (MS) (Attfield et al., 2022; Lodygin et al., 2019).

1.5.2 Meningeal lymphatics

To ensure optimal brain functionality and maintain tissue homeostasis, the clearance of metabolic waste from the brain is crucial, which is achieved via the so-called glymphatic (glial-lymphatic) system (Mestre et al., 2020). Cerebrospinal fluid (CSF) produced at the choroid plexus is located in the ventricular system and the subarachnoid space and is transported driven by arterial pulsation in the arterial perivascular space towards arterioles and brain capillaries (Humberto Mestre et al., 2018),

where it is mixed with interstitial fluid (ISF) that is pumped through Aquaporin-4 channels on astrocytic end-feet (H. Mestre et al., 2018). The CSF/ISF efflux occurs through perivenous spaces and is transported out of the CNS (Iliff et al., 2012). This system serves as a pseudo-lymphatic fluid drainage from the brain parenchyma and is regulated by the sleep-wake cycle (Holth et al., 2019; Xie et al., 2013). Recent studies have led to a shift in the paradigm of the immune-privileged brain by providing evidence for the existence of a true lymphatic system of the brain and spinal cord in mice (Aspelund et al., 2015; Louveau et al., 2015). The lymphatic vessels were found to be located at the meninges and run alongside the sagittal venous sinus (Louveau et al., 2015) and at the base of skull in mice (Ahn et al., 2019). It could be shown that the connection between the glymphatic system and the meningeal lymphatic vessels allows drainage of brain-derived antigens from the interstitial fluid and CSF to cervical lymph nodes, thus allowing priming of immune cells of the adaptive immune system to fight brain extraneous antigens (Jacob et al., 2022; Louveau et al., 2018) (Figure 4). However, the contribution of the meningeal lymphatics and its exact role for immune cell recruitment is still not well understood. Therefore, it is important to gain a better understanding of the basic biological mechanisms of immune cell recruitment to the brain.

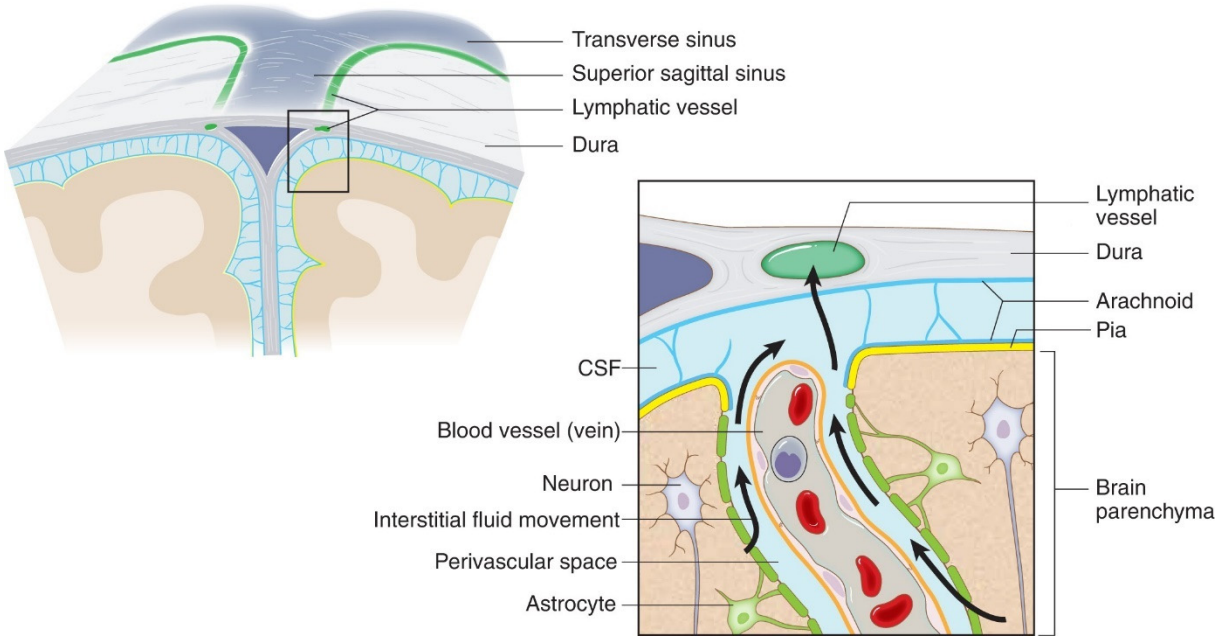

Figure 4: Schematic depiction of the location of meningeal lymphatic vessels

Meningeal lymphatic vessels are located along the superior sagittal sinus of the mouse brain. Interstitial fluid from the perivascular space flows towards the meninges and mixes with CSF, so that its components can enter the lymphatic vessels and can be transported to the cervical lymph nodes. From Louveau et al. 2015 (Louveau et al., 2015)

The choroid plexus has been proposed to be another structure important for immune surveillance and T cell entry to the CNS (Ghersi-Egea et al., 2018; Kivisäkk et al., 2003; Schmitt et al., 2012). Choroid plexus endothelial cells resemble peripheral endothelial cells without the features of a blood-brain barrier. The blood-cerebrospinal-fluid barrier (BCSFB) – a layer of epithelial cells surrounding the choroid plexus stroma – represents the barrier between the choroid plexus stroma and the CSF. It could be shown *in vitro* that a choroid plexus epithelial cell layer expressed the Intercellular adhesion molecule 1 (ICAM-1) and VCAM-1 (Nishihara et al., 2020) and allowed T cell diapedesis through the BCSFB dependent on CCR6/CCL20 chemokine signaling (Reboldi et al., 2009). However, *in vivo* evidence for lymphocyte migration across the BCSFB has not been presented yet (Mapunda et al., 2022), although the development of novel intravital imaging methodologies for microscopy of the ventricle choroid plexus (Shipley et al., 2020) might be a promising tool to investigate this further.

1.6 How T cells enter the CNS during autoimmunity

Multiple sclerosis is an autoimmune disease of the CNS, characterized by infiltration of immune cells directed against proteins of the CNS, leading to tissue destruction and neuronal loss within the CNS (Attfield et al., 2022). Although it is a disease completely different from brain tumors, it has given rise to a related research field, which also aims to uncover mechanisms of lymphocyte recruitment to the CNS parenchyma. Both fields try to translate their findings into restoring the balance of immune regulation in either direction; the intention of MS research is to understand and prevent immune cell entry to the CNS to limit tissue destruction and neuronal impairment, while brain tumor immunology tries to translate findings into enhancing anti-tumor immunity in the brain. It is well conceivable that findings from one research field might be applied to the other as it is likely that mechanisms of lymphocyte entry might share similarities (Mitchell et al., 2021). Brain blood vessels have also been shown to contribute to T cell recruitment to brain parenchyma, however, this has mostly been studied and observed in the context of autoimmunity. The group of B. Engelhardt has done extensive work to elucidate the mechanisms of immune cell entry to the CNS in the context of MS (Mapunda et al., 2022). In models of experimental autoimmune encephalomyelitis (EAE), the animal model of multiple sclerosis, they could show that immune cell entry to the CNS parenchyma involved two steps to induce onset of EAE. The first step is transmigration through the vascular endothelial into the perivascular space of postcapillary venules, and secondly, breaching of the basement membrane of the glia limitans (Owens et al., 2008). Further, it could be shown that endothelial ICAM-1 and ICAM-2 was required for T helper cell 1 (Th1) and Th17 cell transmigration in the brain (Bullard et al., 2007; Haghayegh Jahromi et al., 2019; Lyck et al., 2003), while penetration of the glia limitans depends on matrix metalloproteinases (MMP) 2 and MMP-9 produced by macrophages (Agrawal et al., 2006; Song et al.,

2015). It remains to be investigated if immune infiltration in the setting of a brain tumor happens via a similar mechanism.

1.7 Intravital imaging to investigate dynamic biological processes

Many highly dynamic biological processes, such as migratory behavior of immune cells or the development of tissue in health and diseases, can be very comprehensively studied using intravital imaging. Intravital fluorescence microscopy can be used to visualize the dynamic behavior of, e.g., fluorescently labeled cells, by dynamic imaging in real-time in the range of seconds to hours and also by longitudinal imaging over an extended period of time by repetitive imaging over days and weeks. Thereby, biological processes of different organisms can be observed microscopically in single-cell resolution in the living organism. For example, *in vivo* imaging has been used to study developmental processes in zebrafish embryos (Keller et al., 2008; Pinto-Teixeira et al., 2013; Scherz et al., 2008), the transparent tissue of zebrafish embryos makes it a relatively easily accessible model-organism for intravital microscopy. However, for studying complex biological processes such as immunity, often higher developed organisms are used as a model, for instance mice or rats. Since light penetration through non-transparent tissue and bone is limited, internal organs or tissue of interest have to be made accessible for microscopy. In rodent models, several different types of surgical preparation for intravital imaging of different organs are well established. For example *in vivo* imaging of subcutaneous tumors can by performed after skin-flap preparation (Lau et al., 2020). This procedure involves surgical incisions and careful detachment of the skin above the tumor on a fixated and anesthetized animal, so that the tumor and for example draining lymph nodes can be exposed for imaging (Lau et al., 2020). For longitudinal imaging over an extended period of time, chronic imaging windows can be implanted over the organ of interest (Alieva et al., 2014). After successful implantation and healing of the chronic imaging window, the tissue lying underneath can be imaged without further invasive intervention. For example, long-term imaging can be performed on the mammary gland through a chronic mammary imaging window (Jacquemin et al., 2021; Kedrin et al., 2008), on the gastro-intestinal tract through an abdominal window (Rakhilin et al., 2019; Ritsma et al., 2012), or within the skin through a dorsal skin fold chamber (Alexander et al., 2008; Schreiter et al., 2017). The cortical brain can be observed by intravital imaging through a chronic cranial window (Kienast et al., 2010; Xu et al., 2007). Implantation of a chronic cranial window involves surgical removal of the skin above the skull, craniotomy of the skull and removal of the underlying dura mater, and replacement of the skull by a cover glass (Kienast et al., 2010).

Surgical preparation of the respective organ, e.g., through an imaging window, is often combined with the method of multi-photon microscopy. The physical principle underlying multi-photon microscopy is

the excitation of a fluorescent molecule by two or more photons of a pulsed laser simultaneously (Karreman, 2021). With this, the energy of an individual photon can be lower as compared to single-photon excitation to achieve fluorophore excitation, resulting in the use of wavelengths ranging between 700 nm and 1100 nm, while typical wavelengths for excitation in standard single-photon microscopy lie within the range of 350 – 650 nm (Larson, 2011). The use of near- infrared lasers in two-photon microscopy, allows deeper penetration into the tissue of interest and results in less phototoxicity as compared to single-photon microscopy. Therefore, two-photon microscopy is well suited for *in vivo* application (Karreman, 2021) and allows imaging through a cranial window to up to 500-600 µm in depth in the mouse brain. In this work, *in vivo* two-photon microscopy (IVM) through a chronic cranial window is the method of choice for visualizing intracranial tumor development and T cell infiltration in the brain of mice both longitudinally and in real-time.

1.7.1 Intravital imaging to study immune cell recruitment and migration

Immunohistochemistry and flow cytometry are standardly used to study the immune microenvironment of tumors both in mouse models and on human tumor samples. While these methods, together with the more recent development of transcriptomics, are well suitable for molecular characterization of immune cell subpopulations and their spatial distribution within the tissue, they can only reveal information at a specific moment, and they lack the dimension time. Therefore, these methods do not allow studying highly dynamic processes such as T cell migration patterns in secondary lymphoid organs or in peripheral tissue. The development of intravital microscopy has majorly contributed to gaining a better understanding of motility patterns of immune cells within lymphoid tissue and during anti-tumor immunity. This technology has not only allowed to elucidate basic functions of immune-surveillance (Kanda et al., 2021; Mempel et al., 2004; Stein et al., 2000), but also how immune cell migration is influenced by the microenvironment or by immunotherapies in preclinical models of cancer (Boulch et al., 2019). For example, it could be revealed by *in vivo* imaging, that T cells travel along perivascular pathways of the spleen to be guided to the splenic T zone, a process that is essential for lymphocyte recirculation (Chauveau et al., 2020). Other important findings made with intravital imaging include a better spatiotemporal understanding of T cell mobility within extracranial solid tumors and their periphery *in vivo*. It could be shown that the presence of cognate antigen presented on alive tumor cells is important for T cell arrest at their target cells, while loss of antigen expression during late phases of tumor-immunity restricted T cell infiltration in a migratory state to the tumor periphery (Boissonnas et al., 2007). Moreover, it was demonstrated that during search for antigen cytotoxic T cells exhibit a random migration pattern in the tumor microenvironment before they engage in stable interactions with their target cells (Mrass et al., 2006), to induce tumor cell killing, a process that takes approximately six hours (Breart et al.,

2008). Furthermore, intravital imaging revealed that T cells are dependent on CD44 to maintain a polarized phenotype, which is essential for T cell migration within the interstitium during the screening for cognate tumor antigen (Mrass et al., 2008). Differences in the migratory behavior of different immune cell types to exert cytotoxic functions could be observed for the first time by intravital microscopy. In particular, it could be shown that natural killer (NK) cell mediated tumor cell killing required only short-lived contacts with their tumor target cells to exert effector function, while cytotoxic T cells engaged in long-lasting, stable contacts dependent on extracellular calcium influx (Deguine et al., 2010).

Two-photon based imaging on acute tissue slices has revealed, that in human lung squamous-cell carcinoma macrophages of the tumor stroma impede CD8 T cell motility, excluding T cells to the tumor periphery and thereby diminishing response to anti-PD-1 treatment (Peranzoni et al., 2018). Another study using acute tumor slice imaging showed that CD8 T cell migration was impacted by the extracellular matrix of the tumor stroma, particularly by orientation, density, and spacing of collagen fibers (Bougherara et al., 2015).

Intravital microscopy has proven to be an important tool to enhance our understanding of the effect of ICI on lymphocytes by elucidating how ICI influences lymphocyte migratory behavior. Effective anti-CTLA-4 including combination immunotherapy increased velocities of antigen-specific T cells in a mouse model of subcutaneous melanoma (Pentcheva-Hoang et al., 2014). Another intravital microscopy study of murine melanoma under anti-PD-1/anti-CTLA-4 combination therapy has highlighted the importance of the spatiotemporal features of T cells when interpreting their migratory behavior (Lau et al., 2020). Lau et al. have detected Lévy-like trajectories of adoptively transferred antigen-specific T cells in the tumor periphery with higher velocities than intratumorally. In contrast to the study by Pentcheva-Hoang et al., in the study of Lau et al. anti-CTLA-4/anti-PD-1 treatment decreased T cell velocities (Lau et al., 2020). These apparent discrepancies highlight how difficult, it is to unravel the effect of ICI on T cell functionality, and how strongly interpretation of these T cell motility experiments depend on the spatiotemporal conditions.

Intravital imaging of T cell migration in EAE has revealed yet another layer of complexity when it comes to interpreting immune cell migratory behavior *in vivo*. The research of the group of A. Flügel has demonstrated that a large fraction of antigen-specific T cell in the brain of rats during EAE seem to be tethered to a distinct location, a phenotype they defined as “stationary”, that is dependent on the presence of cognate antigen, thus reflecting stable interactions of T cells with their specific targets (Kawakami et al., 2005). They also have observed VLA-4 dependent intravascular interactions with leptomeningeal blood vessels and subsequent diapedesis, as well as perivascular locomotion

associated with these vessels early after induction of EAE in the spinal cord of rats (Bartholomäus et al., 2009). All in all, these studies demonstrate the importance of intravital microscopy in relevant model systems to uncover the underlying mechanisms of immune cell infiltration and dynamics.

1.7.2 Intravital Imaging of immune cell infiltration in brain tumors

Interestingly, intravital imaging of immune cell infiltration to brain tumors has rarely been conducted so far. Mulazzani et al. have focused on the infiltration dynamics of anti-CD19 chimeric antigen receptor (CAR) T cells in a mouse model of primary central nervous system lymphoma (Mulazzani et al., 2019). As intravenous injection of CAR T cells did not result in successful tumor infiltration and growth control, the authors injected the CAR T cells directly intracerebral, so that the dynamics of T cell recruitment from the blood circulation to the tumor could not be observed in their study (Mulazzani et al., 2019). Thus, further research building on and integrating findings from previous studies is needed to improve our understanding of the effects of immunotherapy in the context of brain tumors.

1.8 Objectives of this study

The state-of the-art studies on T cell migration in intracranial and extracranial tumors and in EAE highlight the important role of the brain vasculature for immunity in the brain and the complex nature of its interactions with immune cells. Principle findings of mechanisms of T cell invasion to the brain parenchyma and T cell migratory behavior during the onset of EAE and could even be similar to mechanisms of T cell recruitment to brain metastasis. This study aims to elucidate the routes of T cell recruitment in the context of brain metastasis by intravital microscopy in mice. Previous knowledge on T cell migratory behavior acquired through EAE research as well as on T cell infiltration outside of the brain is integrated to interpret the findings. A better understanding of the mechanisms of T cell recruitment to the brain is not only important for improving desirable T cell recruitment to the brain tumor by immunotherapeutic strategies, but also for preventing unwanted T cell recruitment to the brain as in autoimmunity or immune-related neurotoxicity as side-effect of immunotherapy (Gust et al., 2017; Martins et al., 2019; Zhao et al., 2021).

The recruitment of T cells to the tumor is very complex and is influenced by a tightly orchestrated interplay of many local and systemic molecular factors and anatomical structures. Specifically, the homing of T cells to brain tumors is still not understood. To improve immunotherapy for brain tumor patients, it will be crucial to gain a deeper understanding of the basic mechanisms of immune cell recruitment to the brain to develop novel approaches for combination therapies allowing efficient lymphocyte homing to the brain tumor lesion.

Most studies using intravital microscopy for analyzing T cell infiltration into extracranial tumors used skin-flap models and tumor exposure on a fixed timepoint (Boissonnas et al., 2007; Breart et al., 2008; Deguine et al., 2010; Lau et al., 2020; Mrass et al., 2008; Mrass et al., 2006) or acute tissue slices (Bougherara et al., 2015; Peranzoni et al., 2018), so that T cell infiltration and migration dynamics could only be observed short term, in a window of maximum several hours. In this study, I exploit the advantage of the chronic cranial window for serial, longitudinal analysis of the brain tumor growth and T cell infiltration over several days up to two weeks, which allows to elucidate the long-term dynamics of T cell infiltration. To gain a better understanding of the mechanisms of immunotherapy on the level of single immune cell behavior, it is crucial to carefully assess the spatiotemporal features of each immune cell. How ICI influences immune cell behavior is likely very distinct depending on the functional state of the lymphocyte. Particularly, long-term dynamics of T cell recruitment during brain tumor development and how this is shaped by ICI has not been studied in preclinical models so far.

By establishing suitable syngeneic mouse models for intravital imaging, I was able to visualize the brain tumor development, T cell infiltration, and the blood vasculature of the brain in living mice over an extended period of time and also in real-time. In these models, I investigated the exact locations and timings of brain infiltrating, adoptively transferred or endogenous T cells in brain tumor models. By exploiting these advantages of *in vivo* two-photon microscopy, I aim to identify the anatomical structures and molecular mechanism, facilitating T cell recruitment to the melanoma brain tumors. Furthermore, this methodology allowed me to elucidate the impact of ICI treatment on T cell migratory behavior in the brain tumor context.

2 Material and Methods

2.1 Material

2.1.1 Mouse lines

Table 1: List of mouse lines

Short name of mouse line	Full name of mouse line	Supplier	RRID
C57BL/6J	C57BL/6J	Janvier Labs	n.a.
Pmel-1	B6.Cg-*Thy1*^{a}/Cy Tg(TcraTcrb)8Rest/J	Inhouse breeding	IMSR_JAX:005023
LCK-Cre	B6-Tg(Lck-cre)548Jxm	Inhouse breeding	IMSR_JAX:003802
LSL-tdTomato	Gt(ROSA)26Sor$^{tm14(CAG-tdTomato)Hze}$	Inhouse breeding	IMSR_JAX:007914
LCK-Cre x LSL-tdTomato	B6-Tg(Lck-cre)548Jxm x Gt(ROSA)26Sor$^{tm14(CAG-tdTomato)Hze}$	Inhouse breeding	IMSR_JAX:003802; IMSR_JAX:007914

Table 2: List of cell lines

Cell line	Alias	Original entity	Derived from transgenic model	Supplier
Ret CM TyrKO	CM TyrKO #43, CM Tyr$^{-/-}$ #43	Murine cutaneous melanoma, C57BL/6 background	Ret transgenic mouse model for melanoma	Iris Helfrich, Dirk Schadendorf, Michael Hölzel, Daniel Hinze
Ret CM TyrKO tdTom	CM TyrKO #43 tdTomato, CM Tyr$^{-/-}$ #43 tdTomato	Murine cutaneous melanoma, C57BL/6 background	Ret transgenic mouse model for melanoma	Iris Helfrich, Dirk Schadendorf, Michael Hölzel, Daniel Hinze
Ret	Ret1	Murine cutaneous melanoma, C57BL/6 background	Ret transgenic mouse model for melanoma	Viktor Umansky
HCmel12	HCmel12 gfp	Murine cutaneous melanoma, C57BL/6 background	HGF-Cdk4^{R24C} mouse model for melanoma	Thomas Tüting, Jennifer Landsberg, Michael Hölzel, Daniel Hinze
HCmel12 TyrKO	HCmel12 Tyr$^{-/-}$	Murine cutaneous melanoma, C57BL/6 background	HGF-Cdk4^{R24C} mouse model for melanoma	Thomas Tüting, Jennifer Landsberg, Michael Hölzel, Daniel Hinze
GL261 gp100		Murine glioma, C57BL/6 background	n.a.	Michael Platten

E0771	Murine mamma carcinoma, C57BL/6 background	n.a.	Cyrus M. Ghajar

2.1.2 Vectors

Table 3: List of retroviral vectors

Name of Vector	Description	Company	Reference number	RRID
LeGO-T2 vector	Cytoplasmic tdTomato expression	Addgene	27324	Addgene_27342
plKO.1-puro-CMV-TurboGFP_shnon-target	cytoplasmatic GFP expression	Sigma-Aldrich	SHC016	Addgene_109012

2.1.3 Antibodies

Table 4: List of antibodies used fluorescence activated cell sorting (FACS) staining panels 1-4

Antibody	Clone	Company	Reference number	Lot	RRID	Dilution used
Antibodies FACS Panel 1						
CD279(PD-1), PE	J43	eBioscience	12-9985-83	E0231-1634	AB_466296	1:100
CD3, PE/Cyanine7	17A2	BioLegend	100220	B185661	AB_1732057	1:100
CD8a, PerCP-Cyanine5.5	53-6.7	eBioscience	45-0081-82	2151510	AB_1107004	1:100
CD4, Pacific Blue	RM4-5	BioLegend	100531	B255834	AB_493374	1:100
CD44, Brilliant Violet 510	IM7	BioLegend	103043	B227210	AB_2650923	1:100
CD69, APC	H1.2F3	eBioscience	17-0691-82	2065643	AB_1210795	1:100
anti-CD16/anti-CD32		eBioscience	14-0161-85		AB_467134	1:100
Antibodies FACS Panel 2						
CD4, FITC	GK1.5	eBioscience	11-0041-85	1987705	AB_464893	1:100
CD366 (Tim-3), Brilliant Violet 421	RMT3-23	BioLegend	119723	B318424	AB_2616908	1:100
CD8a, Brilliant Violet 510	53-6.7	BioLegend	100752	B337862	AB_2563057	1:100

CD223 (LAG-3), PE-Cyanine7	C9B7W	eBioscience	25-2231-82	4284448	AB_2573428	1:100
CD3e, PerCP-Cyanine5.5	17A1	BioLegend	100218	B326440	AB_1595492	1:100
CD62L, APC	MEL-14	BioLegend	104412	B223862	AB_313099	1:100
CD152 (CTLA-4), PE	UC10-4B9	eBioscience	12-1522-82	4275294	AB_465879	1:100
Antibodies FACS Panel 3						
CD4, FITC	GK1.5	eBioscience	11-0041-85	1987705	AB_464893	1:100
CD8a, Brilliant Violet 510	53-6.7	BioLegend	100751	B323243	AB_2561389	1:100
CD45, PE-Cyanine7	30-F11	eBioscience	25-0451-81	2123773	AB_2716950	1:100
CD3e, eFluor 450	17A2	eBioscience	48-0032-82	4314440	AB_1272193	1:100
Antibodies FACS Panel 4						
CD45, PE-Cyanine7	30-F11	eBioscience	25-0451-81	2123773	AB_2716950	1:100
CD19, FITC	6D5	BioLegend	115506	B158637	AB_313641	1:100
Gr1 (Ly-6G/Ly-6C), eFluor450	RB6-8C5	eBioscience	48-5931-80	2241983	AB_1548797	1:100
CD45, PE-Cyanine7	30-F11	eBioscience	25-0451-81	2123773	AB_2716950	1:100
NK-1.1, APC	PK136	BioLegend	108710	B229690	AB_313397	1:100
CD11b, PerCP	M1/70	BioLegend	101230	B256661	AB_2129374	1:100

Table 5: List of *in vivo* antibodies

Antibody	Clone	Company	Reference number	Lot	RRID
Immune checkpoint antibodies for treatment					
anti-PD-1	RMP1-14	BioX Cell	BE0146	665417S1; 695318A1	AB_10949053
anti-CTLA-4	9D9	BioX Cell	BE0164	63617J2	AB_10949609
Isotype for anti-PD-1 (rat IgG2a isotype control, anti-trinitrophenol)	2A3	BioX Cell	BE0089	686318F1	AB_1107769
Isotype for anti-CTLA-4 (mouse IgG2b isotype control)	MPC-11	BioX Cell	BE0086	645417J3	AB_1107791

Antibodies for *in vivo* staining					
anti-ICAM-1, FITC	YN1/1.7.4	eBioscience	11-0541-82	2083928; 2238585	AB_465094
Rat IgG2b kappa Isotype Control, FITC	eB149/10 H5	eBioscience	11-4031-82	1995330, 2122634	AB_470004
Antibodies for *in vivo* functional ICAM-1 blocking					
CD54 (ICAM-1) monoclonal antibody, functional grade	YN1/1.7.4	eBioscience	16-0541-85	2362876, 2452206	AB_468980
Rat IgG2b kappa isotype	eB149/10 H5	eBioscience	16-4031-85	2345592	AB_470152

Table 6: List of antibodies used for immunofluorescence staining on cryo-sections

Antibody	Clone	Company	Reference number	Lot	RRID	Dilution used
Goat anti m/r CD31	Polyclonal IgG	R&D Systems	AF3628	YZU0119021	AB_2161028	1:200
Rat anti-ICAM-1	YN1/1.7.4	eBioscience	14054182	2177738	AB_467301	1:25
AF488 Donkey Anti-Goat	Polyclonal IgG	Invitrogen	A11055	2211210	AB_2534102	1:400
DyLight650 Donkey anti-Rat	Polyclonal IgG	Invitrogen	SA5-10029	VH3056141	AB_2556609	1:400
High Endothelial Venule Marker Monoclonal Antibody (MECA-79), AF488	MECA-79	eBioscience	53-6036-82	2416125	AB_10804391	1:25
Rat IgM Isotype Control (eBRM), AF 488	eBRM	eBioscience	53-4341-80	2332012	AB_493964	1:25
AF633 Donkey anti-goat IgG (H+L)	Polyclonal IgG	Invitrogen	A21082	2309146	AB_2535739	1:400

Table 7: List of antibodies used for immuno-blotting

Antibody	Clone	Company	Reference number	Lot	RRID	Dilution used
anti-gp100	EP4863(2)	Abcam	ab137078	GR304976-9	AB_2732921	1:1000
anti-rabbit IgG HRP	Polyclonal	Novus Biologicals	NB7160	P39	AB_10124655	1:5000
mouse anti-β-actin IgG1	C4	Santa Cruz Biotechnology	sc-47778		AB_2714189	1:1000
anti-mouse IgG1 HRP	Polyclonal	Bethyl Laboratories	A90-205P	A90-205P-3	AB_10634122	1:5000

2.1.4 Reagents

Table 8: List of chemical reagents

Reagent name	Company	Reference number
2-mercaptoethanol	Gibco (Thermo Fisher Scientific)	21985023
4',6-Diamidino-2-phenyl-indol -dihydrochlorid (DAPI)	Sigma-Aldrich (Merck KGaA)	D8417
Accutase solution	Sigma-Aldrich	A6964
ACK lysing buffer	Gibco (Thermo Fisher Scientific)	A104920
Albumin Fraktion V (BSA)	Carl Roth	0163.4
Bepanthen eye cream	Bayer	
Carprofen (Rimadyl 50 mg/ml)	Zoetis	1706155
CellTracker™ Green CMFDA Dye	Thermo Fisher Scientific	C2925
Dexamethason (Fortecortin inject 8mg)	Merck	0415014172 9394
Dulbecco's phosphate-buffered saline (DPBS)	Capricorn Scientific	PBS-1A
Enhanced chemiluminescence (ECL) solution	Amersham, GE Healthcare	RPN2232
Ethylenediaminetetraacetic acid (EDTA)	Sigma Aldrich	E9884
FACS flow	BD Bioscience	18049644
Fixable viability Dye, eFluor780	eBioscience	65-0865-18
Fluoresceinisothiocyanat-Dextran (FITC-Dextran)	Sigma-Aldrich	FD2000S
Fluorescence Mounting Medium DAKO	Agilent	S302380-2
hgp10025-33 peptide	GenScript	RP20344
Human serum AB	Sigma-Aldrich	H4522
Interleukin-2 (IL-2)	Proleukin, Novartis	
Isofluran CP	CP-Pharma	1214

Ketamin (Ketabel 100 mg/ml)	Bela-Pharm	FS1670041
Lämmli buffer	Sigma-Aldrich	S3401
Matrigel	Corning	354234
Milk powder	Carl Roth	T145.2
Moxifloxacin	Stada Pharma	10353917
OneComp eBeads	Invitrogen	01-1111-42
Sodium dodecyl sulfate (SDS)	Sigma-Aldrich	A1112
Sodium chloride (0.9%)	Braun	2350748
Tetramethylrhodaminisothiocyanat-Dextran (TRITC-Dextran)	Sigma-Aldrich	52194
Tissue-Tek O.C.T. Compound	Sakura Finetek Europe B.V.	4583
Tris hydrochloride	Carl Roth	9090.3
Trypan blue	Gibco (Thermo Fisher Scientific)	15250061
Trypsin-EDTA (0.05%)	Gibco (Thermo Fisher Scientific)	25300054
Vectashield Hard set mounting medium	Vector Laboratories	VEC.H.1400
Xylazin (Rompun 2%)	Bayer	(01)04007221031017

2.1.5 Cell culture media and buffers

Table 9: List and composition of cell culture media

Name	Ingredient	Reagent Manufacturer	Catalogue number
RPMI standard growth medium	Roswell Park Memorial Institute 1640 Medium (RPMI-1640)	PAN Biotech	P05-18500
	+10% fetal bovine serum (FBS)	Gibco (Thermo Fisher Scientific)	105000-064
	+100 U/ml penicillin	Sigma-Aldrich	P4333
	+0.1 mg/ml streptomycin	Sigma-Aldrich	P4333
	+2 mM L-glutamine	Gibco (Thermo Fisher Scientific)	25030081
DMEM standard growth medium	Dulbecco's Modified Eagle Medium (DMEM) high glucose	Sigma-Aldrich	D6429
	+10% FBS	Gibco (Thermo Fisher Scientific)	105000-064
	+100 U/ml penicillin	Sigma-Aldrich	P4333
	+0.1 mg/ml streptomycin	Sigma-Aldrich	P4333

Ret cell growth medium	DMEM high glucose	Sigma-Aldrich	D6429
	+ 10% FBS	Gibco (Thermo Fisher Scientific)	105000-064
	+100 U/ml penicillin	Sigma-Aldrich	P4333
	+0.1 mg/ml streptomycin	Sigma-Aldrich	P4333
	+ 5 x 10^{-6} M β-mercaptoethanol	Sigma-Aldrich	M6250
	+ 0.1 mM MEM Non-essential amino acids (NEAA)	Sigma-Aldrich	M7145
T cell proliferation medium	RPMI-1640	PAN Biotech	P05-18500
	2 mM L-glutamine	Gibco (Thermo Fisher Scientific)	25030081
	+ 10% FBS	Gibco (Thermo Fisher Scientific)	105000-064
	+ 100 U/ml penicillin	Sigma-Aldrich	P4333
	+ 0.1 mg/ml streptomycin	Sigma-Aldrich	P4333
	+ 25 mM HEPES pH 7.0-7.6	Sigma-Aldrich	H0887
	+ 1 mM sodium pyruvate	Sigma-Aldrich	S8636
	+ 0.1 mM NEAA	Sigma-Aldrich	M7145
	+ 5 x 10^{-5} M β-mercaptoethanol	Sigma-Aldrich	M6250
Standard freezing medium	DMEM high glucose	Sigma-Aldrich	D6429
	+ 20% FBS	Gibco (Thermo Fisher Scientific)	105000-064
	+ 10% DMSO	Carl Roth	7029.1

Table 10: List and composition of buffers

Buffer	Ingredient	Manufacturer	Catalogue number
FACS buffer	1X PBS	Capricorn Scientific	PBS-1A
	3% FBS	Gibco (Thermo Fisher Scientific)	105000-064
	2 mM EDTA	Sigma-Aldrich	E9884
MACS buffer	1X PBS	Capricorn Scientific	PBS-1A
	3% FBS	Gibco (Thermo Fisher Scientific)	105000-064
	10 mM EDTA	Sigma-Aldrich	E9884
Immunofluorescence blocking buffer	1X PBS	Capricorn Scientific	PBS-1A
	+ 0.3% Triton X-100	Sigma-Aldrich	T8787
	+ 3% BSA	Carl Roth	0163.4

TRIS buffered saline - Tween-20 (TBS-T)	1M Tris-buffered saline (TBS)	AppliChem	A1379
	+ 0.05% Tween-20	Gerbu Biotechnik	2001
PBS-T	1X PBS	Capricorn Scientific	PBS-1A
	+ 0.3% Triton X-100	Sigma-Aldrich	T8787
ris/glycine/SDS running buffer		Bio-Rad Laboratories	1610732
Protein lysis buffer	1M TRIS/HCl	Carl Roth	9090.3
	5 M NaCl	Carl Roth	HN00.2
	1% NP-40	Thermo Fisher Scientific	85124
	250 mM EDTA	Sigma-Aldrich	E9884
	10% Glycerin	Carl Roth	4043.1
	0.2 M DTT	Carl Roth	6908
	2% Complete	Roche	4693132001
	0.7% PMSF Protease Inhibitor	Thermo Fisher Scientific	36978
	1% Phosphatase inhibitor cocktail 2	Sigma-Aldrich	P5726
	1% Phosphataseinhibtor cocktail 3	Sigma-Aldrich	P0044

2.1.6 Kits

Table 11: List of kits

Kit	Manufacturer	Catalogue number
CD8a T cell isolation Kit mouse	Milteny	130-104-075
Cytofix/Cytoperm™ Fixation/Permeabilization kit	BD Biosciences	554714
Pierce ™ BCA Protein Assay Kit	Thermo Fisher Scientific	23225
ArC Amin-reactive Compensation Bead kit	Invitrogen (Thermo Fisher Scientific)	A10346

2.1.7 Primers for genotyping

Table 12: List of primers for genotyping of transgenic mouse lines

All Primers were purchased from Eurofins Genomics.

Primer name	Sequence 5' -3'
LCK-Cre_Tg_ fwd	TGT GAA CTT GGT GCT TGA GG
LCK-Cre_Tg_ rev	CAG GTT CTT GCG AAC CTC AT
LCK-Cre_wt _ fwd	CTA GGC CAC AGA ATT GAA AGA TCT
LCK-Cre_wt_ rev	GTA GGT GGA AAT TCT AGC ATC ATC C
tdTomato mut fwd	CTG TTC CTG TAC GGC ATGG
tdTomato mut rev	GGC ATT AAA GCA GCG TAT CC
tdTomato wt fwd	CCG AAA ATC TGT GGG AAG TC
tdtomato wt rev	AAG GGA GCT GCA GTG GAG TA
Ch2Pmel_Fwd_35	CTT TAG ACC TCC GGC ACT GTT GC
Ch2Pmel_Rev_36	GCA AGT AGC AGT GTA TCA AAT ATG C
Pmel1TCR_Rev_37	GTA GCT TTG TAA GGC TGT GGA GAG

2.1.8 Devices

Table 13: List of devices and associated equipment

Device	Equipped with	Company	comment
ZEISS LSM 7 MP		Carl Zeiss Microscopy	Used for two-photon microscopy
	Chameleon Ultra II laser	Coherent	
	Discovery NX laser	Coherent	
	20x/1.0 W-Plan-Apochromat objective	Carl Zeiss Microscopy	
ZEISS LSM 980 with airyscan2		Carl Zeiss Microscopy	Used for two-photon microscopy
	Discovery NX laser	Coherent	
	20x/1.0 W-Plan-Apochromat objective	Carl Zeiss Microscopy	
Cryo-microtome Leica CM3050 S		Leica	Used for cryo-sectioning
Cryo-microtome Leica CM1950		Leica	Used for cryo-sectioning
Trans-Blot® TurboTM Transfer System		Bio-Rad Laboratories	Used for blotting

ChemiDoc MP imaging system		Bio-Rad Laboratories	Used for imaging of immunoblots and genotyping gels
LSM780 Spinning Disk Microscope		Carl Zeiss Microscopy	Used for imaging of immunofluorescence ICAM-1 stainings
	EMCCD camera QImaging Rolera EM-C2	QImaging	
	63x / 1.4 Oil Plan-Apochromat	Carl Zeiss Microscopy	
Zeiss Axio Scan.Z1		Carl Zeiss Microscopy	Used for imaging of immunofluorescence MECA-79 stainings
	20× / 0.8 Plan-APOCHROMAT, air	Carl Zeiss Microscopy	
BD FACS Canto II, 8-color		BD Biosciences	Flow cytometer
Stereotact with Injector No 53311		Stoelting	Used for intracortical injections
Stereomicroscope Nikon SMZ800		Nikon	Used for surgical procedures
	KL2500 LCD lamp	Schott	
	Nikon Intensilight C-HGFI fluorescence lamp	Nikon	
Electric drill (HP4-917 Brush Type Control Unit)		Foredom	Used for cranial window operation

2.1.9 Software

Table 14: List of software

Software	Version	Company
ZenBlack	Version 2.3	Carl Zeiss Microscopy
ZenBlue	Version 3.5	Carl Zeiss Microscopy
Imaris	Version 7.5.2	Bitplane
Fiji	Image J 1.53c	Public domain
Ilastik	Version 1.3.3post3	Open source
Arivis Vision 4D	Version 3.3	arivis AG
Flow Jo	Version 10	BD Biosciences
Graph Pad Prism	Version 9.4.0	GraphPad Software

Adobe Premiere Pro	Version 15.41	Adobe

2.2 Methods

2.2.1 Animal procedures

Male C57BL/6J mice and male LCK-Cre x LSL-tdTomato mice (>8 weeks of age, >20 g body weight) were used as chronic cranial window and tumor bearing mice. For adoptive T cell transfer experiments, homozygous premelanosome protein 1 (pmel-1) mice were used as T cell donors. All animal procedures were approved by the local governmental authorities (Regierungspräsidium Karlsruhe, Germany) and were conducted according to their standards.

2.2.1.1 Chronic cranial window implantation

For implantation of a chronic cranial window LCK-Cre x LSL-tdTomato mice and C57BL/6J mice (>8 weeks of age, >20g body weight) underwent surgical procedure. Under ketamine (150 mg/kg body weight) and xylazine (10 mg/kg body weight) intraperitoneal (i.p.) injected narcosis, the mouse head was fixated in a customized holder and skin was removed from the top of the head in the region between the eyes and ears. By using a drill, a round piece of skull of 6 mm diameter was carefully removed. With fine scissors and forceps, the underlying arachnoidea mater and dura mater were removed without damaging blood vessels on the brain surface. A round 6 mm cover slip glass was placed on the brain surface and was fixated and sealed to the skull bone with surgical glue. A titan ring was glued onto the skull bone around the window, to ensure painless head fixation during imaging. Mice recovered for a minimum of 2-3 weeks to ensure equal experimental settings without inflammation from the surgical procedure, before further experimental procedures were performed.

2.2.1.2 Flank tumor inoculation

Mice were anesthetized using isoflurane (maximum 5% in 0.5 l/min O_2 for induction, then <2% in 0.5 l/min O_2). The flank was shaved and disinfected followed by injection of 100 µl 1:1 mixture of 150,000 murine melanoma cells in PBS with Matrigel (Corning) was injected subcutaneously (s.c.) using a 27G needle. The flank tumor size was monitored regularly every 2-4 days following injection by measuring the long tumor diameter *D* and the short tumor diameter *d* using a caliper. The tumor volume *V* was calculated by following formula: $V=(D\times d^2)/2$.

2.2.1.3 Cortical tumor injection

For cortical tumor injection (TI) mice were anesthetized with ketamine/xylazine mix (ketamine 100 mg/kg bodyweight, xylazine 10 mg/kg bodyweight, i.p.) for careful removal of the window cover glass. Fluorescently labeled murine melanoma cells were detached from the cell culture plate using accutase, and subsequently washed three times with PBS. 30,000-100,000 melanoma cells suspended in PBS were stereotactically injected into the mouse cortex at a depth of approximately 500 µm using a 10 µl Hamilton syringe. After flushing away excess melanoma cells from the brain surface with PBS using a 10 ml syringe, a new 6 mm cover glass was used to reseal the window using surgical glue.

2.2.1.4 Adoptive cell transfer (ACT) of pmel-1 T cells

Pmel-1 homozygous donor mice were sacrificed on day 5 post cortical tumor injection of acceptor mice. Spleen, inguinal, axial, mesenteric, and cervical lymph nodes were isolated. Single cell suspensions were generated by meshing organs through a 70 µm cell strainer, and next, the cells were washed with PBS. Erythrocytes were lysed by incubating in ammonium-chloride-potassium (ACK) lysing buffer for 90 s on ice with subsequent washing with PBS. For *ex vivo* stimulation of isolated T cells (X.-W. Zhang et al., 2021), the cells were cultured *in vitro* for three days at 37 °C, 5% CO_2 in T cell proliferation medium (see Table 9) and were stimulated with 2 µg/ml human glycoprotein 100 peptide 25-33 ($hgp100_{25-33}$), and 30 U/ml IL-2. *In vitro* activated lymphocytes were harvested on day 8 post cortical tumor injection of acceptor mice and were enriched by using a CD8a+ T cell Isolation kit according to the manufacturer's instructions. CD8+ T cells were fluorescently labeled with 1 µM-2.5 µM CellTracker™ Green 5-chloromethylfluorescein diacetate (CMFDA) dye and 5 x 10^6 T cells in 100 µl PBS were injected intravenously (i.v.) in the lateral tail vein of tumor-bearing acceptor mice using a 1 ml syringe with 30G needle.

2.2.1.5 *In vivo* two-photon laser scanning microscopy (IVM)

For intravital microscopy of fluorescent cells and structures in the murine brain, mice with a chronic cranial window were anaesthetized using maximum 5% Isoflurane in 0.5 l/min O_2 for narcosis initiation and were transferred to a custom-made holder which enables painless fixation of the ring around the window. Anesthesia was continued with <2% isoflurane in 0.5 l/min O_2 through a nose mask for imaging using a Zeiss LSM 7MP equipped with a Chameleon Ultra II or a Discovery NX laser and a 20x/1.0 W-Plan-Apochromat objective. To visualize vasculature *in vivo*, 100 µl 5 mg/ml of tetramethylrhodamine-isothiocyanate-dextran (TRITC-Dextran) or 100 µl 5 mg/ml of fluorescein Isothiocyanate-dextran (FITC-Dextran) was injected into the lateral tail vein i.v. prior to imaging. For visualization of GFP, CMFDA and tdTomato an excitation wavelength of 950 nm or 1040 nm was used,

for FITC 750 nm and for TRITC-Dextran 850 nm was used and fluorescent emission was detected using BP500-550 nm /BP575-610 nm optical filters (Carl Zeiss Microscopy). For image acquisition, lowest adequate laser power and a gains ranging from 600 to 800 was used. Depending on the experiment, z steps between 3-10 µm were used.

Mice were imaged regularly between day 5 and day 14 post cortical TI if they had received ACT, or between day 1 and day 14 post cortical TI for LCK-Cre x LSL-tdTomato mice.

2.2.1.6 Immune checkpoint treatment

Mice were treated with immune checkpoint inhibitors or with respective isotype (Iso) control antibodies. For ICI treatment, 250 µg anti-PD-1, 100 µg anti-CTLA-4 or isotype control antibodies (rat IgG2a isotype control, mouse IgG2b isotype control) in the respective doses in 200 µl 0.9% NaCl were injected i.p. every two days starting from day 7 post cortical TI until the end of the experiment.

2.2.1.7 *In vivo* antibody staining

Intravascular ICAM-1 expression was visualized in blood vessels of the brain of cranial window bearing mice by i.v. injection of 100 µg FITC coupled anti-ICAM-1 in the lateral tail vein on day 10 post cortical TI. As a control, a FITC-conjugated isotype control antibody was used. Intravital microscopy was performed 1-3 h following injection.

2.2.1.8 *In vivo* functional ICAM-1 blocking

For *in vivo* blocking of intravascular ICAM-1, window and tumor bearing LCK-Cre x LSL-tdTomato mice were injected with 100 µg functional grade anti-ICAM-1 antibody or the respective isotype control antibody in a volume of 100 µl i.v. in the lateral tail vein starting from day 3 post cortical TI every three days. Brain tumor growth and T cell infiltration were measured regularly by IVM.

2.2.2 Cell cultivation

The murine melanoma cell line Ret (a kind gift from V. Umansky, Mannheim, Germany) was cultured under standard cell culture conditions (37°C, 5% CO_2) in Ret cell growth medium (see Table 9). Ret CM Tyrosinase knock out (TyrKO) (also known as CM TyrKO #43, a kind gift from I. Helfrich, and D. Schadendorf, Essen, Germany and M. Hölzel, D. Hinze, Bonn, Germany), and HCmel12, and HCmel12 TyrKO (kind gifts from J. Landsberg, and T. Tüting, M. Hölzel, D. Hinze, Bonn, Germany) were cultured under standard cell culture conditions in standard RPMI growth medium (see Table 9).

To increase brain tropism of the cell lines upon transplantation (Manuel Valiente et al., 2020), Ret CM TyrKO cells were *in vivo* brain passaged four times, before using them for *in vivo* experiments.

Gl261 gp100-over expressing cells (a kind gift from M. Platten, Heidelberg, Germany) and E0771 cells (a kind gift from Cyrus M. Ghajar) were cultured under standard cell culture conditions in DMEM standard growth medium (see Table 9).

If tumor cell lines were not kept in culture, they were stored as frozen vials in liquid nitrogen. For cell freezing, cells were harvested from cell culture flasks by trypsinization and resuspension in fresh cell culture medium. Cells were then centrifuged and the cell pellet was resuspended in a density between 10^6 and 10^7 cells/ml in standard freezing medium (see Table 9). 1 ml of cell suspension was transferred into one freezing vial, and vials were frozen in Cell Cool LX boxes (Corning) first at -80°C, then vials were transferred to liquid nitrogen storage.

Regular tests for mycoplasma contamination were performed in-house on all cell lines.

2.2.3 Transduction

The HCmel12 TyrKO cell line and the Ret CM TyrKO cell line were transduced with the retroviral pLKO.1-puro-CMV-TurboGFP_shnon-target-vector (custom made, Sigma Aldrich). Virus was produced from plasmids using HEK cells. A day before the transduction 400,000 tumor cells were seeded per well into a 6-well plate in the respective medium and were cultured under standard conditions overnight. On the day of the transduction, the medium was exchanged with 2 ml of medium containing polybrene (1:1000 diluted) and cells were incubated for 30 min at 37°C and 5% CO_2. Then, 10 µl of concentrated virus particles were added to the pre-incubated cells and cells were cultured under standard conditions. After 24 h, the medium was changed to normal culture medium and cells were expanded for fluorescence activated cell sorting. To generate red fluorescent HCmel12 TyrKO cells, the cells were transduced with retroviral LeGO-T2 vector mediating tdTomato (tdTom) expression as described above. Virus production and transduction were performed under biosafety level 2. Transduced cells were cultivated under biosafety level 2 for at least three passages (including at least three washing steps with PBS) before they were transferred to cultivation under biosafety level 1, where they were cultivated and used for all following experiments.

2.2.4 Fluorescence activated cell sorting (FACS) for enrichment of fluorescently transduced cells

To generate homogenously fluorescent cell lines, several rounds of fluorescence activated cell sorting on GFP or tdTomato were performed with the help of the DKFZ flow cytometry core facility. For this, cells were trypsinized and washed with PBS. Cells were resuspended in FACS buffer for sorting. GFP or tdTomato positive cells were then sorted according to an internal or untransduced negative control

using a BD FACS Aria I or BD FACS Aria II device (both from BD Biosciences) with 100 µm-nozzles into cell culture medium containing 50% FBS. After the sorting, cells were centrifuged once and were resuspended in standard cell culture medium and were cultivated under standard conditions for expansion until further use.

2.2.5 Immuno-blotting

To analyze the expression of melanoma antigen glycoprotein 100 (gp100) in murine melanoma cell lines, cells were harvested by trypsinization and subsequent centrifugation and washing with PBS. Cell pellets were lysed with protein lysis buffer and were diluted 1:4 with Lämmli-Buffer. A Bradford assay was performed to determine the protein concentration of each sample by using the Pierce ™ BCA Protein Assay Kit according to the user manual. 50 µg protein was loaded per well on a 10% acrylamide gel containing sodium dodecyl sulfate (SDS). Proteins were separated by SDS-PAGE at 120 V in 1x Tris/glycine/SDS running buffer using a Mini-PROTEAN® Tetra Cell system (Bio-Rad Laboratories). Semi-dry blotting was used to transfer proteins from the gel to a nitrocellulose membrane using a Trans-Blot® Turbo™ Transfer System. After blotting, the membrane was blocked with 5% powdered milk in Tris-buffered saline-Tween 20 (TBS-T) for 45 min at room temperature. For specific staining of the target protein, the membrane was incubated with primary antibody diluted in 5% milk at 4°C overnight, subsequently it was washed three times with TBS-T and incubated with horseradish peroxidase (HRP) coupled secondary antibody diluted in 5% powdered milk for 45 min at room temperature. The HRP signal was visualized by a ChemiDoc MP imaging system (BioRad Laboratories) upon developing with ECL Substrate according to the manufacturer's instructions.

When required, antibodies were removed from the membrane by incubating with stripping buffer heated to 50°C for 30 min and after washing with TBS-T, the membrane was incubated with a primary antibody diluted in 5% powdered milk directed against a protein used for loading control at 4°C overnight. After subsequent washing with TBS-T the membrane was incubated with the respective HRP coupled secondary antibody diluted in 5% powdered milk at room temperature for 45 min. Images were acquired using ECL substrate and on the ChemiDoc MP imaging system as described above.

2.2.6 Flow Cytometry for analysis of surface markers

For flow cytometric analysis of murine immune cells, lymphocytes were isolated from spleen and lymph nodes (inguinal, axial, cervical, and mesenteric) of Pmel-1 mice or LCK-Cre x LSL-tdTomato mice. Mice were sacrificed by cervical dislocation; organs were isolated and meshed through a 70 µm cell strainer. After washing with PBS, erythrocytes were lysed by incubating with ACK lysing buffer on ice for 90 s and the cell suspension was subsequently washed with PBS. The leukocytes were either directly

used for antibody staining or T cells were stimulated *in vitro* by cultivating in medium containing $hgp100_{25-33}$ peptide and IL-2 with subsequent CD8+ T cell enrichment as described above (see 2.2.1.4 Adoptive cell transfer (ACT) of pmel-1 T cells).

For surface marker staining, the harvested leukocytes were washed with PBS, and blocked with anti-CD16/anti-CD32 (diluted 1:100) for 20 min on ice. Then, the cells were incubated with antibodies directed against surface markers for 45 min on ice. Upon washing three times with PBS, the cell staining was analyzed using a BD FACS Canto II equipped with UV (405 nm), blue (488 nm), and red laser (633 nm), while ArC Amin-reactive Compensation Bead kit and OneComp eBeads were used for compensation of spectral overlap. Data analysis was performed using FlowJo software.

2.2.7 Immunofluorescence of mouse tissue sections

Tumor bearing C57BL/6 mice were sacrificed by cardiac perfusion with first PBS and then 4.5% PFA under deep ketamine/xylazine narcosis. The brains were isolated, incubated in 4.5% PFA at room temperature for 4h and in 30% sucrose in PBS overnight at 4°C. Then, brains were embedded in TissueTek Freezing medium and were frozen in cryo-mold chambers. As control tissue lymph nodes and spleens of untreated LCK-Cre x LSL-tdTomato mice or of ICI treated C57BL/6 mice were isolated and processed in the same way as brains, and 10 µm thick sections were cut. Coronal brain sections of 10 µm thickness were cut and were transferred on microscopy slides. Before staining, sections were air dried at room temperature for 20-30 min in the dark. The tissue was encircled with wax pen before blocking with 3% BSA in 0.3% Triton X-100 in PBS at room temperature for 1h, and subsequent incubation with primary antibody diluted in blocking solution at 4°C overnight in a humid chamber. After incubation the slides were washed three times with 0.3% Triton X-100 in PBS (PBS-T), then the tissue was incubated with fluorescently labeled secondary antibody diluted in blocking buffer for 1 h at room temperature and with 1 µg/ml DAPI diluted in blocking buffer for 5 min at room temperature. After washing three times with PBS-T, a cover slip was mounted using Vectashield mounting medium or DAKO fluorescent mounting medium (Agilent). Microscopy images of ICAM-1 stainings were acquired using a Zeiss LSM780 spinning disk microscope equipped with a 63x oil-immersion objective (1.4 Oil Plan-Apochromat). Unspecific background was subtracted from images by rolling ball background subtraction using Fiji (ImageJ) (Schindelin et al., 2012). Microscopy images of MECA-79 staining were acquired using a Zeiss Axio Scan.Z1 equipped with a 20× / 0.8 Plan-Apochromat air objective.

2.2.8 Image processing and quantification

2.2.8.1 Pre-processing of all IVM images

Tilescan images acquired by Zeiss LSM 7 MP were stitched using ZenBlack. All image processing was always performed on the entire image. Channel subtraction was performed on two-photon microscopy images using ZenBlack or Fiji to remove channel overlap. Images were smoothed using a Gaussian Filter in Imaris (Bitplane) or Fiji.

2.2.8.2 Quantification of T cell density and intracranial tumor volumes in the ACT model

Tumor volume was measured from three-dimensional two-photon microscopy images by intensity thresholding in Fiji, transferred T cells were quantified from these data sets by manually counting in Fiji.

Microregional tumor growth and T cell density were assessed by following the same microregions over time from day 9 to day 12 post cortical TI, as they could be determined by the blood vasculature. The tumor volume and T cell density was quantified in regions of interest of defined cuboid volumes of 200.45 µm x 200.45 µm x 100 µm as described above.

2.2.8.3 T cell tracking for quantification of motility parameters

T cell tracking in four dimensional two-photon timeseries images of the ACT model was performed in a semi-automated way using Imaris (Bitplane). Spot detection and tracking was performed automatically as a first step. Secondly, all T cell tracks were proof-read and corrected manually if necessary. Semi-automated T cell tracking was jointly performed by me and by Manuel Piechutta (Clinical Cooperation Unit Neurooncology, German Cancer Consortium (DKTK), German Cancer Research Center (DKFZ); Heidelberg, Germany). Transferred T cells with mean velocity ≥ 50 nm/s and mean displacement ≥ 10 nm/s were defined as “motile” and T cells with a mean velocity < 50 nm/s and mean displacement < 10 nm/s as “stationary”, as these cells remained within a distance of approximately one cell length during a typical timeseries duration of 25 min. The mean velocity threshold of 50 nm/s was included into this definition to exclude those T cells from the category “stationary”, that travelled further from their track origin and returned to their origin.

To annotate and cut videos from IVM timeseries data after pre-processing with Fiji, Zen Black, Imaris, and Adobe Premiere Pro was used.

Table 15: Total numbers of all T cells analyzed for Figure 22B, D of HCmel12 TyrKO intracranial melanoma

Day	Treatment	Number of motile T cells	Number of stationary T cells	Number of mice analyzed
D9	ICI	417	161	4
	Iso	73	87	4
D10	ICI	1586	406	4
	Iso	181	113	4
D12	ICI	1471	194	3
	Iso	183	91	3

Table 16: Total numbers of all T cells analyzed for Figure 22C of Ret CM TyrKO intracranial melanoma

Day	Treatment	Number of motile T cells	Number of stationary T cells	Number of mice analyzed
D9	ICI	98	59	6
	Iso	27	40	6
D10	ICI	408	182	6
	Iso	59	32	6
D12	ICI	112	13	4
	Iso	20	14	4

Table 17: Total numbers of all T cells analyzed for Figure 22E, F of HCmel12 TyrKO intracranial melanoma

Day	Treatment	Number of motile T cells	Number of stationary T cells	Number of mice analyzed
D9	ICI	57	76	4
	Iso	52	44	4
D10	ICI	286	199	4
	Iso	57	57	4
D12	ICI	440	98	3
	Iso	131	62	3

Table 18: Total numbers of all motile T cells analyzed for Figure 23A-C of HCmel12 TyrKO intracranial melanoma

Day	Treatment	Number of motile T cells	Number of mice analyzed
D9	ICI	417	4
	Iso	73	4
D10	ICI	1586	4
	Iso	181	4
D12	ICI	1471	3
	Iso	183	3

Table 19: Total numbers of all motile T cells analyzed for Figure 23D-F of Ret CM TyrKO intracranial melanoma

Day	Treatment	Number of motile T cells	Number of mice analyzed
D9	ICI	98	6
	Iso	27	6
D10	ICI	408	6
	Iso	59	6
D12	ICI	112	4
	Iso	20	4

Table 20: Total numbers of all motile T cells of N=4 mice per treatment group analyzed for Figure 24B-D of HCmel12 TyrKO intracranial melanoma on day 10 post cortical TI

Region	Treatment	Number of motile T cells
PVV	ICI	553
peritumoral	ICI	557
Tumor edge	ICI	159
intratumoral	ICI	286
PVV	Iso	40
peritumoral	Iso	10
Tumor edge	Iso	67
intratumoral	Iso	57

2.2.8.4 Pre-processing and quantification of T cells in the LCK-Cre x LSL-tdTomato mice

For the analysis of spatiotemporal distribution of endogenous T cells at distinct vessel types in the LCK-Cre x LSL-tdTomato model, machine learning by Ilastik software (Berg et al., 2019) was used for pixel classification of vessel structures and T cells. As a second step, segmented images were further

analyzed using Arivis Vision 4D by using semi-automated 3D modeling of the vasculature and automated detection of T cells. Based on the vessel 3D modeling, a distance map was calculated, which allowed measuring distance of each T cell from the nearest blood vessel. For quantification and comparison between different groups, the volume of T cells within 15 µm proximity of the respective blood vessel was measured and normalized to the respective vessel surface area.

2.2.8.5 Quantification of *in vivo* ICAM-1 staining and *in vivo* functional ICAM-1 blocking

In vivo ICAM-1 staining as detected by IVM was analyzed by measuring peak intensities of fluorescence signal at the vessel walls using Fiji. These ICAM-1 signal intensities at vessel walls were then normalized to mean ICAM-1 signal intensities at brain surface capillaries of the respective mouse to balance out batch differences between different mice, antibody batches and potentially differences in laser power settings during image acquisition. The amount of T cells present in the perivascular space was measured as mean intensity of a binary T cell mask generated by thresholding using Fiji within 30 µm of distance from the vascular lining.

For the analysis of *in vivo* ICAM-1 functional blocking experiments, IVM images were used for machine learning based pixel classification for T cells and for tumor cells using Ilastik. The resulting probability maps were exported and by thresholding binary images were created by FIJI. By using the 3D Voxel counter Plugin in Fiji, cumulative volumes of T cells and of tumor were determined. To ensure that quantification of T cell infiltration was not biased by the size and location of the brain area that was imaged, a 200 µm margin was defined around the tumor binary image by distance map calculation. By multiplying this defined volume with the T cell binary image, and applying the 3D voxel counter plugin, on the resulting image, T cell volume of the defined volume including the tumor and its peripheral margin could be determined and to quantify T cell infiltration, the cumulative T cell volume was normalized to the defined volume including tumor and margin. In cases of complete tumor regression, a defined volume was estimated at the location and of comparable size based on an earlier timepoint, when tumor mass could be well detected.

2.2.9 Schematic illustrations

All graphical and schematic illustrations were made using Inkscape.

2.2.10 Statistics

Statistics were calculated using GraphPad Prism Version 9.1.2. All data are represented as mean ± standard error of the mean (SEM), if not indicated differently in the figure captions.

3 Results

3.1 Establishment of an *in vivo* model to study T cell infiltration into brain tumors

To study the dynamics of T cell recruitment during brain tumor growth it was crucial to establish suitable *in vivo* models of intracranial tumors. This requires a preclinical model that elicits a sufficient immune response against the brain tumor, resulting in immune cell infiltration into the brain. Both in pre-clinical models as well as in patients, melanoma tumors have a high mutational load and thus high immunogenicity as compared to other entities (Alexandrov et al., 2013). For eliciting a complete anti-tumor immune response, closely modeling the human situation, it is important that all components of the adaptive and innate immune system are present. Therefore, fully immunocompetent mice and syngeneic murine melanoma cell lines, namely HCmel12 and Ret CM were chosen for pre-clinical *in vivo* modeling of melanoma brain metastasis. Both cell lines were derived from primary cutaneous melanoma tumors from transgenic mice spontaneously developing melanoma with C57BL/6 background.

To be able to visualize the tumor by *in vivo* two-photon microscopy, T cells and tumor cells needed to express a fluorescent reporter gene. For this, the murine melanoma cell lines HCmel12 TyrKO and Ret CM TyrKO were transduced with a lentiviral vector mediating the pan-cellular expression of turboGFP (plKO.1-puro-CMV-TurboGFP_shnon-target) and transduced cells were enriched by up to 6 rounds of fluorescently activated cell sorting. Red fluorescent Ret CM TyrKO cells were generated by M. Hölzel and D. Hinze (Bonn), and to generate red fluorescent HCmel12 TyrKO cells, these cells were transduced with the lentiviral vector LeGO-T2 resulting in expression of tdTomato fluorescent protein, which were enriched by several rounds of FACS sorting.

To achieve high quality images in single cell resolution of tumor growth in the brain by intravital two-photon microscopy, it was necessary to use amelanotic tumor cells for brain tumor induction. Cell pigmentation by melanin production occurs frequently in melanoma cells, especially in murine cell lines. Melanin pigmentation affects the quality of the fluorescence image. Melanin is released to the microenvironment and oxidized melanin can emit fluorescence when exposed to light (Kayatz et al., 2001), which interferes with the intravital two-photon microscopy by causing unspecific auto-fluorescent background in the tumor and its periphery, resulting in poor image quality. As tyrosinase is a main component of the melanin synthesis pathway (Iozumi et al., 1993; Kameyama et al., 1993), genetic knock-out of the *tyrosinase* (*Tyr*) gene in murine melanoma cell lines leads to depigmentation. To ensure good image quality, Tyrosinase knock-out ("TyrKO") cell lines HCmel12 $Tyr^{-/-}$ and Ret CM $Tyr^{-/-}$, here referred to as HCmel12 TyrKO and Ret CM TyrKO respectively, were used for IVM,

which were generated using clustered regularly interspaced short palindromic repeats/CRISPR associated protein 9 (CRISPR/Cas9) technology by D. Hinze and M. Hölzel.

To study the complete brain metastatic cascade, starting with a circulating tumor cell arresting in the brain capillaries, extravasation and finally establishment of micro- and macro-metastases, intracardiac injection of a suspension of tumor cells is a commonly used method in the field of brain metastasis research (Valiente et al., 2018). One disadvantage of syngeneic tumor models for modeling brain metastases is their inability to stably generate large brain metastases upon intracardiac injection. Usually even before a large brain metastasis can develop, the humane endpoints of the mouse experiments are reached due to the extracranial tumor burden (M. Valiente et al., 2020). To enhance brain tropism of cell lines after intracardiac injection, several *in vivo* brain passages can be performed (M. Valiente et al., 2020). This involves that following intracardiac injection and successful establishment of micro- or macro-metastases, living tumor cells are isolated from the brain again, and taken back into *in vitro* cultivation. Several rounds of this procedure can be performed, thus selecting those cells that grow well in the brain increasing brain tropism of the line. The Ret CM TyrKO tdTom cell line used in this work had been *in vivo* passaged four times, the Ret CM TyrKO GFP cells had been *in vivo* passaged twice. However, despite multiple rounds of *in vivo* passaging, Ret CM TyrKO cells do not reliably form micro- or macro-metastases upon intracardiac injection.

To establish a novel syngeneic murine melanoma model to study brain metastasis upon intracardiac injection, I first attempted to passage the HCmel12 TyrKO tdTomato cells *in vivo*. To increase the likelihood for the successful formation of micrometastases and subsequent *in vivo* passaging, immunodeficient NSG mice were used for the intracardiac injection of HCmel12 TyrKO cells. Due to the depletion of a functional immune system in NSG mice, circulating cancer cells cannot be detected by immune cells in the blood or in the tissue after extravasation, and are not cleared by the immune system, so that *in vivo* passaging could enhance brain tropism without the interference of the immune system.

After injection of 500 000 murine HCmel12 TyrKO cells into the left ventricle of a cranial window-bearing NSG mouse, only four cells could be detected intravascularly at day 1 using IVM (Figure 5). Three of those cells disappeared already by day 3 from the vessels, even before extravasation. One cell could still be detected intravascularly at day 5 post injection, at a slightly different position. Supposedly, this cell had slowly moved within the brain capillaries; it was in the same region, but in a different vessel. Like the others, this cell also failed to extravasate and was flushed back into circulation at day 7 post injection. All attempts to image the metastatic cascade in these models failed, as the cells did not develop into micrometastases upon intracardiac injection. Moreover, increasing brain tropism

by *in vivo* brain passaging also failed, as no viable cells could be isolated from the brain at 14 days after heart injection.

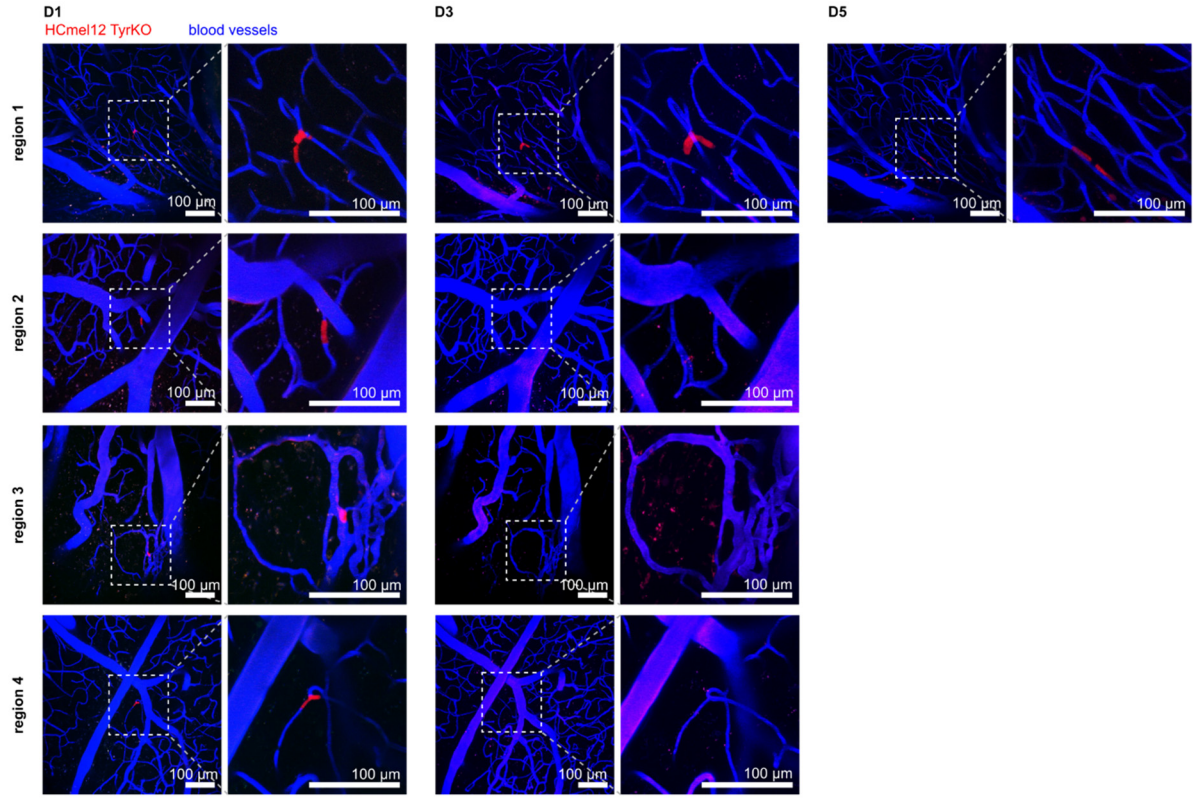

Figure 5: Intravascular HCmel12 TyrKO melanoma cells upon intracardiac injection

HCmel12 TyrKO tdTomato melanoma cells were injected intracardially into one window bearing NSG mouse. 1, 3 and 5 days post intracardiac injection, the mouse was analyzed by intravital two-photon microscopy. Blood vessels were visualized by i.v. injection of FITC- or TRITC-coupled dextran. In four different regions, single melanoma cells trapped in brain capillaries could be detected by IVM 1 day post injection, while three of these cells had disappeared on day 3 post injection, while one cell could still be seen at day 5 post injection intravascularly at a slightly different position.

3.2 Adoptive T cell transfer in cortically injected intracranial melanoma models

To ensure stable tumor growth in the brain for analyzing the immune response to well established brain tumors, an experimental approach other than intracardiac injection was needed that allows the formation of large, well-established melanoma brain tumors. For this purpose, the murine syngeneic melanoma cell lines HCmel12 TyrKO and Ret CM TyrKO were directly injected into the mouse brain cortex (intracortical injection). To visualize T cell infiltration in these melanoma brain tumors using IVM, I applied a model for adoptive T cell transfer (ACT) of *in vitro* stimulated and fluorescently stained pmel-1 CD8+ T cells (Overwijk et al., 2003). For ACT, the lymphocytes were isolated from a pmel-1 homozygous transgenic mouse. The T cells of this mouse line express a transgenic TCR directed against

the MHC class I presented peptide $gp100_{25-33}$. gp100, also known as premelanosome protein (Pmel), is an immunogenic melanocyte differentiation antigen, frequently expressed by melanocytes and melanoma cells (Overwijk et al., 1998). gp100 expression in the HCmel12 TyrKO and Ret CM TyrKO cell lines was confirmed by immunoblotting (Figure 6A). The levels of gp100 expression in HCmel12 TyrKO and Ret CM TyrKO cells were lower compared to the wildtype control cell lines HCmel12 and Ret respectively, however still clearly detectable by immunoblotting. Therefore, it was assumed that the expression was sufficient to allow for immune detection by pmel-1 CD8+ T cells.

Lymphocytes were isolated from spleen and lymph nodes of pmel-1 homozygous mice, and next, the T cells were stimulated *in vitro* with IL-2 and $hgp100_{25-33}$ peptide. Finally, enrichment of CD8+ T cells was done by untouched magnetic cell separation. *In vitro* stimulated T cells were characterized by expression of T cell activation markers CD69, CD44 and CD62L (Figure 6B, C), indicating a central memory T cell phenotype (Natalini et al., 2021). The immune checkpoint molecules PD-1 and LAG-3 were also expressed (Figure 6B, C), but not TIM-3 and CTLA-4, indicating that T cells were activated after antigen encounter, but not yet exhausted (Benichou et al., 2017; Natalini et al., 2021).

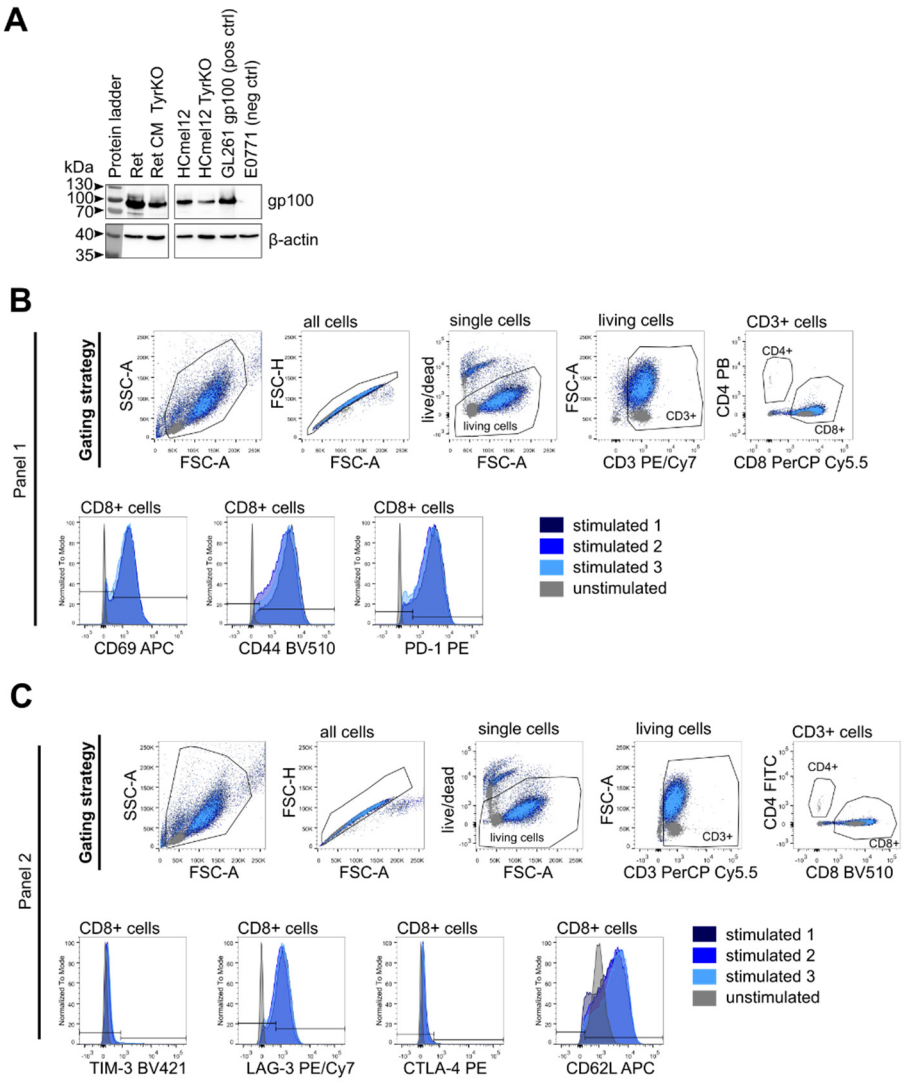

Figure 6: gp100 expression of murine melanoma cells and characterization of *in vitro* stimulated pmel-1 T cells used for ACT

(**A**) Melanoma antigen gp100 expression analysis of murine melanoma cell lines with and without TyrKO by immuno blotting of cell lysates. Lanes from left to right show: Protein ladder, Ret cells, Ret CM TyrKO, HCmel12, HCmel12 TyrKO. GL261 over-expressing gp100 glioma cells were used as a positive control, E0771 breast cancer cells were used as a negative control. Upper bands depict anti-gp100 antibody staining, lower bands depict β-actin loading controls stained for each lane.

(**B, C**) Pmel-1 T cells isolated from pmel-1 homozygous mice were characterized by flow cytometry analysis after 3 day *in vitro* stimulation with hgp100$_{25\text{-}33}$ and IL-2 (stimulated 1-3) or directly after isolation (unstimulated). Two antibody panels for T cell surface markers were used to stain CD3, CD4, CD8, CD69, CD44 and PD-1 (panel 1, B), and for CD3, CD4, CD8, TIM-3, LAG-3, CTLA-4, and CD62L (panel 2, C). Gating strategies for each antibody panel are indicated in the upper row. Histograms of each activation and immune checkpoint surface marker expression are shown as overlays in blue for stimulated T cells, and unstimulated in grey.

3.3 Intravital imaging of adoptively transferred T cell infiltration and brain tumor growth control under ICI treatment

Recent work has shown that T cell infiltration to brain tumors is enhanced by the presence of an extracranial tumor in combination with immune checkpoint inhibitor treatment with anti-PD-1/anti-CTLA-4 (Song et al., 2020; Taggart et al., 2018). Moreover, the presence of a primary tumor better mimics the clinical situation in patients. Therefore, I established an experimental procedure combining extracranial, intracranial tumor implantation with ACT and ICI treatment in window bearing mice, as schematically depicted in Figure 7A. After complete recovery of the chronic cranial window operation, I first injected a subcutaneous flank tumor of the respective melanoma cell line followed by intracortical tumor implantation two days later. On day 5 following intracortical TI, pmel-1 T cells were isolated, stimulated *in vitro* and CD8+ T cells were stained with a fluorescent dye on day 8, directly before tail vein injection into the tumor bearing acceptor mice. Starting from day 5, melanoma brain tumor growth and T cell infiltration was analyzed by IVM in regular intervals. ICI or isotype control antibody treatment was performed every two days starting from day 7 (Figure 7A).

This unique model together with the methodology of IVM allowed long-term analysis of brain tumor growth and T cell infiltration in relation to brain- and tumor microenvironment at high spatial and temporal resolution (Figure 7A, B).

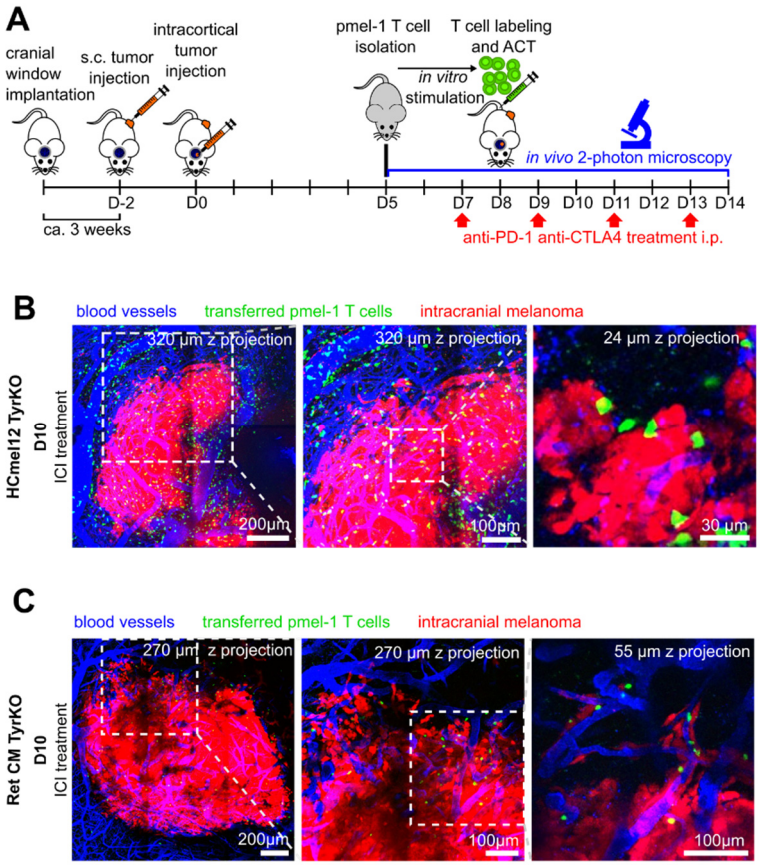

Figure 7: Establishment of an ACT *in vivo* model for IVM analysis of melanoma brain tumor growth and T cell infiltration

(**A**) Schematic representation of the experimental design for modeling intracranial melanoma growth and ACT and subsequent analysis by IVM. Minimally three weeks after chronic cranial window implantation in C57BL/6 mice, melanoma cells were injected first subcutaneously on day -2, then intracortically on day 0. Pmel-1 T cells were isolated from donor mice at day 5, and *in vitro* stimulated, fluorescently labeled CD8+ pmel-1 T cells were adoptively transferred into cranial window- and tumor-bearing acceptor mice. Treatment with ICI or isotype control antibodies was performed every 2 days starting from day 7. IVM was used to analyze tumor growth and T cell infiltration on days 5, 8, 9 ,10, 12, and 14.

(**B, C**) IVM of ICI-treated melanoma brain tumor (B, HCmel12 TyrKO and C, Ret CM TyrKO) and intracranial T cell infiltration at day 10 post cortical injection shown as maximum intensity projection (MIP). MIP depth is indicated in each panel.

IVM demonstrated inhibition of intracranial tumor growth under ICI treatment in both melanoma models (Figure 8A-D). Moreover, ICI treatment increased the number of transferred pmel-1 T cells in both models as early as one day after ACT, which became more pronounced in the subsequent three days (Figure 8E, F).

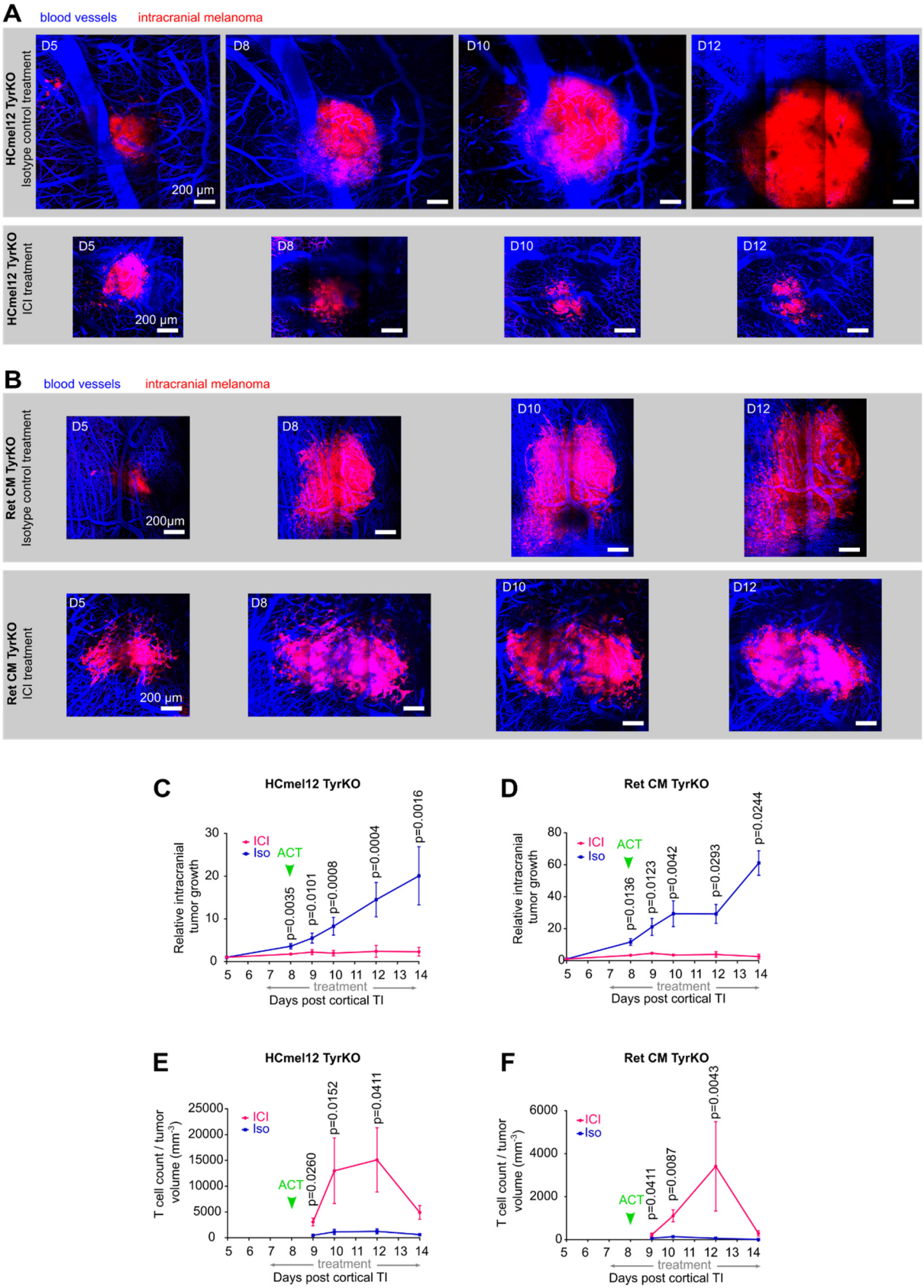

Figure 8: Combining ACT of antigen specific T cells and ICI treatment controls brain tumor growth in two melanoma models

(**A, B**) IVM of melanoma brain tumor growth of ICI or isotype control (Iso) treated HCmel12 TyrKO (A) and Ret CM TyrKO (B) with ACT between day 5 and day 12 post cortical tumor injection, shown as MIP. Scale bars, 200 µm.

(**C, D**) Quantification of relative intracranial tumor growth of HCmel12 TyrKO (C) and Ret CM TyrKO (D). Measured tumor volume was normalized to the tumor volume on day 5 post cortical tumor injection. n=6 mice per group on D5-D12; D14 n=6 mice ICI, n=5 mice Iso (C). n=6 mice per group D5-D12; n=3mice per group D14 (D), two-tailed ratio paired t-test per timepoint.

(**E, F**) Quantification of peri- and intratumoral pmel-1 T cell count of HCmel12 TyrKO (E) and Ret CM TyrKO (F) intracranial tumors normalized to brain tumor volume between day 9 and 14 post TI under ICI treatment. (E) n=6 mice per group on D5-D12; D14 n=6 mice ICI, n=5 mice Iso, two-tailed ratio paired t-test per timepoint. (F) Mann-Whitney test, n=6 mice per group D5-D12; n=3 mice per group D14.

3.4 T cell infiltration to the brain is not enhanced by the procedure of cortical injection

The procedure of intracortical injection induces trauma to the brain, which could cause inflammation and therefore local T cell infiltration, irrespective of the presence of the brain tumor. To verify if the intracranial tumor growth, rather than cortical injection itself caused T cell homing to the lesion, I performed a sham injection of PBS instead of tumor cells. The experimental procedure was performed completely analogously to the ACT model, including cranial window implantation, flank tumor implantation followed by the cortical injection, but here PBS was injected instead of tumor cells. T cell isolation and ACT of *in vitro* stimulated fluorescently labeled T cells was again performed on day 8. To ensure maximal T cell activation, both control mice with sham-injection were treated with ICI starting from day 7, and continued every other day. IVM enabled following T cell infiltration at the same timepoints of interest in tumor-bearing mice, in a large area around the injection site, but notably revealed no considerable T cell infiltration of adoptively transferred T cells to the injection site (Figure 9). Only very few T cells, mostly located close to the brain surface could be detected in both sham-injected mice. The presence of these T cells indicates that the adoptively transferred T cells were in principle able to home to the brain, and thus were not affected in that sense by the procedure of T cell enrichment and fluorescent labeling. However, since I observed much less T cells at the site of the sham-injection compared to a tumor injection, this experiment confirmed that intracortical injection itself was not sufficient to cause substantial T cell recruitment to the brain tumor lesion.

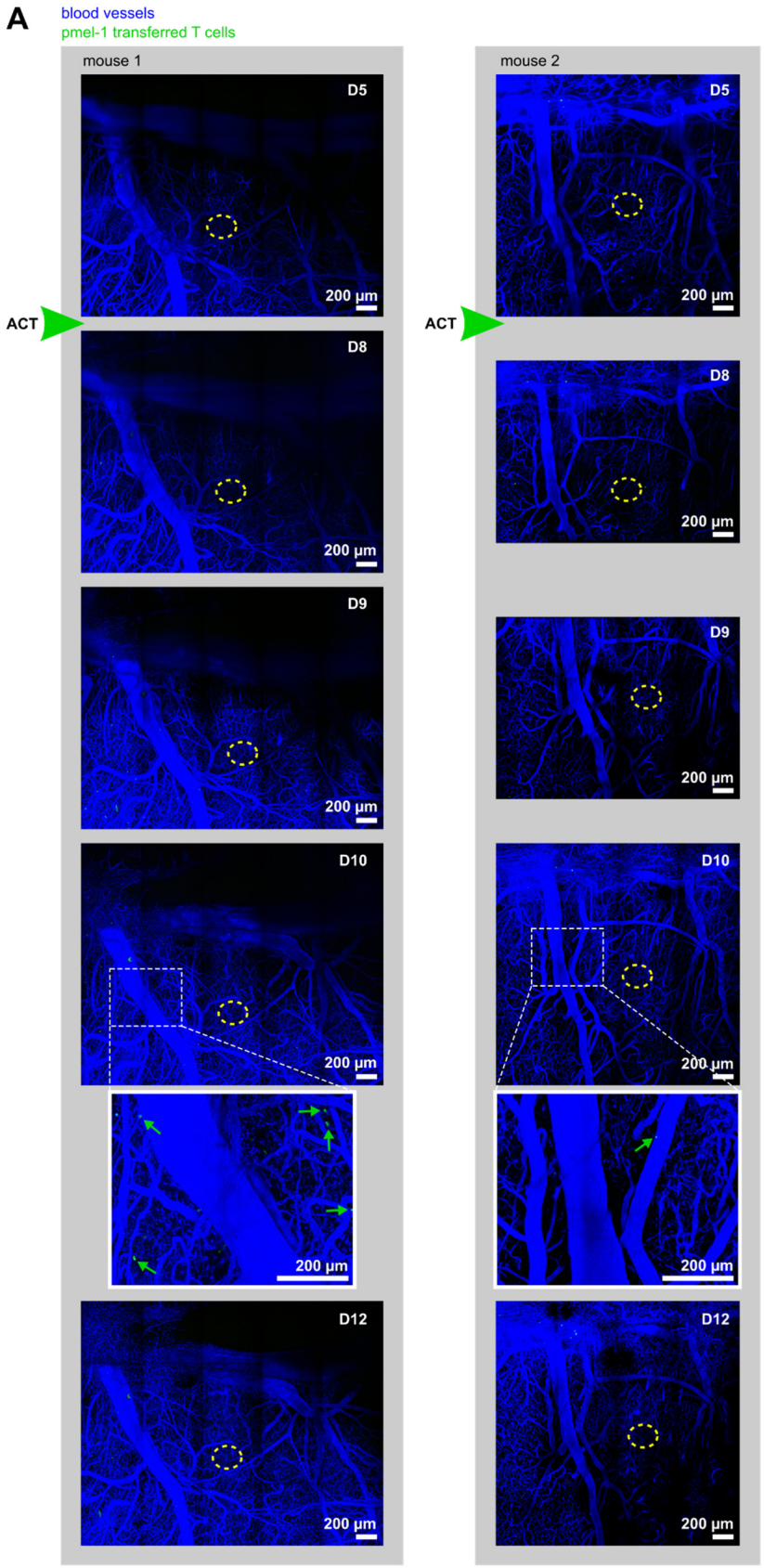

Figure 9: Sham injection does not cause T cell infiltration to the site of injection

Two C57BL/6 with chronic cranial window and were implanted a subcutaneous flank tumor of HCmel12 TyrKO melanoma on day -2. On day 0 analogous to the procedure of intracortical tumor injection, an intracortical sham

injection with PBS was performed, and ACT of pmel-1 T cells was performed on day 8. Both mice were treated with ICI starting from day 7, every two days. The position of the sham injection is indicated by yellow dashed ellipses, the timepoint of the ACT is indicated by green arrow heads. T cell infiltration to the brain was analyzed by IVM on days 5, 8, 9, 10, and 12. Overview images of the brain hemisphere surrounding the injection site are shown for each timepoint as MIPs, images in higher magnifications of day 10 are shown as MIPs, green arrows indicate singe T cells. Scale bars 200 µm.

3.5 Adoptively transferred pmel-1 T cells are associated with microregional brain tumor regression under ICI treatment

Next, I investigated whether the adoptively transferred T cells actively contribute to local anti-tumor immunity under ICI treatment. For this, I quantified local pmel-1 T cell densities at different regions of the tumor edge from IVM recordings. These microregions were followed over time by IVM and changes in their local tumor volume between days 9 and 12 post cortical TI were quantified. Local pmel-1 T cell density in distinct brain tumor microregions and the microregional brain tumor growth rate of these regions negatively correlated (Figure 10A-C). This indicates that the adoptively transferred T cells exert anti-tumor effects in the brain, reducing tumor growth or even leading to tumor regression.

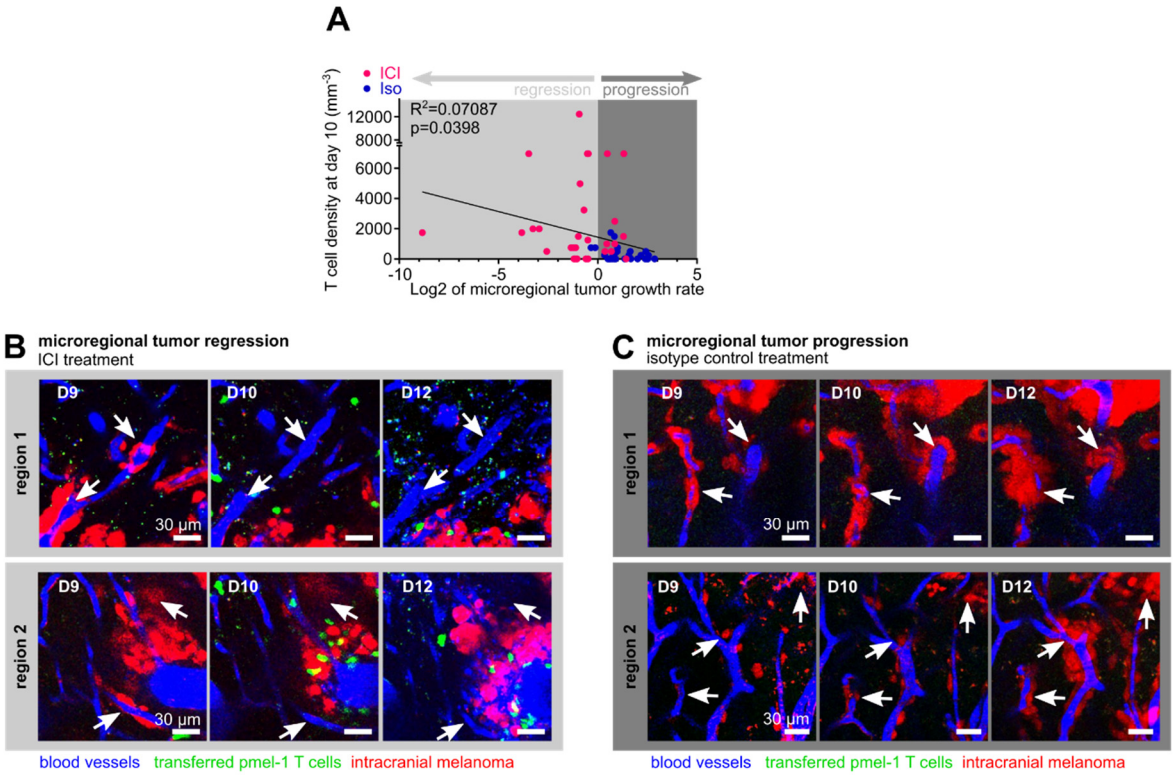

Figure 10: Density of transferred pmel-1 T cells is associated with microregional brain tumor regression

(**A**) Negative correlation of microregional tumor growth rate (log 2 of day 12 regional tumor volume / day 9 regional tumor volume) with density of pmel-1 transferred T cells on day 10 post cortical TI in HCmel12 TyrKO

intracranial melanoma under ICI and Iso control treatment. N=6 mice per group with n=5 distinct regions per mouse.

(**B**) IVM images of pmel-1 T cell abundance and microregional brain tumor regression (HCmel12 TyrKO) under ICI treatment in two example regions between days 9 and 12 post cortical TI. MIPs of 20 µm depth, arrows indicate tumor regression at distinct vessels followed over time.

(**C**) IVM images of microregional brain tumor progression (HCmel12 TyrKO) under isotype control treatment in two example regions between days 9 and 12 post cortical TI. MIPs of 20 µm depth, arrows indicate tumor progression at distinct vessels followed over time. Correlation of microregional tumor growth rate with microregional T cell density was calculated by using linear regression analysis and was conducted collectively on 5 microregions of cuboid volumes of 200.45 µm x 200.45 µm x 100 µm at the tumor edges per mouse of a total of n=6 mice per group (ICI or isotype control treated).

The growth of the extracranial flank tumors, which were implanted in combination with the intracranial tumors, was also inhibited under ACT and ICI treatment compared to isotype control treatment in both models. However, the flank tumors exhibited a distinct dynamic from the intracranial tumor growth (Figure 11A, B). The growth of extracranial HCmel12 TyrKO tumors seemed to be partially inhibited even without ICI treatment, which was not the case in Ret CM TyrKO flank tumors, suggesting an effect of the ACT alone on extracranial growth of HCmel12 TyrKO cells, but not Ret CM TyrKO cells. This observation might indicate differences of the two model cell lines with respect to their immunogenicity and their potential of being recognized and targeted by pmel-1 T cells. The benefit of combining both therapeutic strategies, seems to be especially effective to target intracranial tumor growth.

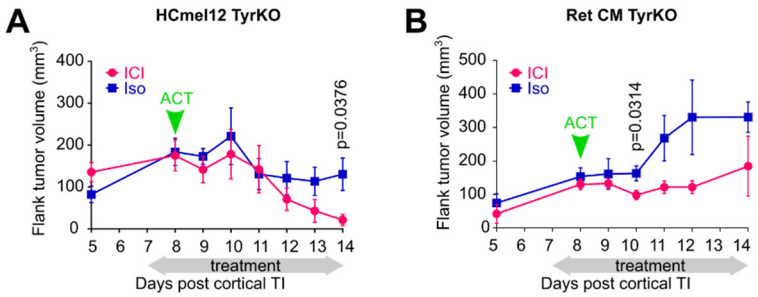

Figure 11: Extracranial flank tumor growth is inhibited under ACT and ICI treatment

(**A, B**) Quantification of extracranial flank tumor growth in mice injected with HCmel12 TyrKO (A) and Ret CM TyrKO (B) and treated with ACT and ICI or Isotype control antibodies. Two-tailed paired t-test per timepoint. n=6 mice per group D5-D12; n=5 mice per group D13-D14 (A). D5-D12: ICI group n=6 mice, isotype control group n=5 mice; D14: ICI group n=3 mice, isotype control group n=2 mice (B).

3.6 A transgenic T cell reporter mouse model allows visualization of endogenous T cells by intravital microscopy

The ACT model enables visualizing T cell infiltration into melanoma brain tumors, but it suffers from a few disadvantages. Firstly, the fluorescence of adoptively transferred pmel-1 T cells is based on staining with a chemical dye, therefore the T cell fluorescence fades with time due to dilution effects caused by cell proliferation and cellular metabolism. Thus, the signal of the fluorescent dye in the transferred T cells was only visible by IVM up to a maximum of 4-6 days following ACT. A notable decrease in T cell fluorescence intensity could even be observed after 4 days post ACT already. Secondly, recruitment of pmel-1 T cells as visualized by IVM was majorly dependent on the timepoint of the adoptive T cell transfer, so that timepoints before and further after the ACT could not be observed. Furthermore, pilot experiments of flow cytometry and CD3 immunofluorescence staining of the brain of ACT-model mice with Ret CM TyrKO intracranial melanoma, revealed that a much higher number of endogenous T cells compared to transferred T cells could be detected in the brain (data not shown). The latter findings suggest that endogenous T cell contribute to ICI-mediated anti-tumor activity and are thus an important focal point for this study.

Thus, to study brain-homing and dynamic interactions between endogenous T cells and tumor, and to circumvent the technical limitations of the ACT model, I generated a transgenic T cell reporter mouse line. Hereto, I crossed LCK-Cre mice, which express cyclization recombinase (Cre) under the control of the T cell specific lymphocyte protein tyrosine kinase (LCK) promoter, with a Lox-Stop-Lox (LSL)-tdTomato mouse line encoding a floxed-STOP cassette in front of a tdTomato gene. This resulted in a mouse line (LCK-Cre x LSL-tdTomato) expressing the red fluorescent protein tdTomato specifically in all cells of the T lymphocyte lineage.

Validation of TdTomato expression in leukocytes isolated from LCK-Cre x LSL-tdTomato mice was performed by flow cytometry (Figure 12A-G). 92.4% - 99.1% of $CD4^+$ and $CD8^+$ T cells isolated from spleen and lymph nodes of LCK-Cre x LSL-tdTomato mice (LCK-$Cre^{+/-}$ LSL-$tdTomato^{+/+,\ +/-}$) expressed tdTomato (Figure 12A-D), while only 0.5% -2.8% of non-T cell leukocytes tdTomato expression could be detected (Figure 12E). To determine the amount of unspecific labeling of other immune cells, tdTomato fluorescent signal was analyzed in non-T cell immune cell populations. The contribution of non-T cells to $CD45^+$ $tdTomato^+$ cells from LCK-Cre x LSL-tdTomato mice could be attributed to a small proportion of natural killer (NK) cells in the leukocytes isolated from spleen with ca. 3%, and between approximately 4% and 6% of $CD11b^-$ $Gr\text{-}1^+$ cells (Figure 12F, G). At first glance, it is tempting to identify the tdTomato positive, $CD11b^-$ $Gr\text{-}1^+$ cells as granulocytes, however it has to be taken into account that the T cell markers anti-CD3, anti-CD4, and anti-CD8 were not included in panel 4. Therefore, the panel

design did not allow for T cell subset identification. It could therefore be conceivable, that the $CD11b^{-}$ $Gr\text{-}1^{+}$ cells are not granulocytes, which are normally characterized by double positive staining for CD11b and Gr-1, but they could rather reflect a certain subset of T cells, which had been detected in other studies to stain positive for the Gr-1 marker component Ly-6C (DeLong et al., 2016; Fleming et al., 1993; Hänninen et al., 2011). Summarized, this data confirms robust tdTomato expression in endogenous T cells of LCK-Cre x LSL-tdTomato mice, with only minor leakage of tdTomato expression in non-T cell leukocyte subsets. Therefore, this new transgenic mouse line is well suitable to be used as a T cell reporter mouse model for studying T cell dynamics of infiltration and motility by intravital fluorescence microscopy.

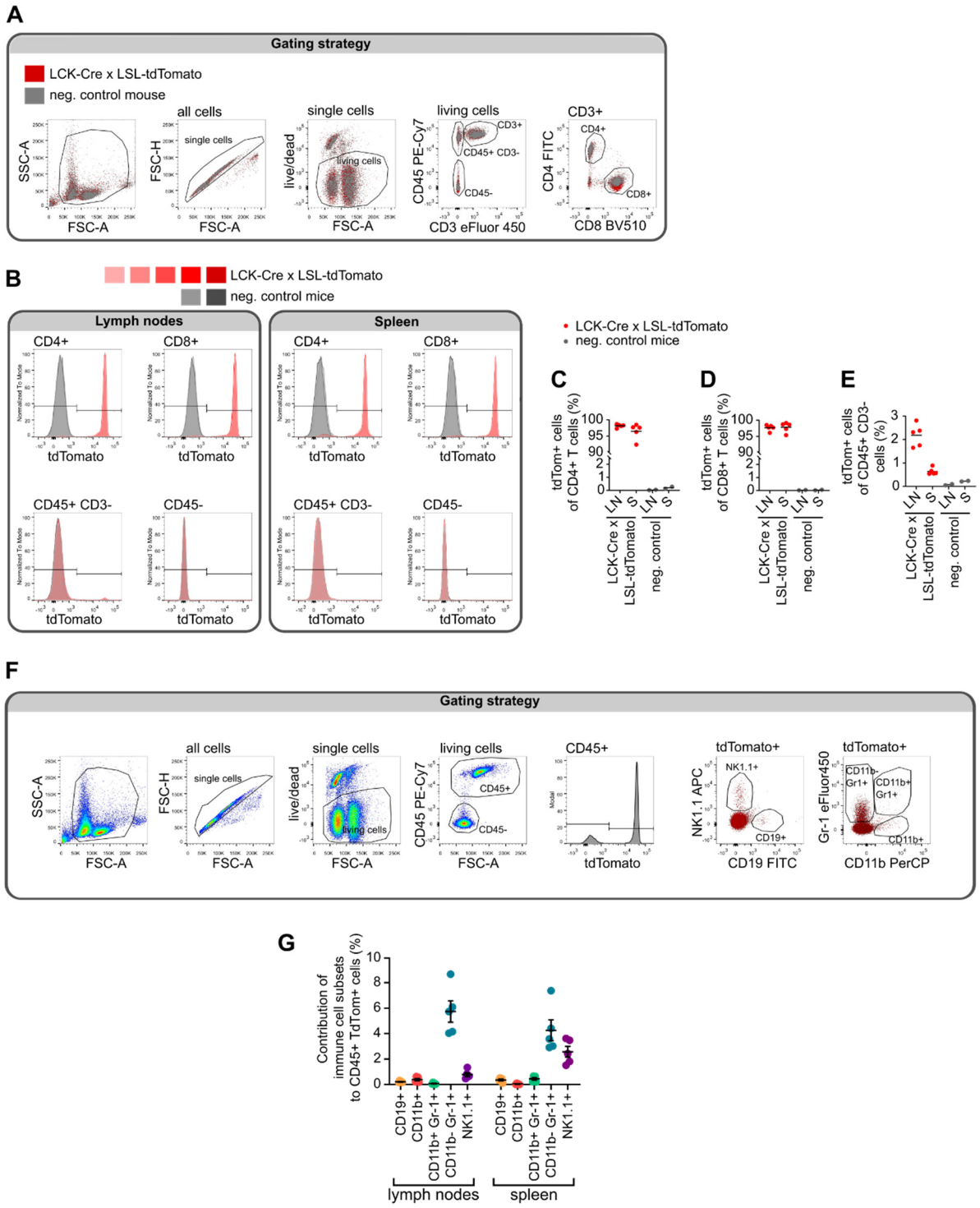

Figure 12: TdTomato expression in leukocytes isolated from LCK-Cre x LSL-tdTomato T cell reporter mice.

Flow cytometric characterization of tdTomato fluorescence of lymphocytes isolated from spleen (S) and lymph nodes (LN) of 5 LCK-Cre x LSL-tdTomato (LCK-Cre$^{+/-}$ LSL-tdTomato$^{+/+, +/-}$) and 2 negative control mice (LCK-Cre$^{+/-}$ LSL-tdTomato$^{-/-}$).

(**A**) Gating strategy to determine CD4+ and CD8+ T cell subsets shown as examples of one LCK-Cre x LSL-tdTomato mouse (red) and for one negative control mouse (grey) stained with antibodies of panel 3 (see Material and Methods).

(**B**) TdTomato fluorescence shown as overlays of histograms of fluorescence intensities in CD4+ and CD8+ T cell subsets and CD3- leukocytes and CD45- cells based on gating shown in (A) of 5 LCK-Cre x LSL-tdTomato mice (red) and of 2 negative control mice (grey).
(**C, D**) Quantification of the fraction of tdTomato positive cells of CD4+ (C) and CD8+ (D) T cells isolated from spleen (S) and lymph nodes (LN) as determined by A and B. Black bars represent means.
(**E**) Quantification of the fraction of tdTomato positive cells of CD45+ CD3- non-T cell leukocytes of 5 LCK-Cre x LSL-tdTomato mice (red) compared to two negative control mice (grey). Black bars represent means.
(**F, G**) Gating strategy (F) and contribution of non-T cell immune cell subsets to CD45 and tdTomato double positive cells isolated from spleen and lymph nodes of 5 LCK-Cre x LSL-tdTomato mice, stained with antibodies of panel 4 (see Material and Methods).

3.7 ICI treatment inhibits intracranial tumor growth in LCK-Cre x LSL-tdTomato T cell reporter mice

Analogically to the experimental procedure of the ACT model, the LCK-Cre x LSL-tdTomato T cell reporter mouse model was used to visualize T cell infiltration and intracranial tumor growth dynamics through a chronic cranial window by IVM (Figure 13A). After complete healing of a chronic cranial window implantation in LCK-Cre x LSL-tdTomato mice, a subcutaneous flank tumor was implanted followed two days later by intracortical injection of syngeneic fluorescent melanoma cells. The mice were treated with ICI or isotype control antibodies every two days starting from day 7 post cortical TI.

Intracranial tumor growth dynamics of HCmel12 TyrKO melanoma were similar as observed in the C57BL/6 mice with ACT. Importantly, both intracranial tumor growth and extracranial flank tumor growth were inhibited under ICI treatment as compared to isotype control treatment (Figure 13B-D). Comparable to the ACT model, the T cell reporter mouse model could be used to visualize fluorescent T cells in high resolution and reveals simultaneously their relation to blood vessels and tumor cells (Figure 13E). Due to the robust expression of tdTomato in the T cell lineage, endogenous T cells could be visualized at any timepoint of intravital microscopy (Figure 13E). T cells could be detected as early as one day post cortical tumor injection and T cell number observed in the brain in tumor proximity was increasing over time (Figure 13E). Whereas the ACT model allows the visualization of a very defined, antigen-specific, CD8+ T cell subpopulation, in the transgenic LCK-Cre x LSL-tdTomato model the complete heterogenous T cell population can be monitored. This likely explains the much higher overall number of observed T cells in the LCK-Cre x LSL-tdTomato mice as compared to the number of transferred T cells visualized by IVM in the ACT model.

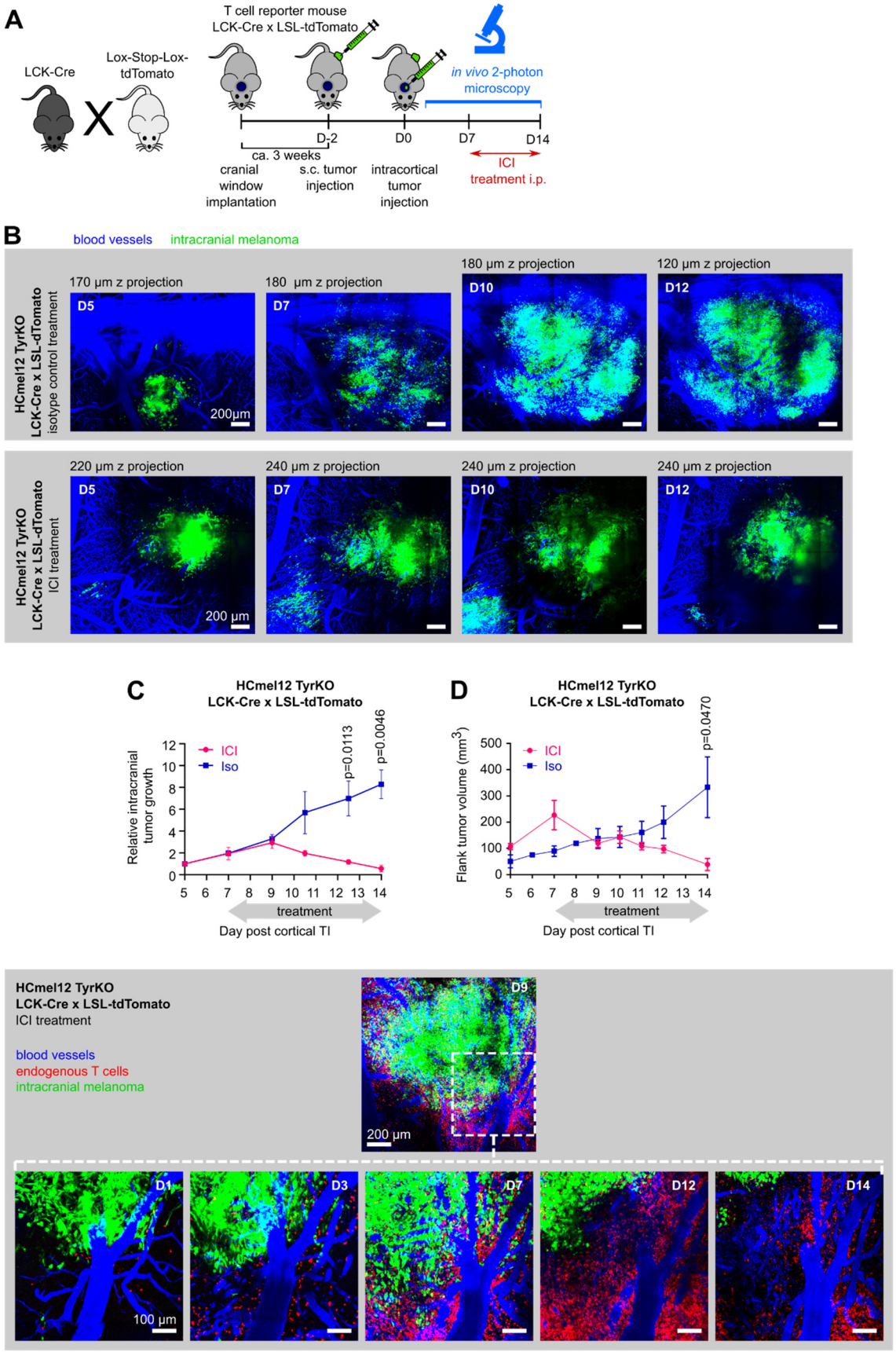

Figure 13: IVM of intracranial tumor growth and endogenous T cell infiltration in a transgenic T cell reporter mouse model

(**A**) Schematic representation of the experimental design for intravital imaging of brain tumor growth and T cell infiltration in LCK-Cre x LSL-tdTomato mice.
(**B**) IVM images of intracranial tumor growth of HCmel12 TyrKO melanoma in LCK-Cre x LSL-tdTomato mice over time between day5 and day 12 post cortical tumor injection treated with ICI or isotype control antibodies shown as MIP.
(**C**) Quantification of relative intracranial HCmel12 TyrKO growth (tumor volumes normalized to day 5 intracranial tumor volume) in LCK-Cre x LSL-tdTomato mice under ICI or isotype control treatment. Tumor volumes measured either on day 10 or 11 were analyzed together as day 10.5, and on day 12 or day 13 were analyzed together as day 12.5. Multiple two-tailed unpaired *t-tests* per timepoint with Holm-Šídák method for multiple comparison correction, n=4 mice per group on D5-D12.5; n=3 on D14.
(**D**) Quantification of flank tumor growth of HCmel12 TyrKO bearing LCK-Cre x LSL-tdTomato mice treated with ICI or isotype control antibodies. Two-tailed *t-test* per timepoint, n=4 mice per group.
(**E**) IVM images of intracranial melanoma and endogenous T cell infiltration in LCK-Cre x LSL-tdTomato mice under ICI treatment. Overview image of the whole tumor (top) is shown as MIP of 110 µm depth and in higher magnifications and over time between days 1 and 14 (bottom), shown as MIPs of 30 µm depth. Intravital imaging reveals high T cell density at distinct peritumoral venous vessels in the brain

3.8 Intravital imaging reveals high T cell density at distinct peritumoral venous vessels in the brain

Four-dimensional imaging revealed particularly high T cell numbers around certain intracranial blood vessels in both the ACT model and the T cell reporter mouse model (Figure 14A, B). These were identified as large peritumoral venous blood vessels, hereafter referred to as peritumoral venous vessels (PVVs), which drain into the sagittal venous sinus.

PVVs could be detected as early as one day post cortical tumor injection (Figure 14B), indicating that these vessels already existed before the intracranial tumors could induce angiogenesis and alter brain vasculature (Lockman et al., 2010; Lyle et al., 2016), which are changes that are not expected to be detectable within one day.

To investigate the exact route of T cells to melanoma brain tumors, I followed pmel-1 T cell infiltration in different peritumoral and intratumoral regions by IVM at day 9, 10 and 12 post cortical TI, meaning 1, 2, and 4 days after ACT. T cell densities at the PVVs were compared with other regions such as interspace (peritumoral capillary region between PVV and tumor), intratumoral, peritumoral capillary bed, sagittal sinus, and peritumoral brain surface (Figure 14C). Already one day post ACT, under ICI treatment I observed a trend towards increased T cell density at PVVs compared to all other regions. This difference became significant starting 2 days post ACT and increased even more with time (Figure

14C). T cells could also be detected in the spaces between the PVV and the tumor (here termed interspace) and intratumorally under ICI treatment, but T cell density in these regions was lower compared to at the PVVs. The trend of increasing T cell numbers in the interspace and intratumorally with time seemed to follow behind of the increase in T cell density at the PVVs. Therefore, the interregional spatiotemporal dynamics suggests a T cell recruitment from the PVVs passing the peritumoral capillary interspace between PVV and tumor, to the tumor mass. Interestingly, this spatiotemporal T cell recruitment pattern could not be observed under isotype control treatment (Figure 14C).

Analysis of spatiotemporal T cell recruitment of the more frequently detectable endogenous T cells in the LCK-Cre x LSL-tdTomato mouse model confirmed a PVV-induced T cell recruitment pattern. Due to the high density of T cells in this model, I developed a machine learning-based and semi-automated analysis to measure T cell density within 15 µm of proximity of four distinct brain vessel types, namely PVVs, peritumoral capillaries, intratumoral vessels, and sagittal sinus. Here, I detected a trend of increased T cell accumulation at PVVs until day 7 in both treatment groups. While T cell numbers at PVVs remained high, at days 9-14 T cell numbers were also rising at intratumoral vessels, and at peritumoral capillaries, which was more pronounced under ICI treatment compared to control (Figure 14D).

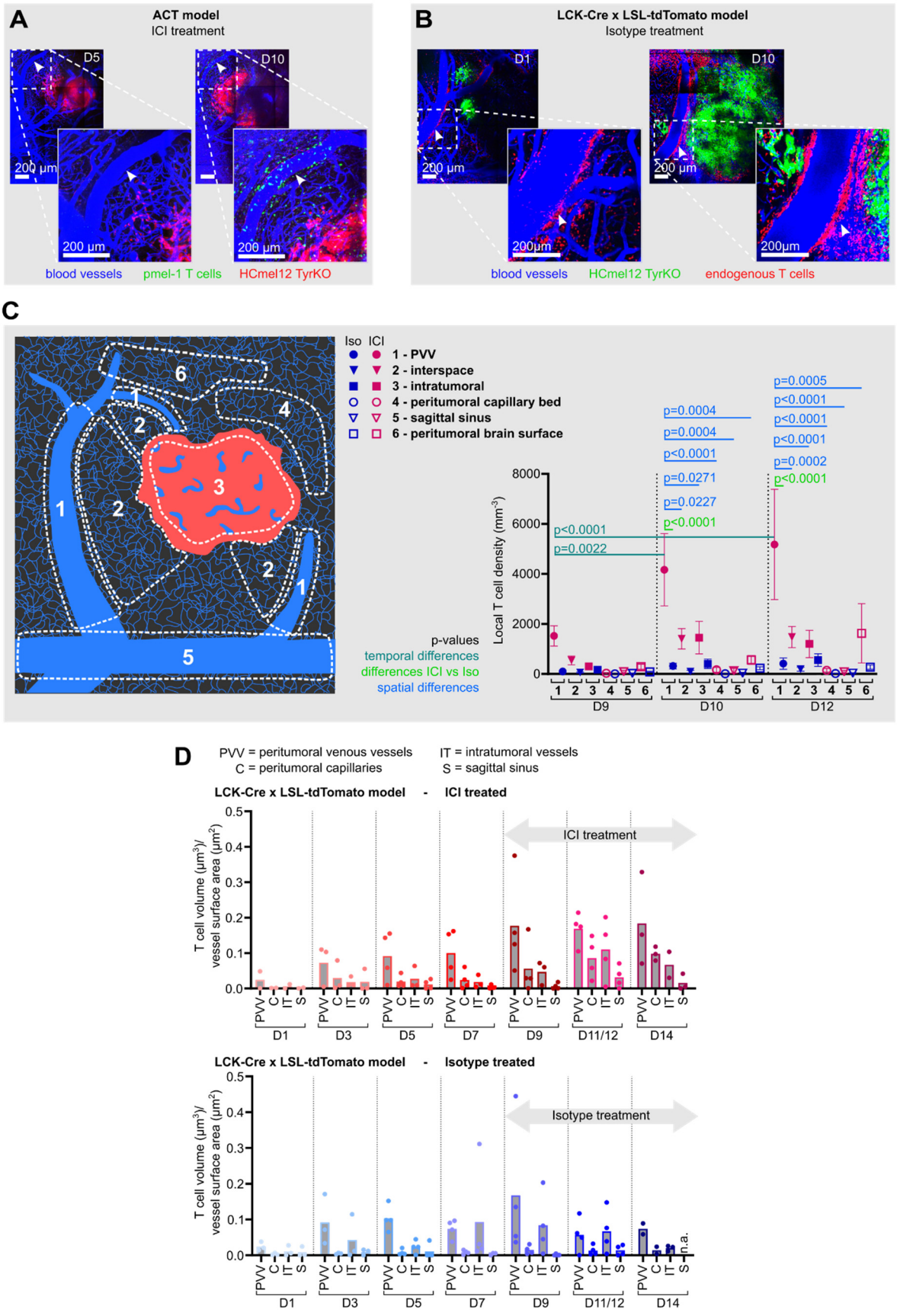

Figure 14: High T cell abundance of endogenous and transferred T cells at PVVs

(**A**) IVM images of HCmel12 TyrKO intracranial melanoma and adoptively transferred pmel-1 T cells at days 5 and 10 post cortical tumor injection and under ICI treatment. Images are shown as MIPs of 230 µm depth (day 5) and 160 µm depth (day 10). High T cell density at PVVs is indicated by arrow heads.
(**B**) IVM images of HCmel12 TyrKO intracranial melanoma and endogenous T cell infiltration in LCK-Cre x LSL-tdTomato mice at days 1 and 10 post cortical tumor injection under isotype control antibody treatment. Images are shown as MIPs of 110 µm depth (day 1) and 40 µm depth (day 10). High T cell density at PVVs is indicated by arrow heads.
(**C**) Schematic representation (left) of the localization of peritumoral and intratumoral regions as indicated by numbers 1-6 (1 PVVs, 2 interspace, 3 intratumoral, 4 peritumoral capillary bed, 5 sagittal sinus, and 6 peritumoral brain surface) selected used for T cell density quantification (right). Quantification of local T cell density of transferred pmel-1 T cells at day 9, day 10 and day 12 post cortical tumor injection at distinct regions in intracranial HCmel12 TyrKO melanoma under ICI (red) or isotype control (blue) treatment. N=6 mice per group D9 and D10, n=5 mice per group D12, statistics were calculated by two-way analysis of variance (ANOVA) with Tukey's *post-hoc* test.
(**D**) Quantification of the dynamics of local T cell density of endogenous T cells in HCmel12 TyrKO intracranial melanoma in the LCK-Cre x LSL-tdTomato mouse model treated with ICI (top) or isotype control antibodies (bottom) between day 1 and day 14. T cell density within 15 µm proximity of distinct vessel types (PVVs, peritumoral capillaries, intratumoral, sagittal sinus) was analyzed as described in methods section.

Since the PVVs appeared to be of critical importance during T cell recruitment, I next set out to characterize the PVVs. Hereto, blood flow velocities were measured in blood vessels of a non-tumor bearing LCK-Cre x LSL-tdTomato mouse that were anatomically located likewise to their PVV counterparts in tumor bearing mice. These vessels had a diameter ranging from 30 µm and 180 µm and could also clearly be identified to drain into the sagittal venous sinus (Figure 15A-C). Positions of measurement of the different blood vessel types are indicated in Figure 15A. The PVV-like vessels of the non-tumor-bearing mice, here depicted as medium large and large vessels, exhibit blood flow velocities of 13.8 mm/s ± 1.3 mm/s (Figure 15B). This result is close to the velocities that have been measured in venous vessels of a mouse cortex by another study (Kim et al., 2012), and which confirms the venous nature of PVVs.

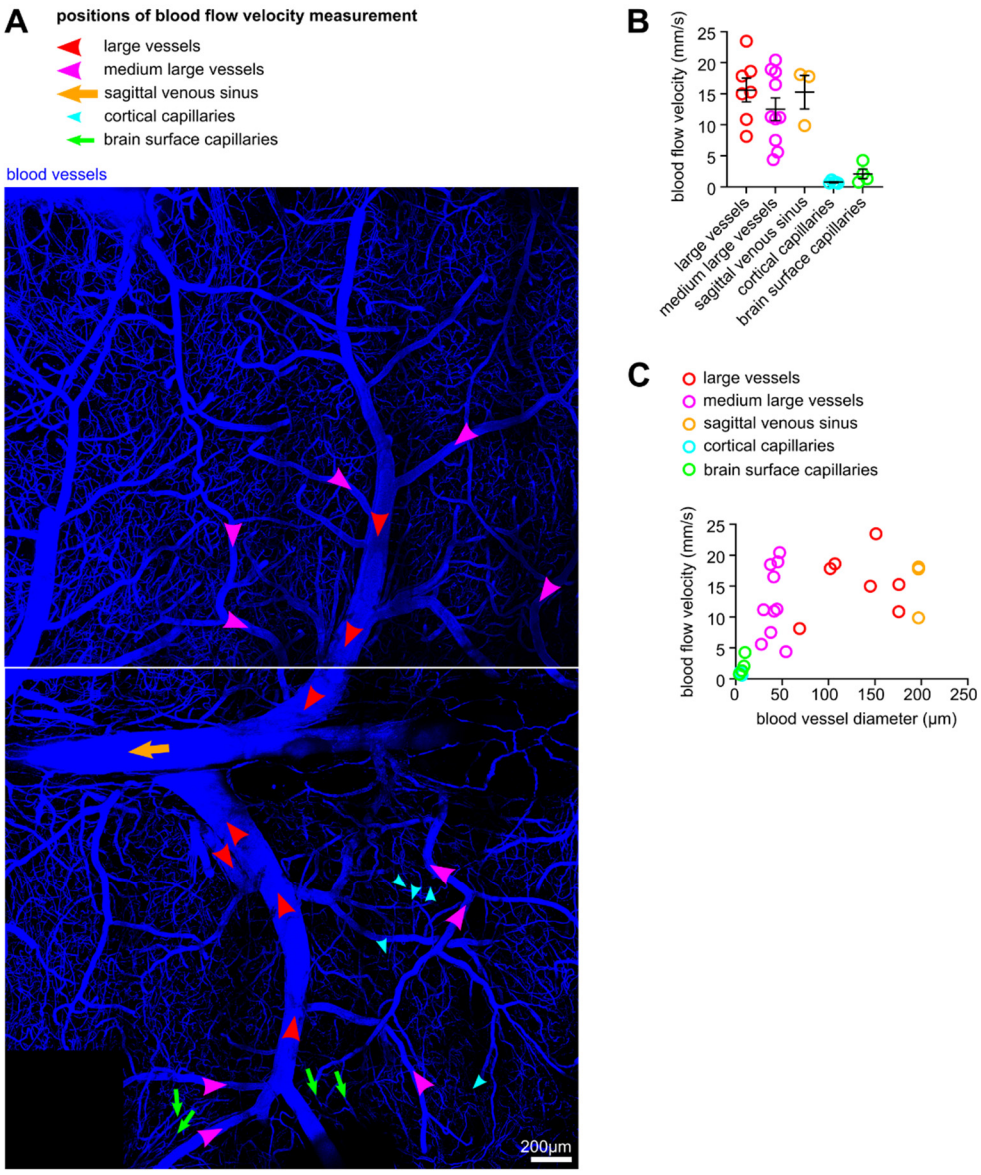

Figure 15: Blood flow velocity in brain vessels of a non-tumor bearing LCK-Cre x LSL-tdTomato T cell reporter mice measured by IVM linescan analysis

(**A**) IVM image of a brain angiogram shown as a MIP of a non-tumor bearing LCK-Cre x LSL-tdTomato mouse. Arrow heads and arrows indicate positions of blood flow velocity measurements at different vessel categories (large vessels, medium large vessels, sagittal venous sinus, cortical capillaries, and brain surface capillaries).

(**B**) Measurement of blood flow velocity (mm/s) was performed by IVM based linescan analysis at 7 large vessels, 10 medium large vessels, 5 cortical capillaries and 4 surface capillaries

(**C**) Blood flow velocity (mm/s) at different vessel types plotted against the diameter (µm) of the respective blood vessel.

3.9 PVVs provide sites of T cell entry to the brain by allowing T cell extravasation from the blood

The early increase of T cell abundance at PVVs suggests that PVVs harbor the sites of T cell entry from the blood to the brain parenchyma. To validate this assumption, I used the advantage of real-time imaging by two-photon microscopy in tumor-bearing cranial window mice with ACT. The ACT model was chosen for this analysis, because it facilitated visualizing and tracking of the movement of single transferred T cells due to their lower density, as compared to the LCK-Cre x LSL-tdTomato model. I recorded 20-30 min timeseries of different brain and tumor regions with different vessel types, such as tumor microvessels, peritumoral capillaries and PVVs. With this, I was able to detect events of firm T cell attachment to the vascular walls (T cell rolling or crawling), which is a prerequisite for T cell extravasation to the brain parenchyma (Bartholomäus et al., 2009; Kerfoot & Kubes, 2002), and T cell extravasation events. T cell rolling and extravasation almost exclusively occurred at PVVs (Figure 16A, B), most frequently on day 9, one day post ACT. At tumor microvessels or peritumoral capillaries, intravascular T cells could mostly be observed without showing signs of stable vascular attachment, but rather moving fast through the vessel with the blood flow (Figure 16C).

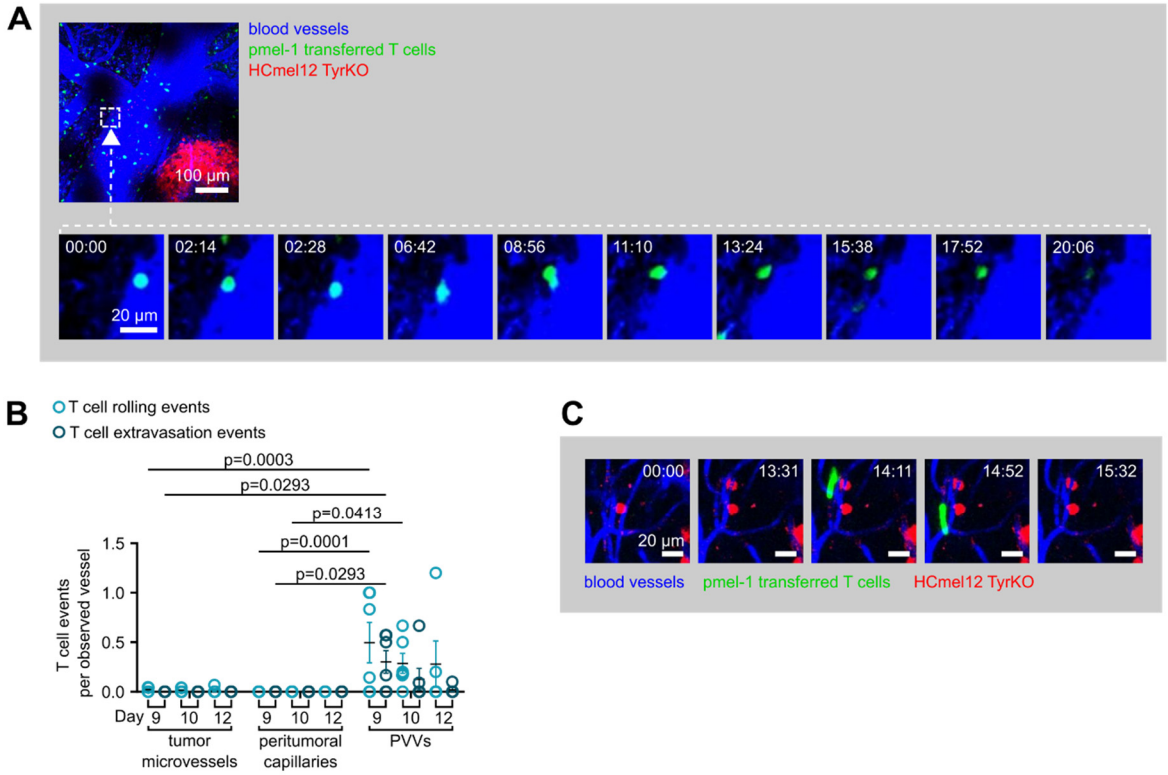

Figure 16: T cell attachment to vessel wall and extravasation at PVVs

(**A**) IVM time series images of a pmel-1 T cell extravasating from a PVV of HCmel12 TyrKO intracranial melanoma on day 12 post cortical tumor injection treated with ICI. Zoomed-in time course of 20:06 min is shown as single z-planes; overview image (top) is shown as MIP of 90 µm depth.

(**B**) Quantification of pmel-1 transferred T cell rolling events (intraluminal retention for > 2 min) and T cell extravasation events at distinct vessel types (tumor microvessels, peritumoral capillaries, PVVs) of ICI treated intracranial HCmel12 TyrKO intracranial melanoma at days 9, 10, and 12 post cortical TI depicted as events per number of observed vessels. Statistics were calculated by two-way ANOVA with Tukey's *post-hoc* test, dots represent individual mice, for numbers of observed mice and vessels see Table 21.

(**C**) IVM time series images of a pmel-1 T cell 4 hours post ACT on day 8 post cortical TI flushed through a peritumoral capillary without stable adhesion to vascular endothelium of HCmel12 TyrKO intracranial melanoma under ICI treatment. Time course of 15:32 min, MIPs of 70 µm depth.

Table 21: Number of mice and vessel types observed on days 9, 10, and 12 as described in Figure 16B

Day post cortical TI	**D9**	**D10**	**D12**
Number of observed mice	6	6	5
Count of intratumoral microvessels observed per mouse (mean)	20	28	36
Count of peritumoral capillaries observed per mouse (mean)	69	104	133
Count of PVVs observed per mouse (mean)	5	7	5

To better understand the characteristics and development of PVVs, I used the LCK-Cre x LSL-tdTomato mouse model and exploited the advantage of readily detectable fluorescent T cells at any timepoint. IVM of chronic cranial window bearing, untreated mice without extracranial and intracranial tumors revealed far less T cells in the brain as compared to tumor-bearing mice. Interestingly, in brains of healthy mice, T cell accumulation of endogenous T cells could be observed around certain regions of venous vessels of comparable size and anatomical location to PVVs in brain tumor bearing mice (Figure 17A). Around parenchymal capillaries of healthy brain, only very few T cells could be detected (Figure 17B), while T cell numbers at the sagittal venous sinus and at the brain surface beneath the cranial window were elevated compared to the brain parenchyma (Figure 17A-E). These findings in healthy brain confirm what has also been described in another study, showing that the meningeal brain surface and the sagittal venous sinus are sites of lymphocyte mediated immune surveillance of healthy brain (Rustenhoven et al., 2021). However, this data suggests that in the context of local inflammation induced by the presence of a brain tumor, immune surveillance might differ from surveillance of the healthy brain. The data presented in this work invites to speculate that large venous vessels exhibiting T cell clusters already in healthy brain might be prone to develop into PVVs in the brain tumor context, thus taking over the major function of T cell recruitment to the brain tumors.

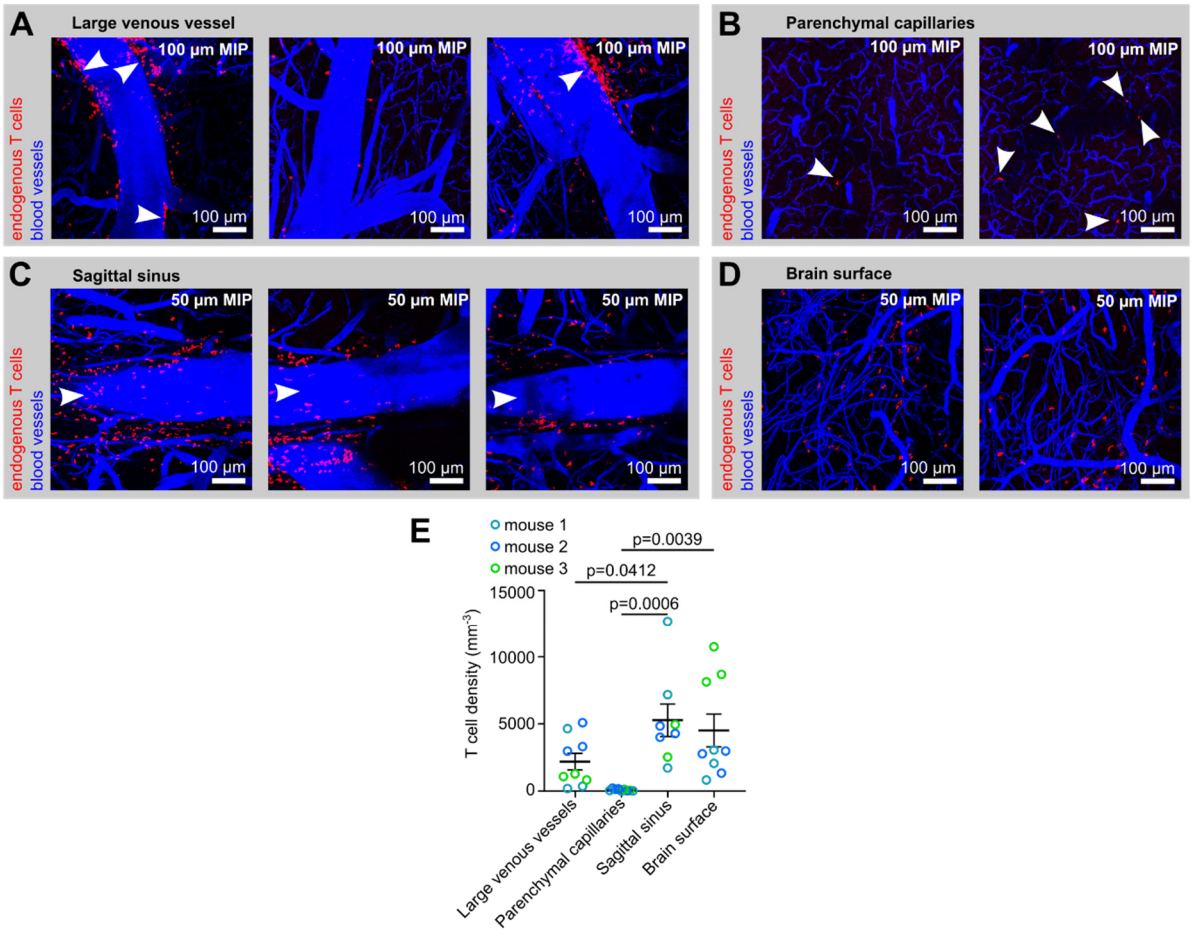

Figure 17: Distribution of endogenous T cells in non-tumor bearing T cell reporter mice

(**A-D**) IVM images of endogenous T cells in distinct brain regions (A: large venous vessels, B: parenchymal capillaries, C: sagittal venous sinus, D: brain surface) of non-tumor bearing, untreated LCK-Cre x LSL-tdTomato mice with chronic cranial window. Images are shown as MIPs.

(**E**) Quantification of endogenous T cell densities at distinct brain regions and vessel categories as shown in A-D. T cells were counted manually at three different regions per mouse of n=3 mice of an area of 600 µm x 600 µm and a depth of 50 µm – 100 µm. Statistics were calculated by two-way ANOVA with Tukey's *post-hoc* test on 9 regions per group combining different mice.

3.10 Molecular characteristics of PVVs

3.10.1 ICAM-1 expression on PVVs

Blood vessels outside of the brain that allow lymphocyte transmigration share certain molecular characteristics, such as expression of cell adhesion molecules, integrin receptors and members of the integrin family (Alon et al., 1995; Staunton et al., 1988; Vestweber, 2015). One of these important molecular binding partners, crucial for immune cell recruitment, is ICAM-1 (Haghayegh Jahromi et al., 2019; Lyck et al., 2003). Therefore, I investigated ICAM-1 expression on brain sections of ACT-mice with intracranial HCmel12 TyrKO melanoma and treated with ICI. ICAM-1 expression could be detected by

immunofluorescence on CD31 positive endothelial cells of PVVs and on the brain surface around these PVVs (Figure 18A). ICAM-1 expression was not associated with other vessel types, such as intratumoral tumor microvessels and peritumoral capillaries (Figure 18A) or vessels on the non-tumor hemisphere (Figure 18B).

Previous studies have shown that chemo-attraction of lymphocytes to sites of inflammation in and outside of the brain could be mediated by CXCL10 and its receptor CXCR3. I attempted to stain for CXCR3 on brain sections of HCmel12 TyrKO tumor bearing mice, but unfortunately this staining did not work and CXCR3 could not be detected on these sections (data not shown).

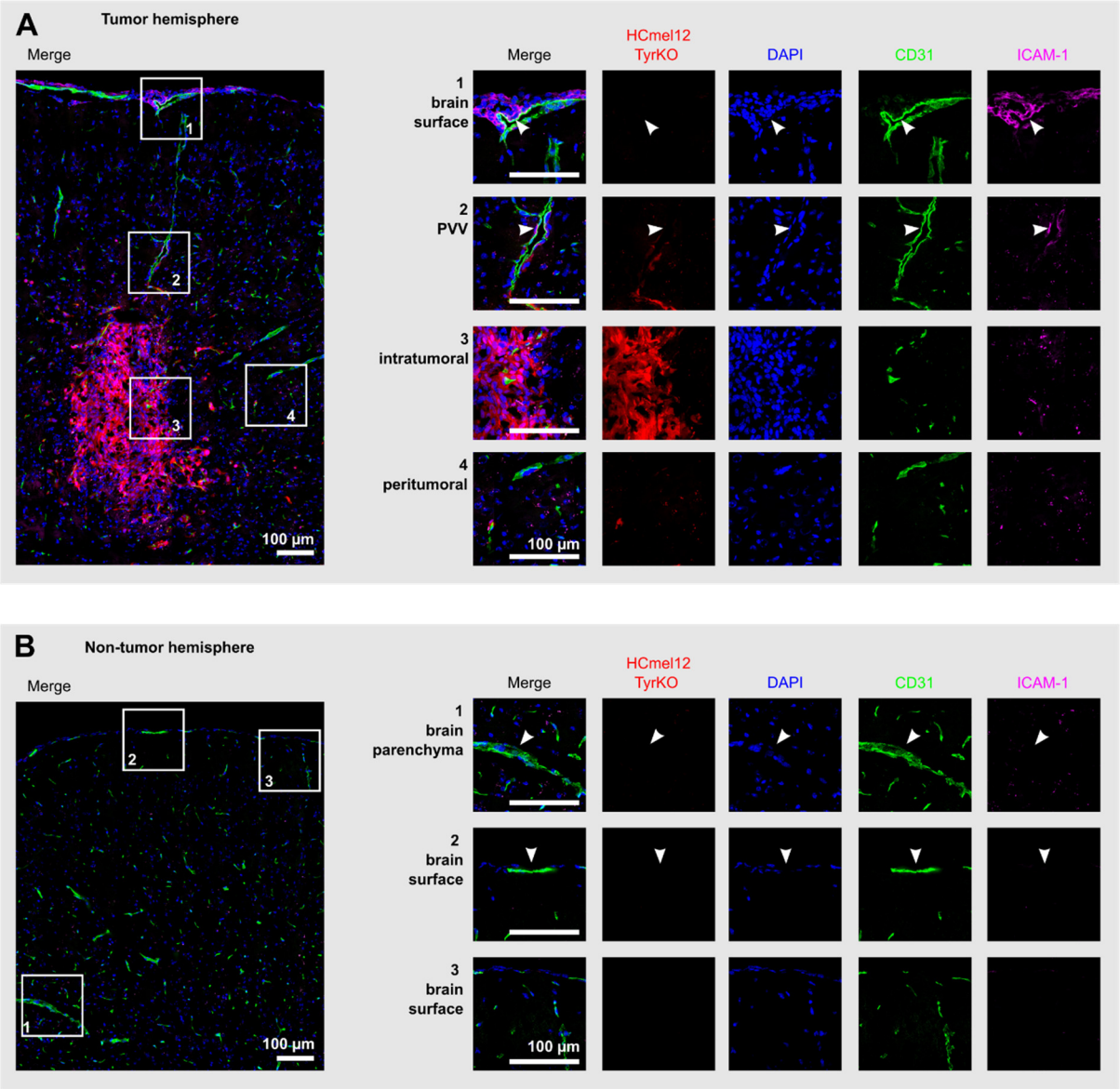

Figure 18: ICAM-1 immunofluorescence staining on HCmel12 TyrKO intracranial melanoma brain sections

(**A, B**) Immunofluorescence analysis on coronal brain sections of intracranial melanoma of the ACT model of HCmel12 TyrKO intracranial tumor on day 10 post cortical TI treated with ICI. (A) Whole tumor and peritumoral

brain tissue overview is shown on as merged image with numbered boxes indicating specific regions shown in higher magnification as color merged images and as single channel images (right). Arrow heads indicate ICAM-1 positive vessels. Scale bars 100 µm. (B) Overview image of a coronal section of the non-tumor bearing hemisphere (left) with numbered boxes indicating specific regions shown in higher magnifications (right). Arrow heads indicate vessels.

To confirm ICAM-1 expression in PVVs and link it to T cell behavior, I performed *in vivo* intravascular antibody staining by injection of FITC-coupled anti-ICAM-1 intravenously into HCmel12 TyrKO tumor bearing, ICI treated LCK-Cre x LSL-tdTomato mice and monitored T cell dynamics by IVM. In accordance with the immunofluorescence staining on brain sections, ICAM-1 signal could not be detected in intratumoral vessels and also only very faintly in some peritumoral capillaries, while most peritumoral capillaries were ICAM-1 negative (Figure 19A-C). High ICAM-1 staining could be detected at the endothelial lining of PVVs, particularly at regions, with high abundance of perivascular T cells (Figure 19D). This was quantified by correlating the normalized ICAM-1 fluorescent signal at PVVs with the binarized T cell fluorescent signal in direct proximity of 30 µm of the vascular wall at the respective position (Figure 19E). Such relation was not detectable at brain surface capillaries (Figure 19F) or at the sagittal sinus (Figure 19G). The vessel diameters of neither PVVs, nor brain surface capillaries, nor sinus correlated with T cell abundance at the respective position (Figure 19H-J). This indicates that the vessel diameter itself is not associated with T cell abundance at PVVs, but rather that particularly high ICAM-1 expression at PVVs allows T cell adhesion to endothelium and facilitates extravasation of circulating T cells for their recruitment to the brain tumor.

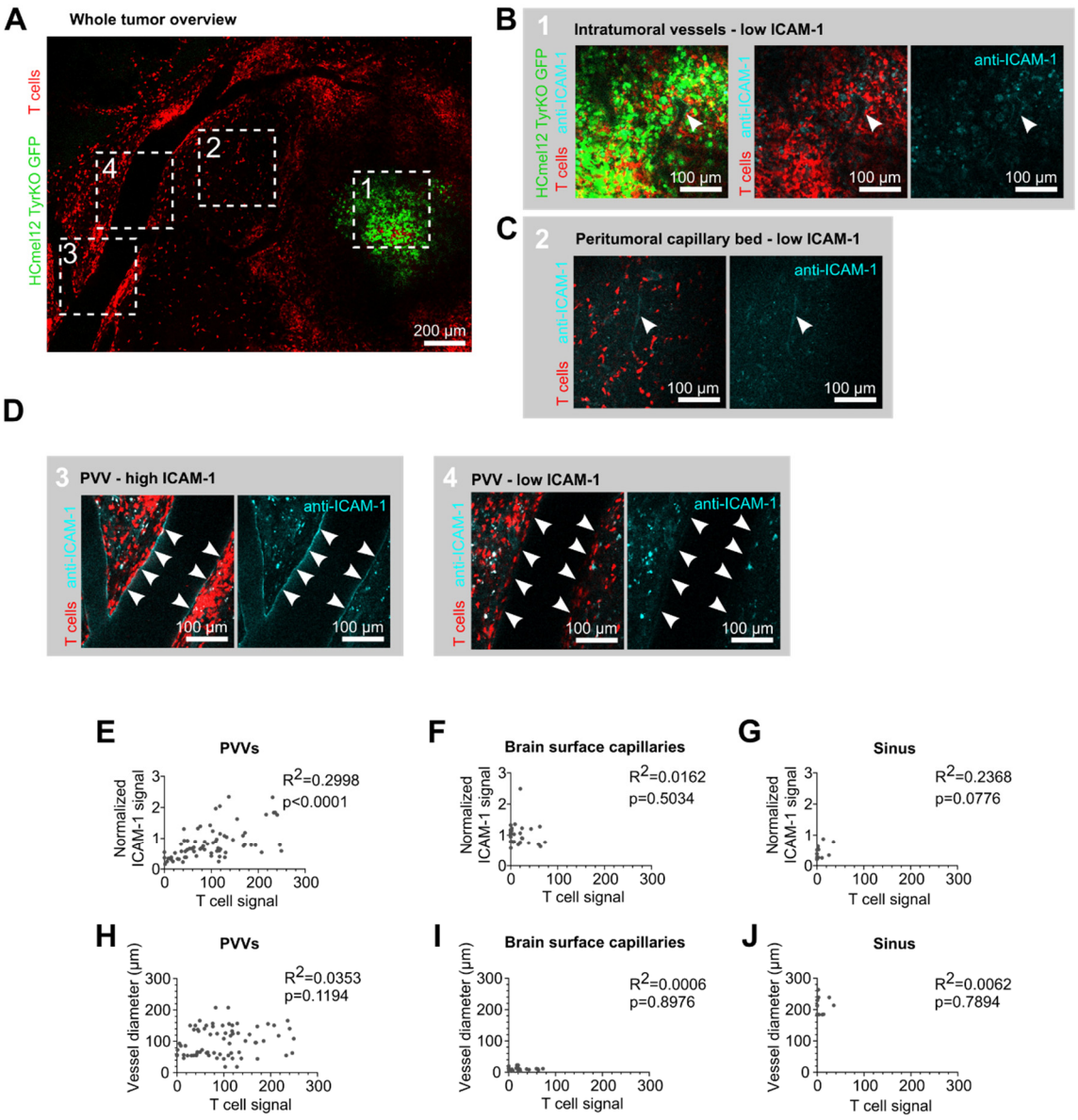

Figure 19: *In vivo* ICAM-1 intraluminal staining in vessels of intracranial melanoma

(**A-D**) IVM images of *in vivo* ICAM-1 staining upon i.v. injection of FITC-coupled anti-ICAM-1 1-3h post injection in LCK-Cre x LSL-tdTomato mice with intracranial HCmel12 TyrKO melanoma at day 10 post cortical tumor injection under ICI treatment. (A) Overview image of the brain tumor (green) and distribution of T cells (red) in its periphery directly before anti-ICAM-1 i.v. injection. Distinct regions shown in higher magnifications (B-D) are indicated by numbered boxes. (B-D) IVM images 1-3h post anti-ICAM-1 FITC injection of an intratumoral region (B), the peritumoral capillary bed (C), and two regions of a PVV with high and low ICAM-1 staining (D). Arrow heads point to the vascular walls of the respective vessel types in each region corresponding to the numbered boxes of panel A.

(**E-G**) Quantification of binarized T cell fluorescence signal in the perivascular space within a 30 µm distance from the vessel walls plotted against normalized intraluminal ICAM-1-FITC fluorescence signal intensities. Pearson correlation was calculated for PVVs (E) and brain surface capillaries (F) and sinus (G).

(**H-J**) Correlation analysis of quantified T cell signal in vessel proximity to the respective vessel diameter at PVVs (H), at brain surface capillaries (I) and at the sagittal sinus (J). N=2 mice for PVVs and brain surface capillaries (E,F,H,I), n=72 position on PVVs (E,H), n=30 positions on brain surface capillaries (F,I), N=1 mouse for sinus with n=14 positions (G,J).

3.10.2 Functional blocking of ICAM-1 *in vivo* leads to a trend to mitigate ICI-mediated anti-tumor immunity

To validate the functional importance of intraluminal ICAM-1 expression on PVVs, I blocked ICAM-1 *in vivo* by using an inhibitory antibody and measured HCmel12 TyrKO tumor growth and endogenous T cell infiltration in LCK-Cre x LSL-tdTomato mice by IVM (Figure 20A). To guarantee sufficient T cell infiltration to the brain, the subcutaneous and cortical tumor bearing mice were all treated with immune checkpoint inhibition starting at day 7. For blocking intraluminal ICAM-1 already in the earliest stages of T cell recruitment to the brain, the mice were injected i.v. with anti-ICAM-1 neutralizing antibody starting from day 3 post cortical tumor every three days. I observed a clear trend suggesting that ICI-mediated tumor growth inhibition was stronger in the control mice as compared to anti-ICAM-1 treated mice, as seen in an earlier and steeper drop of the growth curve (Figure 20B). Interestingly, this trend only became apparent after the start of ICI treatment at day 7 post cortical TI (Figure 20B). In contrast, all subcutaneous tumors of both treatment groups showed a complete regression, with a slight trend towards later onset of tumor regression under ICAM-1 blocking (Figure 20C). ICAM-1 blocking also resulted in a trend towards reduced T cell infiltration upon start of the ICI treatment (Figure 20D). This supports the findings on tumor growth inhibition under ICAM-1 blockage (Figure 20B) and suggests that intraluminal ICAM-1 expression is functionally relevant for sufficient T cell recruitment, as facilitated by ICI, and for efficient tumor growth inhibition.

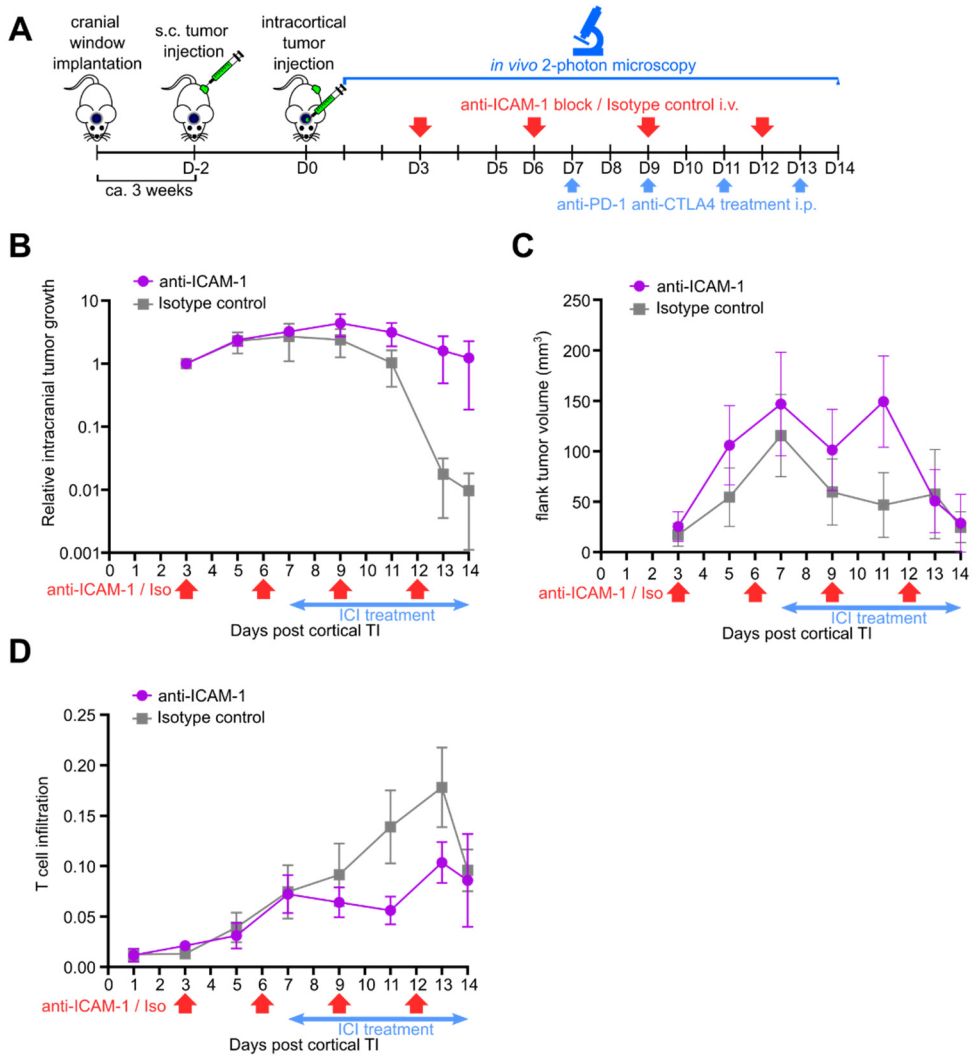

Figure 20: *In vivo* functional ICAM-1 blocking in intracranial melanoma

(**A**) Schematic depiction of the ICAM-1 functional blocking experiment. HCmel12 TyrKO GFP melanoma cells were injected subcutaneously and two days later intracortically in cranial window bearing LCK-Cre x LSL-tdTomato mice. Mice were treated either with 100 µg anti-ICAM-1 functional blocking antibody by i.v. injection starting from day 3 every three days or with the respective Isotype control antibody. Both groups were additionally treated with ICI starting from day 7. The intracranial tumor growth and T cell infiltration was analyzed by IVM regularly starting from day 1 post cortical TI.

(**B**) Quantification of HCmel12 TyrKO brain tumor growth in ICI treated LCK-Cre x LSL-tdTomato mice over time normalized to the starting tumor volume measured at day 3 post cortical TI shown as relative growth in logarithmic scale under ICAM-1 blocking antibody or Isotype control treatment. N=4 mice per group.

(**C**) Quantification of subcutaneous flank tumor growth over time as described in (A). N= 4 mice per group.

(**D**) Quantification of T cell infiltration in brain tumors of LCK-Cre x LSL-tdTomato mice as described in (A). For each brain tumor a volume including the tumor volume plus 200 µm distance from the tumor to its periphery was determined and the cumulative volume of all T cells within this volume was determined and T cell infiltration is depicted as the fraction of T cell volume / defined tumor plus periphery volume. In cases of complete tumor

regression, the observed volume and location was estimated from a timepoint before, when tumor mass was well detectable. N=4 mice per group.

As *in vivo* ICAM-1 blocking showed trends, but not significant results in inhibiting anti-tumor immunity, it is very likely that ICAM-1 is not the only molecular feature of PVVs. Probably other molecular factors are also upregulated during inflammation of PVVs that also facilitate T cell extravasation and recruitment.

3.10.3 Brain vessels in intracranial melanoma in mice do not express a high endothelial venule marker

In extracranial solid tumors, tumor associated vessels share characteristics of high endothelial venules (HEVs) by expression of the HEV marker peripheral lymph node adressin (PNAd), a sulfated carbohydrate epitope expressed on the endothelial cell surface (Allen et al., 2017; Asrir et al., 2022). These tumor-associated HEVs are associated with T cell recruitment under ICI treatment and are abundant in metastatic melanoma patients and correlate with better response to ICI therapy (Asrir et al., 2022). To determine whether PNAd might be co-expressed with ICAM-1 in the brain and act as another factor for T cell recruitment to the brain tumors, I used a PNAd specific antibody, MECA-79, to stain cryo-sections of ICI treated mouse brain tumors (day 10 post cortical TI). I stained and analyzed 17, 12, and 12 individual sections per brain tumor of three different mice, and MECA-79 positive vessels could not be detected intratumorally, on peritumoral vessels or on large vessels on the brain surface in any of these sections (Figure 21A, B). Technical difficulties of the MECA-79 antibody staining could be excluded as staining of lymph node cryo-sections as a positive control clearly showed positive staining of high endothelial venules (Figure 21C).

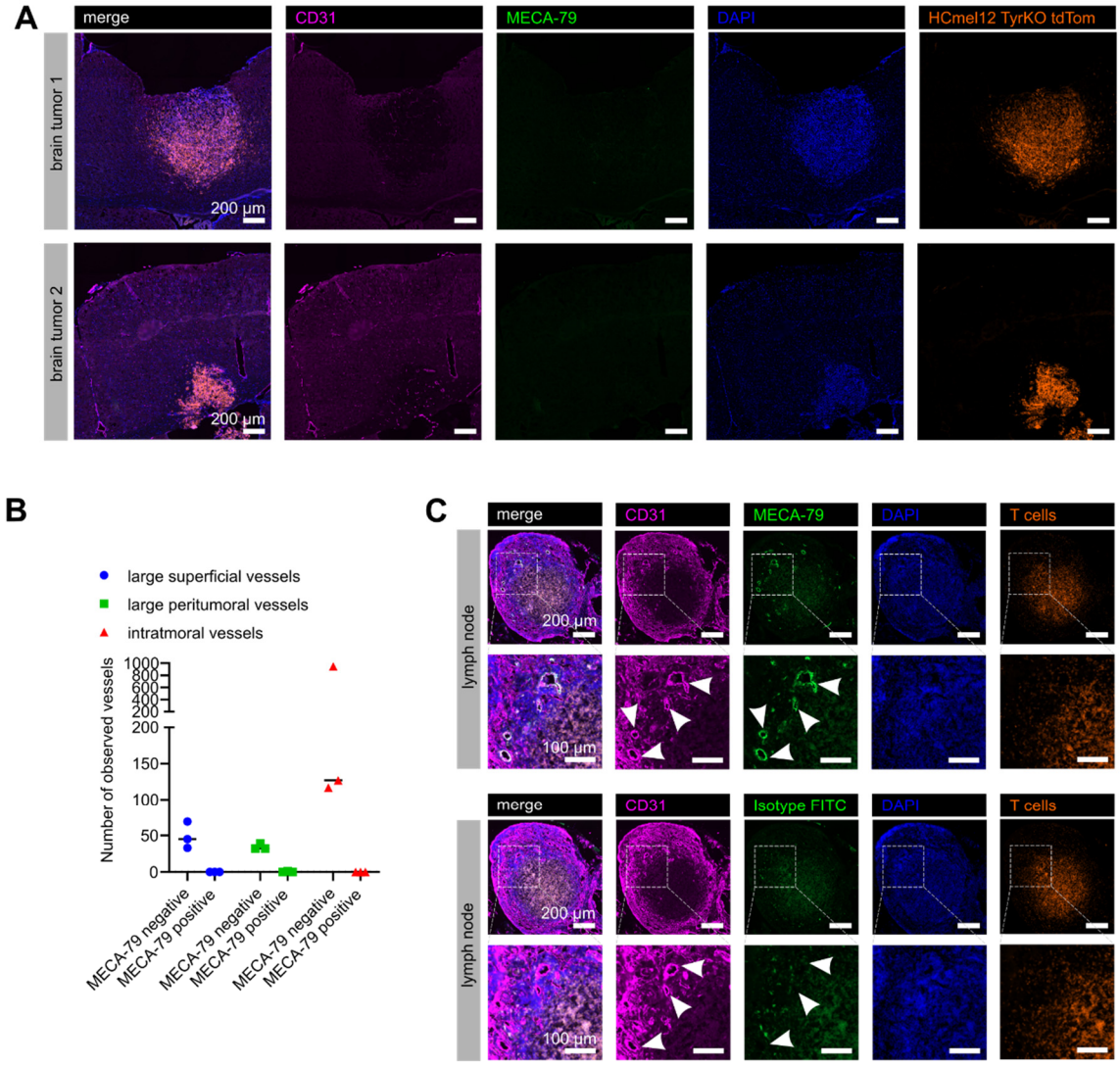

Figure 21: Immunofluorescence PNAd staining on HCmel12 TyrKO intracranial melanoma brain sections

(**A, B**) Immunofluorescence analysis of PNAd stained by a FITC labeled MECA-79 antibody on coronal brain sections of intracranial melanoma of the ACT model of HCmel12 TyrKO intracranial tumor on day 10 post cortical TI treated with ICI. (A) A whole tumor cross section and its periphery of two individual mice are shown as merged image and as single channel images (CD31 (blood vessels) – magenta, MECA-79 (PNAd) – green, DAPI (nuclei) – blue, HCmel12 TyrKO (tumor) – orange). (B) Quantification of the number of MECA-70 negative and positive large vessels on the brain surface, large peritumoral vessels, and intratumoral vessels of each 17, 12, and 12 distinct sections from three mice.

(**C**) Immunofluorescence analysis of PNAd stained by a FITC labeled MECA-79 antibody on sections of LCK-Cre x LSL-tdTomato lymph node as a positive control. Upper part: Overview images of the lymph node are shown in the upper row and as zoom-ins on a specific region in the row shown each as merge and as single channel images (CD31 – magenta, MECA-79 – green, DAPI – blue, T cells – orange). Arrow heads indicate position of high endothelial venules. Lower part: Adjacent serial section to the section of the upper part stained with the FITC conjugated isotype control antibody. Images are shown as overview and zoom-ins as in the upper part.

3.11 ICI treatment increases motility parameters of brain homing T cells

T cell motility is an important aspect of effective T cell functionality (Masopust & Schenkel, 2013). How ICI treatment influences T cell motility has rarely been studied in extracranial tumors and if so, only by short-term intravital imaging (Boissonnas et al., 2007; Bougherara et al., 2015; Breart et al., 2008; Deguine et al., 2010; Lau et al., 2020; Mrass et al., 2008; Mrass et al., 2006; Peranzoni et al., 2018) and has not been studied in the context of brain tumors yet. Here, I applied the advantages of long-term imaging and the ability to make real-time timeseries to uncover the effects of ICI treatment on T cell motility parameters in brain tumors. I performed post-imaging three-dimensional tracking of pmel-1 transferred T cells in timeseries images at different positions in the brain tumor and its periphery. By considering their migratory behavior, two main T cell phenotypes became apparent. T cells seemed to either move freely or they appeared to be anchored to a certain position, only hovering around their anchor point within a radius of approximately one cell length, during the whole duration of the timeseries. These “stationary” or “motile” T cell phenotypes have also been observed in the brain by intravital microscopy in rodent models of experimental encephalomyelitis, showing that stationary T cells were associated with antigen recognition (Kawakami et al., 2005). To quantitatively distinguish between these two phenotypes, T cells with mean velocity ≥ 50 nm/s and mean displacement ≥10 nm/s were defined as “motile” and T cells with a mean velocity < 50 nm/s and mean displacement < 10 nm/s as “stationary”, as shown in two exemplary timeseries IVM images in Figure 22A.

Previous studies in primary mouse tumors have shown that T cells undergo a migratory phase preceding a stationary phase reflecting stable interactions between T cells and target cells as a result of target cell recognition (Lau et al., 2020; Mrass et al., 2006). To better understand and differentiate between these two distinct T cell states, T cells within and surrounding intracranial melanoma were categorized accordingly and the percentage of these phenotypes were assessed. ICI treatment led to a trend of moderate increase of the fraction of motile transferred T cells *in vivo* in both intracranial melanoma models (Figure 22B, C), which was significant on day 12 in the HCmel12 TyrKO melanoma model (Figure 22B). Moreover, a trend towards higher absolute T cell numbers of both motile T cells and stationary T cells under ICI treatment was found, despite large variability between individual mice (Figure 22D). When only intratumoral T cells were included in the analysis, T cells of ICI treated mice exhibited a higher percentage of stationary T cells than motile T cells on day 9, which was higher than day 12 (Figure 22E). Although not significant, this trend could also be observed for the isotype treated mice. No differences in motile/stationary T cell fractions could be detected when comparing ICI to isotype control treatment (Figure 22E). In absolute numbers, more T cells of both motile and stationary phenotype were observed under ICI treatment, however, differences were not significant due to

strong variability between individual animals and due to the lack of normalization to the observed volume (Figure 22F). Taken together, these findings indicate that antigen recognition at tumor target cells, which is associated with a stationary phenotype (Boissonnas et al., 2007; Kawakami et al., 2005) of intratumoral transferred T cells, happens early after ACT at days 9 and 10.

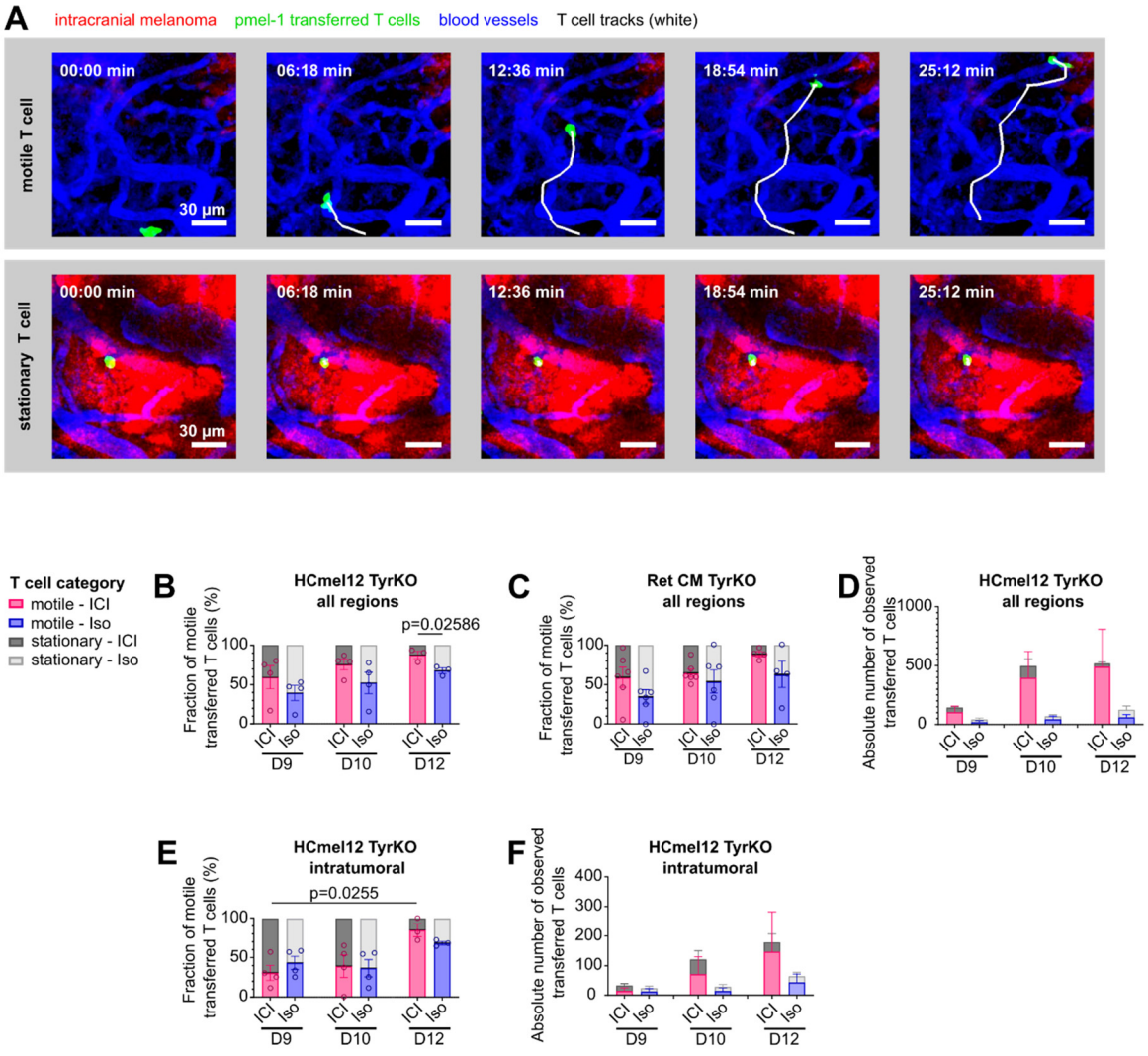

Figure 22: Motile and stationary phenotypes of adoptively transferred T cells in intracranial melanoma

Real-time analysis of T cell motility phenotypes of adoptively transferred pmel-1 T cells in intracranial melanoma measured by IVM and T cell tracking. Semi-automated T cell tracking data was produced jointly with Manuel Piechutta.

(**A**) IVM timeseries images spanning a period of ca. 25 min of one T cell with "motile" phenotype (mean velocity ≥ 50 nm/s and mean displacement ≥10 nm/s, top row) and one with "stationary" phenotype (mean velocity < 50 nm/s and mean displacement <10 nm/s, bottom row). Ret CM TyrKO intracranial melanoma (red), blood vessels (blue), pmel-1 T cells (green), T cell tracks (white), images are shown as MIPs. Scale bars 30 µm.

(**B, C**) Quantification of the percentage of motile and stationary T cells of all regions covered by IVM (intratumoral and peritumoral) in HCmel12 TyrKO (B) and Ret CM TyrKO (C) intracranial melanoma treated with ICI or isotype

control. Statistics were calculated by two-tailed, unpaired *T-test.* (B) Day 9, D10 N=4 mice, D12 N=3 mice. (C) Day 9, D10 N=6 mice, D12 N=4 mice. For n numbers of analyzed T cells per group see Table 15 (B) and Table 16 (C).
(**D**) Absolute number of adoptively transferred pmel-1 T cells observed in all peritumoral and intratumoral regions of HCmel12 TyrKO intracranial melanoma under ICI or control treatment. T cell tracks of N=4 mice per group on day 9 and 10, and of N=3 mice on day 12 were analyzed. For n numbers of analyzed T cells per group see Table 15.
(**E**) Quantification of the fraction of motile and stationary intratumoral T cells in intracranial HCmel12 TyrKO melanoma with and without ICI treatment. Day 9, D10 N=4 mice, D12 N=3 mice, statistics were calculated by two-way ANOVA with Tukey's *post-hoc* test. For n numbers of analyzed T cells per group see Table 17.
(**F**) Absolute numbers of pmel-1 T cells intratumorally in HCmel12 TyrKO intracranial melanoma on days 9, 10, and 12 post cortical TI. T cell tracks of N=4 mice per group on day 9 and 10, tracks of N=3 mice on day 12 analyzed. For n numbers of analyzed T cells per group see Table 17.

Next, I used semi-automated T cell tracking in three-dimensional real-time timeseries IVM images of intratumoral regions and of regions surrounding the intracranial melanoma brain tumor. I distinguished between motile and stationary T cells, and I analyzed the motility parameters mean velocity (track length/time), mean displacement (track displacement/time) and track straightness (track displacement/track length) of only motile T cells (Figure 23A-F).

T cell mean velocity and mean displacement were significantly higher under ICI treatment as compared to isotype control treatment in both tumor models (Figure 23A, B, D, E). The parameter indicating direct T cell movement, track straightness, was also significantly increased under ICI compared to control treatment, but at distinct timepoints in the two tumor models (Figure 23C, F). These findings suggest that ICI treatment facilitates T cell migration in the brain by increasing overall T cell motility and supports the capacity for directed movement.

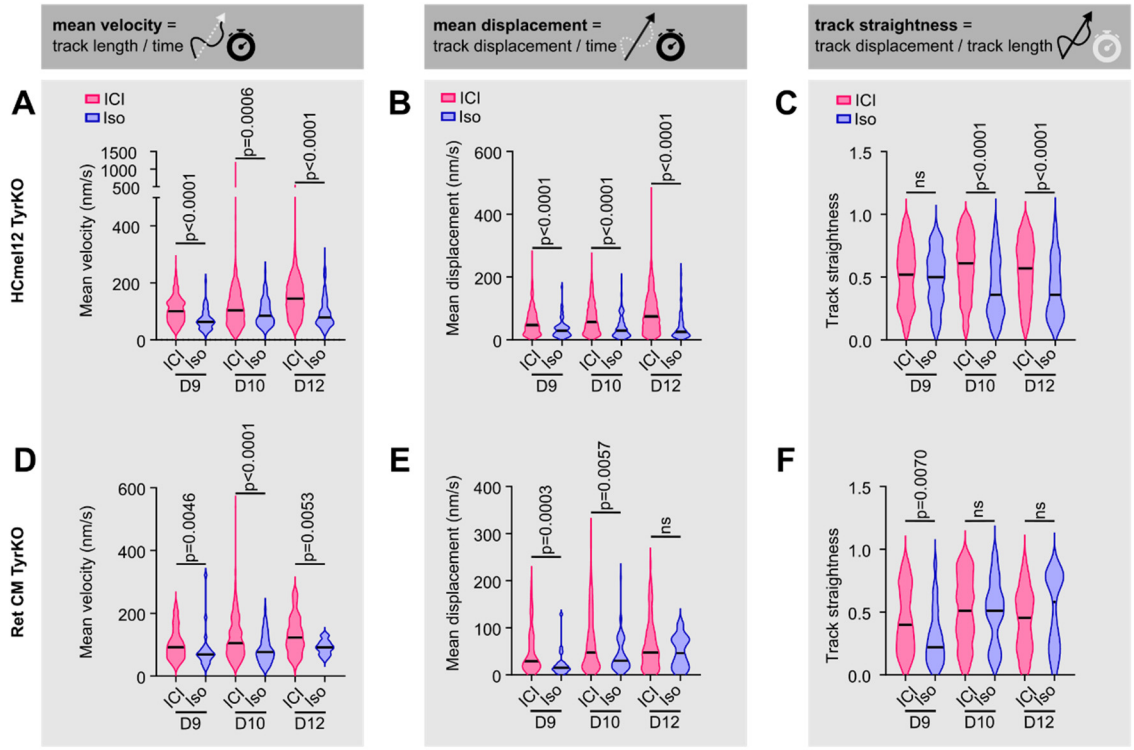

Figure 23: Motility parameters of motile T cells in intracranial melanoma under ICI treatment

Semi-automated T cell tracking data was produced jointly with Manuel Piechutta.

(**A, B, C**) Quantification of motility parameters of motile pmel-1 T cells in intracranial HCmel12 TyrKO melanoma measured by IVM depicted as violin plots of mean velocity (track length/time) (A), mean displacement (track displacement/time) (B) and track straightness (track displacement/track length) (C) from all intratumoral and peritumoral regions combined on days 9, 10, and 12 post TI while under ICI or isotype control treatment. Statistics were calculated by Mann-Whitney tests per timepoint; N=4 mice per group on day 9 and 10, N=3 mice per group on day 12. Black bars represent medians. For n numbers of analyzed T cells per group see Table 18.

(**D, E, F**) Violin plots of mean velocity (D), mean displacement (E) and track straightness (F) of pmel-1 transferred T cells categorized as motile as a total of all intratumoral and peritumoral regions of Ret CM TyrKO intracranial melanoma on days 9, 10, and 12 post TI treated with ICI or isotype control. Statistics were calculated by Mann-Whitney test between ICI and isotype control per timepoint, black bars represent medians, T cell tracks of N=6 mice per group on day 9 and 10, T cell tracks of N=4 mice per group on day 12 were analyzed. For n numbers of analyzed T cells per group see Table 19.

3.12 Perivascular spaces of PVVs are sites of high T cell motility

Previous studies have highlighted the importance of the lymphocyte location and their microenvironmental properties on T cell migration ability (Boissonnas et al., 2013; Bougherara et al., 2015). Therefore, to include the spatial effect on T cell motility and ICI treatment in the brain tumor context, T cell motility parameters of motile transferred T cells were compared at different brain and tumor regions in HCmel12 TyrKO intracranial melanoma. T cell tracks located at PVVs and at PVV-

associated peritumoral regions exhibited the highest values of mean velocity and mean displacement. The closer the T cells were located to the tumor, however, their mean velocity and displacement were decreasing (Figure 24A-C). This spatial effect could be observed in both treatment groups. Directed T cell movement, as measured by track straightness was increased under ICI treatment at the tumor edge, suggesting that ICI facilitates directed movement to the tumor target cells in the brain (Figure 24D).

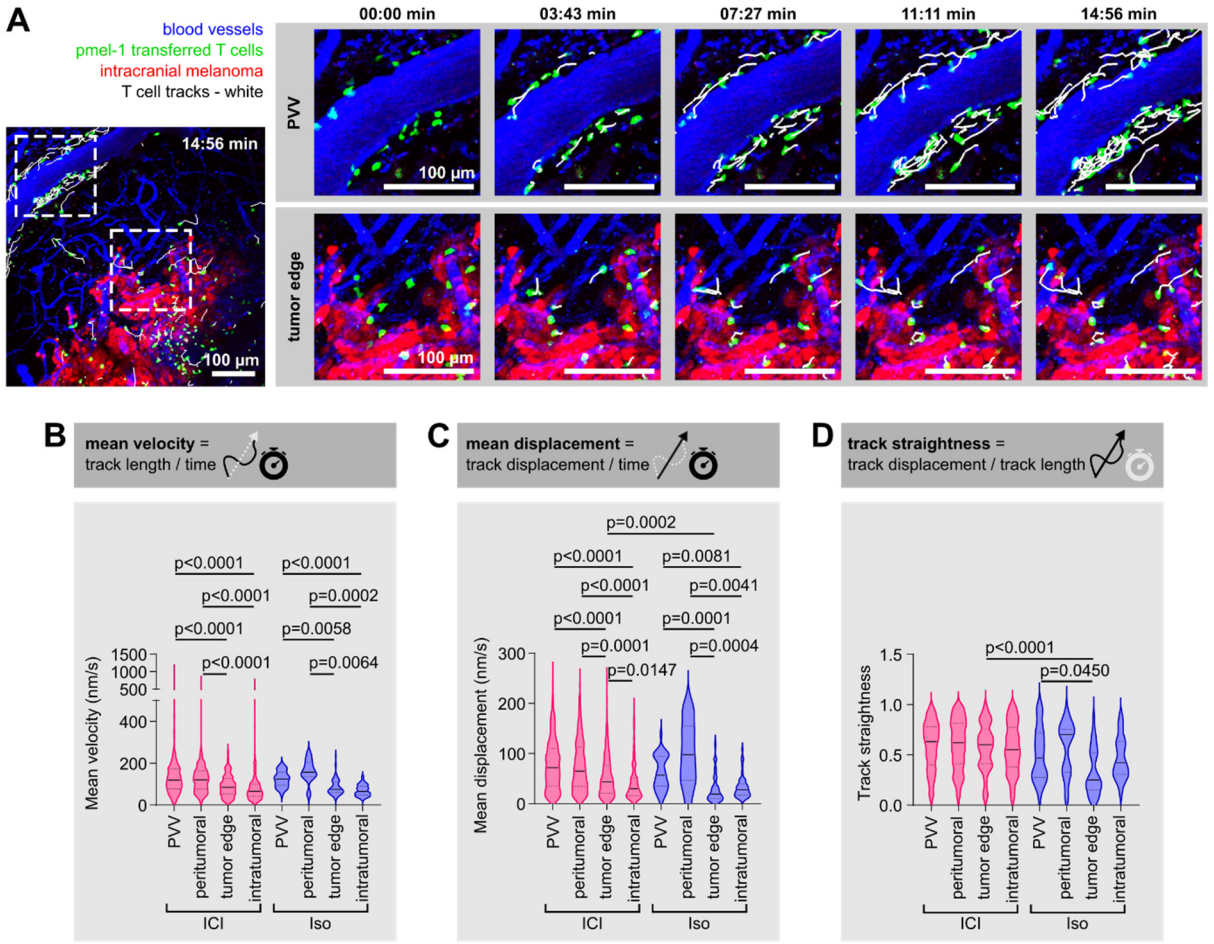

Figure 24: Spatiotemporal effect on T cell motility parameters

(**A**) IVM timeseries images over a period of 14:56 min of pmel-1 T cells (green) and their tracks (white) at day 10 post cortical tumor injection at a PVV and at the tumor edge of HCmel12 TyrKO intracranial melanoma (red) treated with ICI, blood vessels (blue). Regions shown in higher magnification over time (right) are indicated on the overview image (left) as dashed boxes. Images are shown as MIPs.

(**B, C, D**) Quantification of T cell motility parameters mean velocity (B), mean displacement (C), and track straightness (D) of motile pmel-1 T cells in different regions (PVV, peritumoral, tumor edge, intratumoral) of intracranial HCmel12 TyrKO melanoma on day 10 post cortical tumor injection treated with ICI or isotype control. Statistics were calculated by Kruskal-Wallis test with Dunn's *post-hoc* test, N=4 mice per group, black bars represent medians, dotted lines represent quartiles. For n numbers of analyzed T cells per group see Table 20. Semi-automated T cell tracking data was produced jointly with Manuel Piechutta.

4 Discussion

In summary, the data presented in this work, shows that PVVs provide sites for T cells to enter the brain, allowing T cell extravasation from the blood (Figure 16A, B), which is a prerequisite for T cell recruitment to the brain tumor. T cells located next to PVVs migrate at a fast pace (Figure 22A-F) to travel from the site of extravasation to the brain tumor (Figure 24A-C). Thus, PVVs are exploited in multiple ways for T cell recruitment to intracranial tumors. Importantly, I found that this major T cell route to the brain tumor can be used much more efficiently under ICI treatment, as compared to control treatment, which in turn results in increased T cell infiltration (Figure 8 E, F). Finally, molecular characterization of PVVs revealed that ICAM-1 is expressed on the PVV endothelium. Inhibition of ICAM-1 *in vivo* results in a trend of reduced T cell recruitment to the brain tumor and of impaired ICI-mediated tumor growth inhibition (Figure 19A, D, E, Figure 20B, D). Increasing the number of T cells in the tumor is associated with more effective cytotoxic effects on tumor cells (Figure 10A-C) and consequently overall inhibition of intracranial tumor growth (Figure 8A-D, Figure 13B-D).

4.1 Establishment of suitable brain metastasis tumor models

The establishment of reliable mouse models for studying intracranial melanoma growth and simultaneously, T cell infiltration over time was crucial for the work presented here. Developing syngeneic models based on intracortical injection of murine melanoma cell lines allowed the development of large, well established brain tumors. Adoptive transfer of labeled T cells allowed visualization of a well specified cell population, while in transgenic LCK-Cre x LSL-tdTomato mice, the dynamic of all cells of the T cell lineage could be traced. Others have used similar transgenic models for analyzing immune cell populations, mostly of innate immune cells, in brain tumor models by IVM. For example dynamics of microglia during glioma (Bayerl et al., 2016) or lung cancer brain metastasis (W. Zhang et al., 2021) development were studied by IVM in CX3CR1-GFP$^{GFP/wt}$ mice. Others have used an inducible model to trace brain-resident macrophages in Cx3cr1:CreERT2-IRES-YFP;Rosa26:lslTdTomato mice, which express tdTomato in macrophages upon tamoxifen induction, and visualized the recruitment of peripheral immune cells to the brain using a Flt3:Cre based transgenic mouse line (Zomer et al., 2022). Within the field of brain metastasis research, it is under debate whether cortically injected brain tumor models represent a relevant model for metastatic disease (Miarka & Valiente, 2021). Intracranially injected brain tumors do not undergo the brain metastatic cascade that involves survival in the circulation, tumor cell arrest within brain capillaries, tumor cell extravasation, and outgrowth from micrometastases to macrometastases within the brain

parenchyma (Kienast et al., 2010). For studying steps of the brain metastatic cascade, intracardiac injection is a commonly used model (M. Valiente et al., 2020).

Attempts to establish a syngeneic model based on intracardiac injection by increasing brain tropism of a murine tumor cell line by *in vivo* passaging unfortunately failed to result in large macrometastatic growth (Figure 5). Others have also faced this difficulty; in most attempts of brain passaging of murine cell lines in syngeneic hosts following intracardiac injection, humane endpoints were reached due to extracranial tumor development before brain macro metastases could form (Miarka & Valiente, 2021). Even though patient-derived models of brain-metastases exist, including those that form metastases following intracardiac injection, xenograft models were not used for this work. This is because the use of human cell lines would have required immunodeficient mice as hosts (Manuel Valiente et al., 2020). However, the use of syngeneic tumor models was essential for studying recruitment of circulating lymphocytes to the brain tumor. Due to the complex interplay of systemic factors, such as cytokines and chemokines produced by cells of the innate and adaptive immune system, modelling of T cell recruitment from the circulation would not have represented the human situation in immunodeficient mouse models adequately. Furthermore, considering that even the presence of an extracranial tumor was necessary to induce sufficient lymphocyte recruitment in the syngeneic models (Taggart et al., 2018), it would even have been questionable if T cell recruitment from the circulation to a xenografted brain tumor would be successful. As seen in the work of Mulazzani et al., xenograft models required intracerebral application of transferred CAR T cells to elicit an effective immune response (Mulazzani et al., 2019), and thus could not be used to model T cell homing from the circulation. Therefore, I established syngeneic melanoma brain tumor models based on direct intracortical injection, which could successfully be used to study T cell recruitment to the brain by IVM.

To closely model the patient situation a combination of an intracranial and extracranial tumor was injected in the mouse models of intracranial melanoma. Previous studies indicate that tumor antigens present at extracranial locations are important for T cell activation outside of the brain (Song et al., 2020; Taggart et al., 2018). Furthermore, evidence was presented that ICI treatment acts on these activated T cells extracranially, releasing them for recruitment to the brain (Taggart et al., 2018). My findings in this work resonate well with these previous studies, as I could show that ICI treatment facilitates the T cell recruitment process through PVVs resulting in efficient intracranial anti-tumor-immunity. In patients, surgical removal of the primary melanoma lesion is usually the first step of melanoma therapy, so that the primary tumor is no longer present when brain metastases occur. However, as the immune system has had a chance to recognize melanoma antigens before tumor removal, it is conceivable that the primary tumor could have induced an immune response. In mouse models of melanoma it could be shown that melanoma antigen specific skin-resident memory T cells

remain in the skin after surgical removal of the tumor and mediate durable protection (Malik et al., 2017; Park et al., 2019). For translating the extracranial immune activation necessary for efficient T cell recruitment to the brain tumor to the clinic, an approach mimicking the antigenic presence extracranially would be beneficial. Therefore, it would be interesting to further investigate if this extracranial priming could also be achieved and by substituting the presence of an extracranial tumor with a peptide- (Reed et al., 2015) or mRNA-based (Sahin et al., 2017) cancer vaccine (Blass & Ott, 2021) and how this might influence intracranial response to ICI. Similarly, another interesting question, but more controversial, would be whether, and how, the presence of an extracranial tumor-antigenic source – be it extracranial tumor growth or a vaccination approach – would influence immunotherapy response in primary brain tumors, such as gliomas.

4.2 Differences in immunogenicity between ACT and transgenic tumor models

The adoptive transfer of antigen specific T cells can be considered a therapeutic intervention itself, and its efficacy against melanoma has been proven in preclinical and clinical studies (Nguyen et al., 2019; Overwijk et al., 2003; Rosenberg & Restifo, 2015; Rosenberg et al., 2011). Therefore it is surprising to see very similar intracranial tumor growth kinetics of HCmel12 TyrKO intracranial tumors in C57BL/6 mice treated with ICI and ACT (Figure 8C) as compared to HCmel12 TyrKO brain tumors in LCK-Cre x LSL-tdTomato mice only treated with ICI (Figure 13C). Pmel-1 T cell density was associated with microregional tumor regression, which suggest activity of transferred pmel-1 T cells (Figure 10). However, the anti-tumor immunity of the transferred pmel-1 T cells likely was dampened by the reduction in gp100 expression in the TyrKO cell lines (Figure 6A). Moreover, the murine $gp100_{25\text{-}33}$ peptide, which is endogenously expressed by the melanoma cell lines used in this work, has a lower peptide-MHC affinity than the human $gp100_{25\text{-}33}$ peptide (Engels et al., 2013). Therefore, the murine gp100 (mgp100) is recognized by the transgenic $CD8^+$ TCR of pmel-1 T cells, but T cell stimulation is stronger by TCR interaction with human gp100-MHC than with the murine gp100-MHC (Engels et al., 2013). In this work, T cells were stimulated *ex vivo* with the human $gp100_{25\text{-}33}$ peptide, resulting in notable T cell activation prior to ACT (Figure 6B). To increase pmel-1 T cell activity at the tumor target, it would have been necessary to use murine cell lines genetically engineered to express only the human gp100 protein (Effern et al., 2020). However, as the purpose of this work was to investigate mechanisms of T cell recruitment, which I could already observe in the current models, this was not necessary.

A key difference between the two models is the expression of fluorescent proteins of the tumor cell lines. For the ACT model, T cells were labeled with green fluorescence dye, so that this model was paired with red fluorescent tdTomato expressing tumor cell lines. In the transgenic LCK-Cre x LSL-

tdTomato mouse model endogenous T cells were labeled red, so that this model was paired with GFP expressing tumor cells. It has been reported that enhanced GFP is weakly immunogenic in C57BL/6 mice (Skelton et al., 2001). Even slight differences in baseline immunogenicity of GFP and tdTomato might be enhanced under immunotherapy, which might explain the observed similarities of tumor growth kinetics of a potentially more immunogenic GFP expressing tumor cell line in the LCK-Cre x LSL-tdTomato model. Differences in immunogenicity between the two models might also be caused by the distinct mouse lines. Although the founding lines of the LCK-Cre x LSL-tdTomato mouse line had been back-crossed on a C57BL/6 mouse background, there still could remain subtle differences influencing the immune response against the tumor cells. Combined, these methodological parameters could explain why I did not observe an enhanced effect on tumor growth of ACT plus ICI treatment as compared to ICI treatment only in the different models.

4.3 T cell recruitment through non-pathologic blood vessels

The blood vasculature of tumors is strongly altered (Hanahan & Folkman, 1996), as tumors grow co-optively along existing vessels (Bridgeman et al., 2017; Kuczynski et al., 2019), or induce vasculogenesis (Maniotis et al., 1999) or angiogenesis (Folkman et al., 1989; Weidner et al., 1991) to form new, altered vessels. Therefore, tumor associated blood vessels have very pathologic, structurally and functionally abnormal characteristics (Jain et al., 2007; Wang et al., 2010). For example, they appear to be contorted, rather unorganized without a clear distinction between arterial or venous nature and blood flow can be disturbed in these vessels (Jain et al., 2007; Kimura et al., 1996; Yuan et al., 1994). Particularly in primary brain tumors and brain metastasis with large tumor masses, the integrity of the blood-tumor barrier is disturbed, resulting in increased permeability (Fidler et al., 2002; Lyle et al., 2016; Tiwary et al., 2018; Winkler et al., 2004; Zhang et al., 1992). In non-pathological conditions, most chemotherapeutic agents used for cancer treatment are not able to cross the blood-brain barrier and drug compounds can even actively be effluxed from the brain (Agarwal et al., 2010; Kim et al., 2019; Sprowls et al., 2019). Although heterogenous leakiness of the blood-tumor barrier in experimental models of breast cancer brain metastasis resulted in increased distribution of chemotherapeutic agents in the brain tumors as compared to healthy brain, cytotoxic concentrations were not reached in most cases (Lockman et al., 2010). Several recent approaches for improving therapeutic options for brain tumor patients include further disrupting the blood-tumor barrier and blood-brain barrier to increase drug distribution within the brain (Arvanitis et al., 2018; Kovacs et al., 2017; Sprowls et al., 2019; Zhao et al., 2018). Some of these approaches are based on brain radiation therapy, which induces apoptosis of endothelial cells (Peña et al., 2000; Peña et al., 2000) and can lead to increased neuroinflammation (Yuan et al., 2003). These studies suggest that the disruption of the blood-brain

barrier could also be linked to increased leukocyte infiltration into the brain. However, the data presented in this work proposes a different mechanism for T cell recruitment through seemingly normal peritumoral vessels, but not through strongly pathologic, leaky tumor microvessels. Therefore, it is tempting to hypothesize that normalization of the blood vasculature by anti-angiogenic therapy (de Groot et al., 2010; Jain, 2005; Stegmayr et al., 2017), might be beneficial in combination with immunotherapeutic approaches for the treatment of brain metastases. For the treatment of glioblastoma, a recent preclinical study has even applied this strategy by normalizing glioblastoma vascularity through inhibition of p21-activated kinase 4, which resulted in increased vascular expression of adhesion molecules such as ICAM-1 and improved chimeric antigen receptor T cell based immunotherapy (Ma et al., 2021).

4.4 Interdependency of brain blood vessels and anti-tumor immunity

Previous studies on experimental models of extracranial tumors have demonstrated that the presence of high endothelial venules is associated with immune cell infiltration and response to immune checkpoint blockade (Allen et al., 2017; Asrir et al., 2022). However, PNAd, the marker for high endothelial venules, could not be detected on vessels within and peritumoral of tumors of HCmel12 intracranial melanoma treated with ICI in this work. This indicates that ICI-mediated T cell infiltration to the brain requires different molecular mechanism than T cell recruitment to extracranial tumors. In support of this, Allen et al. could show that combinatorial treatment of anti-angiogenic (anti-vascular endothelial growth factor receptor 2, anti-VEGFR2) and anti-PD-L1 antibodies induce HEVs in extracranial tumor models, but not in a model of glioblastoma. In their study, treatment with a lymphotoxin β receptor agonist was able to induce HEV formation in glioblastoma, thus sensitizing tumors to the combination of VEGFR2 and PD-L1 inhibition (Allen et al., 2017). Whether this difference between glioblastoma and extracranial tumors is caused by the distinct features of the brain microenvironment, or whether it is a distinction of primary brain tumors, and how it compares to metastatic brain tumors remains to be uncovered. In parallel to my findings, the presence of HEVs could not be detected by immunohistochemical analysis in human breast cancer brain metastasis (Karpathiou et al., 2021). These studies, combined with the current work, highlight how strongly intertwined yet complexly regulated tumor vascularization and anti-tumor immunity are and provide first experimental hints that treatment combinations targeting both tumor vessels and immune checkpoints might benefit the treatment of brain metastasis.

4.5 Role of meningeal lymphatic vessels for the recruitment of T cells

The breakthrough discoveries of meningeal lymphatic vessels have tremendously improved our understanding of brain immune surveillance (Aspelund et al., 2015; Louveau et al., 2015). Lymphatic vessels could however not be visualized in the models applied in this work. The surgical procedure of implanting a chronic cranial window includes removal of the dura from most part of the cranial window area. However, along the sagittal venous sinus, the dura and the underlying sinusoidal vasculature are relatively tightly connected, so that during the cranial window operation the dura above the sagittal sinus cannot be removed but is cut in parallel to the sinus on each hemisphere. Considering the description of the location of the meningeal lymphatic vasculature running closely in parallel to the sagittal sinus (Aspelund et al., 2015; Louveau et al., 2015), it can be assumed that the lymphatic vasculature remains mostly intact after the surgical implantation of a chronic cranial window. Rustenhoven et al. could not only identify the perisinusoidal space as sites of brain-derived antigen exposure and presentation through APCs to patrolling T cells, but they could also observe T cell extravasation under homeostatic conditions from the dural sinuses by intravital microscopy of craniotomized mice. They found events of T cell adhesion and extravasation mainly at the vasculature of dural sinuses, and to a lesser extent at larger veins draining into the sinuses (Rustenhoven et al., 2021). The intravital imaging data of T cell distribution in the non-tumor bearing brains of LCK-Cre x LSL-tdTomato mice presented in this work reflect these findings well, as T cell accumulation could also be observed preferentially in the perisinusoidal space under homeostatic conditions (Figure 17). This supports the assumption that the surgical procedure of chronic cranial window implantation does not damage the meningeal vasculature in a way that homeostatic immune surveillance by T cells is impaired. Interestingly, in the presence of an intracranial tumor, PVVs seem to gain importance for T cell recruitment, exceeding the sagittal venous sinus in terms of perivascular T cell accumulation. Therefore, it can be assumed that under tumor-induced inflammatory conditions, enhanced by ICI treatment, pathways of T cell recruitment to the brain differ from the homeostatic immune surveillance. How this change is induced by inflammation and how it could be manipulated is still unclear and represent interesting subjects for further experimental investigation.

4.6 Immune cell recruitment from skull bone marrow

Recent studies have collected evidence of a direct connection between the skull bone marrow and the brain meninges by vascular channels (Cai et al., 2019; Herisson et al., 2018; Yao et al., 2018). These microscopic channels were associated with myeloid cell migration in an experimental model of stroke (Cai et al., 2019; Herisson et al., 2018) and could even be exploited by acute lymphoblastic leukemia cells to invade the CNS and form meningeal metastases (Yao et al., 2018). Cugurra et al. could show

that under homeostatic conditions these channels provide structures that can be used as a scaffold for myeloid cell migration from a bone marrow reservoir in the adjacent skull directly to the brain meninges, thus circumventing crossing of the blood-brain barrier through recruitment from the blood (Cugurra et al., 2021). However, recruitment of T cells via these skull-meningeal connections could neither be observed during homeostasis nor during experimental neuroinflammation as in EAE (Cugurra et al., 2021). Whether this could be similar in the brain tumor context or if the bone marrow might also yield a reservoir of lymphocytes ready for recruitment under certain inflammatory conditions, is another open question. As the models for *in vivo* imaging used in this thesis work included the removal of the skull for the implantation of a chronic cranial window, these questions could not be addressed by this methodology. Although I demonstrated that effective T cell infiltration into the melanoma brain tumor occurs via PVVs, it still has to be taken into account that the removal of the skull might have indirect effects on T cell recruitment, by possibly altering the meningeal myeloid cell composition.

4.7 Interpreting T cell motility

In vivo and *ex vivo* time-lapse imaging studies have been crucial to better understand T cell motility and how it is influenced by different stimuli (Boissonnas et al., 2007; Bougherara et al., 2015; Breart et al., 2008; Deguine et al., 2010; Lau et al., 2020; Mrass et al., 2006; Peranzoni et al., 2018). However, it is quite challenging to interpret T cell motility behavior correctly. It is well recognized that engagement of the TCR with its cognate antigen leads to a halt in T cell migration (Dustin et al., 1997); a process necessary for the T cell to engage in stable immune synapses with antigen presenting cells, which in turn is fundamental for T cell activation (Bousso & Robey, 2003; Hugues et al., 2004; Miller et al., 2002). Imaging studies, conducted to elucidate the function of CTLA-4, have revealed that stimulation of CTLA-4 signaling by ligation leads to increased T cell motility and reduced dwell times at APCs (Schneider et al., 2006; Schneider et al., 2008). Based on these observations, the "reverse stop-signal model" was proposed for CTLA-4 function, describing how CTLA-4 signaling overrides the TCR-stop signal, preventing T cell activation (Rudd, 2008). However, another *in vivo* imaging study in a mouse model of extracranial melanoma, treated with anti-CTLA-4 inhibitory antibody in combination with a tumor vaccination approach, has revealed opposing effects of CTLA-4 inhibition on T cell motility (Pentcheva-Hoang et al., 2014). In this work, the authors demonstrated that CTLA-4 inhibition increased T cell motility at the tumor and also within the draining lymph node, which was associated with therapy response (Pentcheva-Hoang et al., 2014). A more recent study has focused on analyzing T cell motility behavior under anti-PD-1/anti-CTLA-4 ICI in a mouse model of primary melanoma (Lau et al., 2020). The authors report diverse migratory patterns of T cells in all treatment groups, while T

cells in the tumor periphery travelled with higher velocities than intratumorally, and ICI treatment increased the proportion of T cell with slower migration and more confined movements, supposedly engaging with their target cells (Lau et al., 2020). By conveying yet another picture of the effect of ICI on T cell motility, this study highlights the necessity to closely evaluate the spatiotemporal context of the observed T cells for properly interpreting T cell motility behavior. In order to avoid skewing the effect of ICI on T cell motility by mixing different functional T cell states in one analysis, I have strictly separated two distinct functional T cell phenotypes (Kawakami et al., 2005), namely "motile" and "stationary" in the work presented here – "Motile" T cells representing T cells during antigen-search phase, and "stationary" representing T cells that likely have engaged the tumor with stable immune-synaptic contacts. Importantly, this work shows that ICI-supported increase in T cell motility, as in accordance with the findings of Pentcheva-Hoang et al., does not seem to override the TCR-stop signal, which is crucial for stable T cell engagement with their target cells. Although ICI treatment increased T cell motility, spatial analysis revealed, that this effect seemed to mostly occur at PVVs, or in the tumor periphery, where T cells are on their way from extravasation towards the brain tumor. Furthermore, analysis of the fraction of T cells with stationary or motile phenotypes showed that under ICI treatment, especially at early timepoints after the ACT, a substantial proportion of stationary T cells could be detected intratumorally (Figure 22E).

4.8 The role of chemokine gradients on T cell recruitment to brain tumors

Under distinct timepoints during ICI I observed an increase in track straightness, indicating directed T cell motility. This leads to the assumption that chemokine gradients might play a role in T cell recruitment in the brain. It might even be conceivable that chemokine gradient distribution is dependent on perivascular spaces of PVVs, however, this was not addressed in this work. Previously it has been described that the chemokines CXCL9 and CXCL10, produced by inflamed brain endothelium, play a critical role in T cell recruitment to the brain in mouse models of experimental cerebral malaria (Sorensen et al., 2018). Staining attempts for CXCR3, the mutual receptor of these two chemokines, unfortunately were not successful and are thus not displayed here. The role of CXCL9 and CXCL10 for T cell recruitment in these models could therefore not be evaluated in these models. Further experimental approaches, for example flow-cytometry based quantification of chemokine-receptor expression or intracellular chemokine staining would be necessary to elucidate their contributions.

4.9 Molecular factors important for T cell recruitment through PVVs

Although functional ICAM-1 blocking under ICI treatment did not have a significant effect on brain tumor growth inhibition and T cell infiltration, I did observe a clear trend toward mitigation of tumor

growth inhibition and reduction of T cell infiltration under ICAM-1 blockage (Figure 20). Therefore, it can be suspected, that ICAM-1 plays an important role for ICI-enhanced T cell recruitment to brain tumors. However, it is very likely that ICAM-1 is not the only molecular player orchestrating and facilitating T cell recruitment to the brain. Other molecules might be able to compensate ICAM-1 function, so that ICAM-1 blockade only partially inhibits T cell recruitment. The gain in knowledge provided by this work, i.e. that T cell extravasation for recruitment to the brain happens mainly at very distinct sites of ICAM-1 expressing peritumoral venous vessels, might help to determine other molecular factors expressed on inflamed endothelium in the brain tumor setting. Another promising approach to identify other molecular players, co-expressed with ICAM-1, is the use of single cell RNA sequencing of specifically this ICAM-1 high, peritumoral venous endothelial cell population of ICI treated brain tumors. Based on the dynamics of T cell infiltration, an optimal timepoint can be selected to harvest and sequence this cell population. By narrowing down to ICAM-1 positive venous endothelial cells, this might allow to identify other, possibly brain-specific molecular factors important for T cell recruitment to the brain. This could reveal potential new candidates for therapeutic targeting, either to prevent T cell infiltration to the brain as in autoimmunity or therapy side effects, or to enhance it for immunotherapeutic treatment of brain tumors.

Single cell RNA and TCR sequencing has mainly been used to characterize the immune microenvironment of human brain metastasis patients (Alvarez-Breckenridge et al., 2022; Gonzalez et al., 2022). A correlation between T cell clonality in the brain with its matched peripheral blood counterpart in response to ICI was found, thus suggesting a strong cross-talk between peripheral and intracranial T cell populations in patients (Alvarez-Breckenridge et al., 2022). Combining single cell sequencing with the spatiotemporal information of T cell infiltration in mouse models could further contribute to uncover the underlying molecular mechanism important for the routes of T cell recruitment via PVVs as described in this work. As a first approach in this direction, in a collaborative effort with Dr. Varun Venkataramani, the single cell sequencing dataset of patient brain metastases biopsies published by Gonzalez et al. was analyzed *in silico* (Gonzalez et al., 2022). This revealed expression of ICAM-1 mainly on venous endothelial cells of breast and lung cancer brain metastasis patients, and on both venous and arterial endothelial cells of melanoma brain metastasis patients. ICAM-1 expression was heterogenous within the endothelial cell subpopulation, possibly reflecting that only a certain subset might share PVV characteristics (data not yet published, and not shown here).

4.10 PVVs as an entry-route to intracranial melanoma – translation to the clinical setting

Studying the dynamic of T cell infiltration over an extended period of time within a living organism could only be accomplished in animal models. Although studies on T cell motility have been conducted in patient-derived acute tissue slices, these approaches only allowed the analysis during a particular short time frame and were not conducted on brain tumor tissue (Bougherara et al., 2015; Peranzoni et al., 2018; You et al., 2021). Since the work presented here is solely based on murine models, the question arises whether T cell recruitment via PVVs is only specific to mouse, or whether it can be translated to human brain tumors. To answer these questions, I have established a collaboration with Dr. Rebekka Wehner (Institut für Immunologie, TU Dresden) and Dr. Dana Westphal (Universitätsklinikum Dresden) to perform multi-parametric immunofluorescence staining of patient-derived human brain metastasis tissue. Through this collaboration, we could demonstrate that examples of peritumoral vessels expressing ICAM-1 could also be found in several melanoma brain metastasis patients (data not yet published and not presented in this work). These findings support that PVVs might be exploited for T cell recruitment to the brain both in mice and human melanoma brain metastases.

4.11 Conclusion and Outlook

Uncovering of the long-term dynamics of T cell recruitment to the brain within a living organism was possible due to the successful establishment of several *in vivo* models for intravital imaging of intracranial melanoma growth and T cell infiltration based on transgenic mouse lines and adoptive T cell transfer. I could show that very distinct, pre-existing, venous vessels in the tumor periphery, provide structures within the brain, which can be exploited for T cell recruitment to melanoma brain tumors. PVVs harbor sites of T cell extravasation and enable fast T cell trafficking in their perivascular space. ICI treatment facilitates the exploitation of this pathway, which leads to intracranial tumor growth control associated with high intracranial T cell infiltration. Moreover, I could correlate intraluminal ICAM-1 staining on PVVs to the T cell density in the adjacent perivascular space. Functional blocking of ICAM-1 partially inhibited T cell recruitment and brain tumor growth-control under ICI treatment. This work contributes profoundly to a general understanding of T cell homing dynamics to melanoma brain tumors. Moreover, revealing that seemingly “normal” vasculature of certain peritumoral vessels is important for T cell recruitment, could reinvigorate the idea of combining therapeutic approaches for the treatment of brain metastasis patients, e.g. targeting of tumor associated vasculature and immunotherapeutics. More pre-clinical research is needed to assess this

approach and find suitable combinations and treatment regimens. Moreover, the knowledge gained from this work might reveal new leverage points for further research to identify more molecular co-factors of PVV-associated ICAM-1. In this way, novel, potentially brain-specific molecules might be identified, which could be pharmacologically targetable to enhance lymphocyte recruitment to the brain and thus improve therapy for brain metastasis patients.

5 References

Achar, S. R., Bourassa, F. X. P., Rademaker, T. J., Lee, A., Kondo, T., Salazar-Cavazos, E., Davies, J. S., Taylor, N., François, P., & Altan-Bonnet, G. (2022). Universal antigen encoding of T cell activation from high-dimensional cytokine dynamics. *Science*, *376*(6595), 880-884. https://doi.org/doi:10.1126/science.abl5311

Agarwal, S., Sane, R., Gallardo, J. L., Ohlfest, J. R., & Elmquist, W. F. (2010). Distribution of gefitinib to the brain is limited by P-glycoprotein (ABCB1) and breast cancer resistance protein (ABCG2)-mediated active efflux. *The Journal of pharmacology and experimental therapeutics*, *334*(1), 147-155. https://doi.org/10.1124/jpet.110.167601

Agrawal, S., Anderson, P., Durbeej, M., van Rooijen, N., Ivars, F., Opdenakker, G., & Sorokin, L. M. (2006). Dystroglycan is selectively cleaved at the parenchymal basement membrane at sites of leukocyte extravasation in experimental autoimmune encephalomyelitis. *J Exp Med*, *203*(4), 1007-1019. https://doi.org/10.1084/jem.20051342

Ahmadzadeh, M., Johnson, L. A., Heemskerk, B., Wunderlich, J. R., Dudley, M. E., White, D. E., & Rosenberg, S. A. (2009). Tumor antigen-specific CD8 T cells infiltrating the tumor express high levels of PD-1 and are functionally impaired. *Blood*, *114*(8), 1537-1544. https://doi.org/10.1182/blood-2008-12-195792

Ahn, J. H., Cho, H., Kim, J.-H., Kim, S. H., Ham, J.-S., Park, I., Suh, S. H., Hong, S. P., Song, J.-H., Hong, Y.-K., Jeong, Y., Park, S.-H., & Koh, G. Y. (2019). Meningeal lymphatic vessels at the skull base drain cerebrospinal fluid. *Nature*, *572*(7767), 62-66. https://doi.org/10.1038/s41586-019-1419-5

Alexander, S., Koehl, G. E., Hirschberg, M., Geissler, E. K., & Friedl, P. (2008). Dynamic imaging of cancer growth and invasion: a modified skin-fold chamber model. *Histochem Cell Biol*, *130*(6), 1147-1154. https://doi.org/10.1007/s00418-008-0529-1

Alexandrov, L. B., Nik-Zainal, S., Wedge, D. C., Aparicio, S. A. J. R., Behjati, S., Biankin, A. V., Bignell, G. R., Bolli, N., Borg, A., Børresen-Dale, A.-L., Boyault, S., Burkhardt, B., Butler, A. P., Caldas, C., Davies, H. R., Desmedt, C., Eils, R., Eyfjörd, J. E., Foekens, J. A., Greaves, M., Hosoda, F., Hutter, B., Ilicic, T., Imbeaud, S., Imielinski, M., Jäger, N., Jones, D. T. W., Jones, D., Knappskog, S., Kool, M., Lakhani, S. R., López-Otín, C., Martin, S., Munshi, N. C., Nakamura, H., Northcott, P. A., Pajic, M., Papaemmanuil, E., Paradiso, A., Pearson, J. V., Puente, X. S., Raine, K., Ramakrishna, M., Richardson, A. L., Richter, J., Rosenstiel, P., Schlesner, M., Schumacher, T. N., Span, P. N., Teague, J. W., Totoki, Y., Tutt, A. N. J., Valdés-Mas, R., van Buuren, M. M., van 't Veer, L., Vincent-Salomon, A., Waddell, N., Yates, L. R., Zucman-Rossi, J., Andrew Futreal, P., McDermott, U., Lichter, P., Meyerson, M., Grimmond, S. M., Siebert, R., Campo, E., Shibata, T., Pfister, S. M., Campbell, P. J., Stratton, M. R., Australian Pancreatic Cancer Genome, I., Consortium, I. B. C., Consortium, I. M.-S., & PedBrain, I. (2013). Signatures of mutational processes in human cancer. *Nature*, *500*(7463), 415-421. https://doi.org/10.1038/nature12477

Alieva, M., Ritsma, L., Giedt, R. J., Weissleder, R., & van Rheenen, J. (2014). Imaging windows for long-term intravital imaging: General overview and technical insights. *Intravital*, *3*(2), e29917-e29917. https://doi.org/10.4161/intv.29917

Allen, E., Jabouille, A., Rivera, L. B., Lodewijckx, I., Missiaen, R., Steri, V., Feyen, K., Tawney, J., Hanahan, D., Michael, I. P., & Bergers, G. (2017). Combined antiangiogenic and anti–PD-L1

therapy stimulates tumor immunity through HEV formation. *Science Translational Medicine*, *9*(385), eaak9679. https://doi.org/doi:10.1126/scitranslmed.aak9679

Alon, R., Kassner, P. D., Carr, M. W., Finger, E. B., Hemler, M. E., & Springer, T. A. (1995). The integrin VLA-4 supports tethering and rolling in flow on VCAM-1. *J Cell Biol*, *128*(6), 1243-1253. https://doi.org/10.1083/jcb.128.6.1243

Alvarez-Breckenridge, C., Markson, S. C., Stocking, J. H., Nayyar, N., Lastrapes, M., Strickland, M. R., Kim, A. E., de Sauvage, M., Dahal, A., Larson, J. M., Mora, J. L., Navia, A. W., Klein, R. H., Kuter, B. M., Gill, C. M., Bertalan, M., Shaw, B., Kaplan, A., Subramanian, M., Jain, A., Kumar, S., Danish, H., White, M., Shahid, O., Pauken, K. E., Miller, B. C., Frederick, D. T., Hebert, C., Shaw, M., Martinez-Lage, M., Frosch, M., Wang, N., Gerstner, E., Nahed, B. V., Curry, W. T., Carter, B., Cahill, D. P., Boland, G. M., Izar, B., Davies, M. A., Sharpe, A. H., Suva, M. L., Sullivan, R. J., Brastianos, P. K., & Carter, S. L. (2022). Microenvironmental landscape of human melanoma brain metastases in response to immune checkpoint inhibition. *Cancer Immunol Res*. https://doi.org/10.1158/2326-6066.Cir-21-0870

Anderson, K. G., Stromnes, I. M., & Greenberg, P. D. (2017). Obstacles Posed by the Tumor Microenvironment to T cell Activity: A Case for Synergistic Therapies. *Cancer Cell*, *31*(3), 311-325. https://doi.org/https://doi.org/10.1016/j.ccell.2017.02.008

Armulik, A., Genové, G., Mäe, M., Nisancioglu, M. H., Wallgard, E., Niaudet, C., He, L., Norlin, J., Lindblom, P., Strittmatter, K., Johansson, B. R., & Betsholtz, C. (2010). Pericytes regulate the blood–brain barrier. *Nature*, *468*(7323), 557-561. https://doi.org/10.1038/nature09522

Arnold, M., de Vries, E., Whiteman, D. C., Jemal, A., Bray, F., Parkin, D. M., & Soerjomataram, I. (2018). Global burden of cutaneous melanoma attributable to ultraviolet radiation in 2012. *International Journal of Cancer*, *143*(6), 1305-1314. https://doi.org/https://doi.org/10.1002/ijc.31527

Arvanitis, C. D., Askoxylakis, V., Guo, Y., Datta, M., Kloepper, J., Ferraro, G. B., Bernabeu, M. O., Fukumura, D., McDannold, N., & Jain, R. K. (2018). Mechanisms of enhanced drug delivery in brain metastases with focused ultrasound-induced blood-tumor barrier disruption. *Proc Natl Acad Sci U S A*, *115*(37), E8717-e8726. https://doi.org/10.1073/pnas.1807105115

Ascierto, P. A., Napolitano, M., Celentano, E., Simeone, E., Gentilcore, G., Daponte, A., Capone, M., Caracò, C., Calemma, R., Beneduce, G., Cerrone, M., De Rosa, V., Palmieri, G., Castello, G., Kirkwood, J. M., Marincola, F. M., & Mozzillo, N. (2010). Regulatory T cell frequency in patients with melanoma with different disease stage and course, and modulating effects of high-dose interferon-alpha 2b treatment. *J Transl Med*, *8*, 76. https://doi.org/10.1186/1479-5876-8-76

Aspelund, A., Antila, S., Proulx, S. T., Karlsen, T. V., Karaman, S., Detmar, M., Wiig, H., & Alitalo, K. (2015). A dural lymphatic vascular system that drains brain interstitial fluid and macromolecules. *Journal of Experimental Medicine*, *212*(7), 991-999. https://doi.org/10.1084/jem.20142290

Asrir, A., Tardiveau, C., Coudert, J., Laffont, R., Blanchard, L., Bellard, E., Veerman, K., Bettini, S., Lafouresse, F., Vina, E., Tarroux, D., Roy, S., Girault, I., Molinaro, I., Martins, F., Scoazec, J.-Y., Ortega, N., Robert, C., & Girard, J.-P. (2022). Tumor-associated high endothelial venules mediate lymphocyte entry into tumors and predict response to PD-1 plus CTLA-4 combination immunotherapy. *Cancer Cell*. https://doi.org/https://doi.org/10.1016/j.ccell.2022.01.002

Attfield, K. E., Jensen, L. T., Kaufmann, M., Friese, M. A., & Fugger, L. (2022). The immunology of multiple sclerosis. *Nature Reviews Immunology*. https://doi.org/10.1038/s41577-022-00718-z

Barber, D. L., Wherry, E. J., Masopust, D., Zhu, B., Allison, J. P., Sharpe, A. H., Freeman, G. J., & Ahmed, R. (2006). Restoring function in exhausted CD8 T cells during chronic viral infection. *Nature*, *439*(7077), 682-687. https://doi.org/10.1038/nature04444

Bartholomäus, I., Kawakami, N., Odoardi, F., Schläger, C., Miljkovic, D., Ellwart, J. W., Klinkert, W. E. F., Flügel-Koch, C., Issekutz, T. B., Wekerle, H., & Flügel, A. (2009). Effector T cell interactions with meningeal vascular structures in nascent autoimmune CNS lesions. *Nature*, *462*(7269), 94-98. https://doi.org/10.1038/nature08478

Bassani-Sternberg, M., Bräunlein, E., Klar, R., Engleitner, T., Sinitcyn, P., Audehm, S., Straub, M., Weber, J., Slotta-Huspenina, J., Specht, K., Martignoni, M. E., Werner, A., Hein, R., H. Busch, D., Peschel, C., Rad, R., Cox, J., Mann, M., & Krackhardt, A. M. (2016). Direct identification of clinically relevant neoepitopes presented on native human melanoma tissue by mass spectrometry. *Nature Communications*, *7*(1), 13404. https://doi.org/10.1038/ncomms13404

Baumgartner, J., Wilson, C., Palmer, B., Richter, D., Banerjee, A., & McCarter, M. (2007). Melanoma induces immunosuppression by up-regulating FOXP3(+) regulatory T cells. *J Surg Res*, *141*(1), 72-77. https://doi.org/10.1016/j.jss.2007.03.053

Bayerl, S. H., Niesner, R., Cseresnyes, Z., Radbruch, H., Pohlan, J., Brandenburg, S., Czabanka, M. A., & Vajkoczy, P. (2016). Time lapse in vivo microscopy reveals distinct dynamics of microglia-tumor environment interactions—a new role for the tumor perivascular space as highway for trafficking microglia. *Glia*, *64*(7), 1210-1226. https://doi.org/https://doi.org/10.1002/glia.22994

Benichou, G., Gonzalez, B., Marino, J., Ayasoufi, K., & Valujskikh, A. (2017). Role of Memory T Cells in Allograft Rejection and Tolerance [Mini Review]. *Frontiers in Immunology*, *8*. https://doi.org/10.3389/fimmu.2017.00170

Berg, S., Kutra, D., Kroeger, T., Straehle, C. N., Kausler, B. X., Haubold, C., Schiegg, M., Ales, J., Beier, T., Rudy, M., Eren, K., Cervantes, J. I., Xu, B., Beuttenmueller, F., Wolny, A., Zhang, C., Koethe, U., Hamprecht, F. A., & Kreshuk, A. (2019). ilastik: interactive machine learning for (bio)image analysis. *Nature Methods*, *16*(12), 1226-1232. https://doi.org/10.1038/s41592-019-0582-9

Blank, C., Brown, I., Peterson, A. C., Spiotto, M., Iwai, Y., Honjo, T., & Gajewski, T. F. (2004). PD-L1/B7H-1 inhibits the effector phase of tumor rejection by T cell receptor (TCR) transgenic CD8+ T cells. *Cancer Res*, *64*(3), 1140-1145. https://doi.org/10.1158/0008-5472.can-03-3259

Blass, E., & Ott, P. A. (2021). Advances in the development of personalized neoantigen-based therapeutic cancer vaccines. *Nature Reviews Clinical Oncology*, *18*(4), 215-229. https://doi.org/10.1038/s41571-020-00460-2

Bode, K., Bujupi, F., Link, C., Hein, T., Zimmermann, S., Peiris, D., Jaquet, V., Lepenies, B., Weyd, H., & Krammer, P. H. (2019). Dectin-1 Binding to Annexins on Apoptotic Cells Induces Peripheral Immune Tolerance via NADPH Oxidase-2. *Cell Rep*, *29*(13), 4435-4446.e4439. https://doi.org/10.1016/j.celrep.2019.11.086

Boissonnas , A., Fetler , L., Zeelenberg , I. S., Hugues , S. p., & Amigorena , S. (2007). In vivo imaging of cytotoxic T cell infiltration and elimination of a solid tumor. *Journal of Experimental Medicine*, *204*(2), 345-356. https://doi.org/10.1084/jem.20061890

References

Boissonnas, A., Licata, F., Poupel, L., Jacquelin, S., Fetler, L., Krumeich, S., Théry, C., Amigorena, S., & Combadière, C. (2013). CD8+ tumor-infiltrating T cells are trapped in the tumor-dendritic cell network. *Neoplasia (New York, N.Y.)*, *15*(1), 85-94. https://doi.org/10.1593/neo.121572

Bougherara, H., Mansuet-Lupo, A., Alifano, M., Ngô, C., Damotte, D., Le Frère-Belda, M.-A., Donnadieu, E., & Peranzoni, E. (2015). Real-Time Imaging of Resident T Cells in Human Lung and Ovarian Carcinomas Reveals How Different Tumor Microenvironments Control T Lymphocyte Migration [Original Research]. *Frontiers in Immunology*, *6*(500). https://doi.org/10.3389/fimmu.2015.00500

Boulch, M., Grandjean, C. L., Cazaux, M., & Bousso, P. (2019). Tumor Immunosurveillance and Immunotherapies: A Fresh Look from Intravital Imaging. *Trends in Immunology*, *40*(11), 1022-1034. https://doi.org/https://doi.org/10.1016/j.it.2019.09.002

Bousso, P., & Robey, E. (2003). Dynamics of CD8+ T cell priming by dendritic cells in intact lymph nodes. *Nature Immunology*, *4*(6), 579-585. https://doi.org/10.1038/ni928

Breart, B., Lemaître, F., Celli, S., & Bousso, P. (2008). Two-photon imaging of intratumoral CD8+ T cell cytotoxic activity during adoptive T cell therapy in mice. *J Clin Invest*, *118*(4), 1390-1397. https://doi.org/10.1172/jci34388

Bridgeman, V. L., Vermeulen, P. B., Foo, S., Bilecz, A., Daley, F., Kostaras, E., Nathan, M. R., Wan, E., Frentzas, S., Schweiger, T., Hegedus, B., Hoetzenecker, K., Renyi-Vamos, F., Kuczynski, E. A., Vasudev, N. S., Larkin, J., Gore, M., Dvorak, H. F., Paku, S., Kerbel, R. S., Dome, B., & Reynolds, A. R. (2017). Vessel co-option is common in human lung metastases and mediates resistance to anti-angiogenic therapy in preclinical lung metastasis models. *J Pathol*, *241*(3), 362-374. https://doi.org/10.1002/path.4845

Brody, J. R., Costantino, C. L., Berger, A. C., Sato, T., Lisanti, M. P., Yeo, C. J., Emmons, R. V., & Witkiewicz, A. K. (2009). Expression of indoleamine 2,3-dioxygenase in metastatic malignant melanoma recruits regulatory T cells to avoid immune detection and affects survival. *Cell Cycle*, *8*(12), 1930-1934. https://doi.org/10.4161/cc.8.12.8745

Bullard, D. C., Hu, X., Schoeb, T. R., Collins, R. G., Beaudet, A. L., & Barnum, S. R. (2007). Intercellular adhesion molecule-1 expression is required on multiple cell types for the development of experimental autoimmune encephalomyelitis. *J Immunol*, *178*(2), 851-857. https://doi.org/10.4049/jimmunol.178.2.851

Cai, R., Pan, C., Ghasemigharagoz, A., Todorov, M. I., Förstera, B., Zhao, S., Bhatia, H. S., Parra-Damas, A., Mrowka, L., Theodorou, D., Rempfler, M., Xavier, A. L. R., Kress, B. T., Benakis, C., Steinke, H., Liebscher, S., Bechmann, I., Liesz, A., Menze, B., Kerschensteiner, M., Nedergaard, M., & Ertürk, A. (2019). Panoptic imaging of transparent mice reveals whole-body neuronal projections and skull–meninges connections. *Nature Neuroscience*, *22*(2), 317-327. https://doi.org/10.1038/s41593-018-0301-3

Carman, C. V., & Martinelli, R. (2015). T Lymphocyte–Endothelial Interactions: Emerging Understanding of Trafficking and Antigen-Specific Immunity [Review]. *Frontiers in Immunology*, *6*(603). https://doi.org/10.3389/fimmu.2015.00603

Chan, T. A., Yarchoan, M., Jaffee, E., Swanton, C., Quezada, S. A., Stenzinger, A., & Peters, S. (2019). Development of tumor mutation burden as an immunotherapy biomarker: utility for the oncology clinic. *Annals of oncology : official journal of the European Society for Medical Oncology*, *30*(1), 44-56. https://doi.org/10.1093/annonc/mdy495

Chapman, P. B., Hauschild, A., Robert, C., Haanen, J. B., Ascierto, P., Larkin, J., Dummer, R., Garbe, C., Testori, A., Maio, M., Hogg, D., Lorigan, P., Lebbe, C., Jouary, T., Schadendorf, D., Ribas, A., O'Day, S. J., Sosman, J. A., Kirkwood, J. M., Eggermont, A. M. M., Dreno, B., Nolop, K., Li, J., Nelson, B., Hou, J., Lee, R. J., Flaherty, K. T., & McArthur, G. A. (2011). Improved Survival with Vemurafenib in Melanoma with BRAF V600E Mutation. *New England Journal of Medicine*, *364*(26), 2507-2516. https://doi.org/10.1056/NEJMoa1103782

Chauveau, A., Pirgova, G., Cheng, H. W., De Martin, A., Zhou, F. Y., Wideman, S., Rittscher, J., Ludewig, B., & Arnon, T. I. (2020). Visualization of T Cell Migration in the Spleen Reveals a Network of Perivascular Pathways that Guide Entry into T Zones. *Immunity*, *52*(5), 794-807.e797. https://doi.org/10.1016/j.immuni.2020.03.010

Chen, Daniel S., & Mellman, I. (2013). Oncology Meets Immunology: The Cancer-Immunity Cycle. *Immunity*, *39*(1), 1-10. https://doi.org/https://doi.org/10.1016/j.immuni.2013.07.012

Cornel, A. M., Mimpen, I. L., & Nierkens, S. (2020). MHC Class I Downregulation in Cancer: Underlying Mechanisms and Potential Targets for Cancer Immunotherapy. *Cancers (Basel)*, *12*(7). https://doi.org/10.3390/cancers12071760

Cugurra, A., Mamuladze, T., Rustenhoven, J., Dykstra, T., Beroshvili, G., Greenberg, Z. J., Baker, W., Papadopoulos, Z., Drieu, A., Blackburn, S., Kanamori, M., Brioschi, S., Herz, J., Schuettpelz, L. G., Colonna, M., Smirnov, I., & Kipnis, J. (2021). Skull and vertebral bone marrow are myeloid cell reservoirs for the meninges and CNS parenchyma. *Science*, *373*(6553), eabf7844. https://doi.org/doi:10.1126/science.abf7844

Dalpke, A. H., Schäfer, M. K., Frey, M., Zimmermann, S., Tebbe, J., Weihe, E., & Heeg, K. (2002). Immunostimulatory CpG-DNA activates murine microglia. *J Immunol*, *168*(10), 4854-4863. https://doi.org/10.4049/jimmunol.168.10.4854

Dangaj, D., Bruand, M., Grimm, A. J., Ronet, C., Barras, D., Duttagupta, P. A., Lanitis, E., Duraiswamy, J., Tanyi, J. L., Benencia, F., Conejo-Garcia, J., Ramay, H. R., Montone, K. T., Powell, D. J., Jr., Gimotty, P. A., Facciabene, A., Jackson, D. G., Weber, J. S., Rodig, S. J., Hodi, S. F., Kandalaft, L. E., Irving, M., Zhang, L., Foukas, P., Rusakiewicz, S., Delorenzi, M., & Coukos, G. (2019). Cooperation between Constitutive and Inducible Chemokines Enables T Cell Engraftment and Immune Attack in Solid Tumors. *Cancer Cell*, *35*(6), 885-900.e810. https://doi.org/10.1016/j.ccell.2019.05.004

Davies, M. A., Liu, P., McIntyre, S., Kim, K. B., Papadopoulos, N., Hwu, W. J., Hwu, P., & Bedikian, A. (2011). Prognostic factors for survival in melanoma patients with brain metastases. *Cancer*, *117*(8), 1687-1696. https://doi.org/10.1002/cncr.25634

de Groot, J. F., Fuller, G., Kumar, A. J., Piao, Y., Eterovic, K., Ji, Y., & Conrad, C. A. (2010). Tumor invasion after treatment of glioblastoma with bevacizumab: radiographic and pathologic correlation in humans and mice. *Neuro-oncology*, *12*(3), 233-242. https://doi.org/10.1093/neuonc/nop027

De Mattos-Arruda, L., Vazquez, M., Finotello, F., Lepore, R., Porta, E., Hundal, J., Amengual-Rigo, P., Ng, C. K. Y., Valencia, A., Carrillo, J., Chan, T. A., Guallar, V., McGranahan, N., Blanco, J., & Griffith, M. (2020). Neoantigen prediction and computational perspectives towards clinical benefit: recommendations from the ESMO Precision Medicine Working Group. *Annals of Oncology*, *31*(8), 978-990. https://doi.org/https://doi.org/10.1016/j.annonc.2020.05.008

References

Deguine, J., Breart, B., Lemaître, F., Di Santo, J. P., & Bousso, P. (2010). Intravital imaging reveals distinct dynamics for natural killer and CD8(+) T cells during tumor regression. *Immunity*, *33*(4), 632-644. https://doi.org/10.1016/j.immuni.2010.09.016

DeLong, J. H., Hall, A. O. H., Muallem, G., & Hunter, C. A. (2016). Ly6C expression on T cells is modulated by IL-27, interferon-gamma and TCR stimulation. *The Journal of Immunology*, *196*(1 Supplement), 196.199-196.199.

Dillon, S., Agrawal, S., Banerjee, K., Letterio, J., Denning, T. L., Oswald-Richter, K., Kasprowicz, D. J., Kellar, K., Pare, J., van Dyke, T., Ziegler, S., Unutmaz, D., & Pulendran, B. (2006). Yeast zymosan, a stimulus for TLR2 and dectin-1, induces regulatory antigen-presenting cells and immunological tolerance. *J Clin Invest*, *116*(4), 916-928. https://doi.org/10.1172/jci27203

Dong, H., Strome, S. E., Salomao, D. R., Tamura, H., Hirano, F., Flies, D. B., Roche, P. C., Lu, J., Zhu, G., Tamada, K., Lennon, V. A., Celis, E., & Chen, L. (2002). Tumor-associated B7-H1 promotes T-cell apoptosis: a potential mechanism of immune evasion. *Nat Med*, *8*(8), 793-800. https://doi.org/10.1038/nm730

Dustin, M. L., Bromley, S. K., Kan, Z., Peterson, D. A., & Unanue, E. R. (1997). Antigen receptor engagement delivers a stop signal to migrating T lymphocytes. *Proceedings of the National Academy of Sciences*, *94*(8), 3909-3913. https://doi.org/doi:10.1073/pnas.94.8.3909

Dutta, T., Spence, A., & Lampson, L. A. (2003). Robust ability of IFN-gamma to upregulate class II MHC antigen expression in tumor bearing rat brains. *J Neurooncol*, *64*(1-2), 31-44. https://doi.org/10.1007/bf02700018

Effern, M., Glodde, N., Braun, M., Liebing, J., Boll, H. N., Yong, M., Bawden, E., Hinze, D., van den Boorn-Konijnenberg, D., Daoud, M., Aymans, P., Landsberg, J., Smyth, M. J., Flatz, L., Tüting, T., Bald, T., Gebhardt, T., & Hölzel, M. (2020). Adoptive T Cell Therapy Targeting Different Gene Products Reveals Diverse and Context-Dependent Immune Evasion in Melanoma. *Immunity*, *53*(3), 564-580.e569. https://doi.org/10.1016/j.immuni.2020.07.007

Eigentler, T. K., Figl, A., Krex, D., Mohr, P., Mauch, C., Rass, K., Bostroem, A., Heese, O., Koelbl, O., Garbe, C., & Schadendorf, D. (2011). Number of metastases, serum lactate dehydrogenase level, and type of treatment are prognostic factors in patients with brain metastases of malignant melanoma. *Cancer*, *117*(8), 1697-1703. https://doi.org/10.1002/cncr.25631

ElTanbouly, M. A., & Noelle, R. J. (2021). Rethinking peripheral T cell tolerance: checkpoints across a T cell's journey. *Nature Reviews Immunology*, *21*(4), 257-267. https://doi.org/10.1038/s41577-020-00454-2

Engels, B., Engelhard, Victor H., Sidney, J., Sette, A., Binder, David C., Liu, Rebecca B., Kranz, David M., Meredith, Stephen C., Rowley, Donald A., & Schreiber, H. (2013). Relapse or Eradication of Cancer Is Predicted by Peptide-Major Histocompatibility Complex Affinity. *Cancer Cell*, *23*(4), 516-526. https://doi.org/https://doi.org/10.1016/j.ccr.2013.03.018

Falcone, I., Conciatori, F., Bazzichetto, C., Ferretti, G., Cognetti, F., Ciuffreda, L., & Milella, M. (2020). Tumor Microenvironment: Implications in Melanoma Resistance to Targeted Therapy and Immunotherapy. *Cancers (Basel)*, *12*(10). https://doi.org/10.3390/cancers12102870

Farber, J. M. (1997). Mig and IP-10: CXC chemokines that target lymphocytes. *J Leukoc Biol*, *61*(3), 246-257.

Fedorenko, I. V., Wargo, J. A., Flaherty, K. T., Messina, J. L., & Smalley, K. S. M. (2015). BRAF Inhibition Generates a Host-Tumor Niche that Mediates Therapeutic Escape. *J Invest Dermatol*, *135*(12), 3115-3124. https://doi.org/10.1038/jid.2015.329

Fidler, I. J., Yano, S., Zhang, R.-d., Fujimaki, T., & Bucana, C. D. (2002). The seed and soil hypothesis: vascularisation and brain metastases. *The Lancet Oncology*, *3*(1), 53-57. https://doi.org/https://doi.org/10.1016/S1470-2045(01)00622-2

Fife, K. M., Colman, M. H., Stevens, G. N., Firth, I. C., Moon, D., Shannon, K. F., Harman, R., Petersen-Schaefer, K., Zacest, A. C., Besser, M., Milton, G. W., McCarthy, W. H., & Thompson, J. F. (2004). Determinants of outcome in melanoma patients with cerebral metastases. *J Clin Oncol*, *22*(7), 1293-1300. https://doi.org/10.1200/jco.2004.08.140

Fleming, T. J., Fleming, M. L., & Malek, T. R. (1993). Selective expression of Ly-6G on myeloid lineage cells in mouse bone marrow. RB6-8C5 mAb to granulocyte-differentiation antigen (Gr-1) detects members of the Ly-6 family. *J Immunol*, *151*(5), 2399-2408.

Folkman, J., Watson, K., Ingber, D., & Hanahan, D. (1989). Induction of angiogenesis during the transition from hyperplasia to neoplasia. *Nature*, *339*(6219), 58-61. https://doi.org/10.1038/339058a0

Ford, A. L., Foulcher, E., Lemckert, F. A., & Sedgwick, J. D. (1996). Microglia induce CD4 T lymphocyte final effector function and death. *J Exp Med*, *184*(5), 1737-1745. https://doi.org/10.1084/jem.184.5.1737

Freeman, G. J., Gribben, J. G., Boussiotis, V. A., Ng, J. W., Restivo, V. A., Jr., Lombard, L. A., Gray, G. S., & Nadler, L. M. (1993). Cloning of B7-2: a CTLA-4 counter-receptor that costimulates human T cell proliferation. *Science*, *262*(5135), 909-911. https://doi.org/10.1126/science.7694363

Frost, J. L., & Schafer, D. P. (2016). Microglia: Architects of the Developing Nervous System. *Trends in cell biology*, *26*(8), 587-597. https://doi.org/10.1016/j.tcb.2016.02.006

Fu, H., Ward, E. J., & Marelli-Berg, F. M. (2016). Mechanisms of T cell organotropism. *Cellular and Molecular Life Sciences*, *73*(16), 3009-3033. https://doi.org/10.1007/s00018-016-2211-4

Galea, I. (2021). The blood–brain barrier in systemic infection and inflammation. *Cellular & Molecular Immunology*, *18*(11), 2489-2501. https://doi.org/10.1038/s41423-021-00757-x

Garbe, C., Keim, U., Eigentler, T. K., Amaral, T., Katalinic, A., Holleczek, B., Martus, P., & Leiter, U. (2019). Time trends in incidence and mortality of cutaneous melanoma in Germany. *Journal of the European Academy of Dermatology and Venereology*, *33*(7), 1272-1280. https://doi.org/https://doi.org/10.1111/jdv.15322

Garibyan, L., & Fisher, D. E. (2010). How Sunlight Causes Melanoma. *Current Oncology Reports*, *12*(5), 319-326. https://doi.org/10.1007/s11912-010-0119-y

Ghersi-Egea, J. F., Strazielle, N., Catala, M., Silva-Vargas, V., Doetsch, F., & Engelhardt, B. (2018). Molecular anatomy and functions of the choroidal blood-cerebrospinal fluid barrier in health and disease. *Acta Neuropathol*, *135*(3), 337-361. https://doi.org/10.1007/s00401-018-1807-1

Gonzalez, H., Mei, W., Robles, I., Hagerling, C., Allen, B. M., Hauge Okholm, T. L., Nanjaraj, A., Verbeek, T., Kalavacherla, S., van Gogh, M., Georgiou, S., Daras, M., Phillips, J. J., Spitzer, M. H., Roose,

J. P., & Werb, Z. (2022). Cellular architecture of human brain metastases. *Cell*. https://doi.org/https://doi.org/10.1016/j.cell.2021.12.043

Gupta, R. G., Li, F., Roszik, J., & Lizée, G. (2021). Exploiting Tumor Neoantigens to Target Cancer Evolution: Current Challenges and Promising Therapeutic Approaches. *Cancer Discovery*, *11*(5), 1024-1039. https://doi.org/10.1158/2159-8290.CD-20-1575

Gust, J., Hay, K. A., Hanafi, L. A., Li, D., Myerson, D., Gonzalez-Cuyar, L. F., Yeung, C., Liles, W. C., Wurfel, M., Lopez, J. A., Chen, J., Chung, D., Harju-Baker, S., Özpolat, T., Fink, K. R., Riddell, S. R., Maloney, D. G., & Turtle, C. J. (2017). Endothelial Activation and Blood-Brain Barrier Disruption in Neurotoxicity after Adoptive Immunotherapy with CD19 CAR-T Cells. *Cancer Discov*, *7*(12), 1404-1419. https://doi.org/10.1158/2159-8290.Cd-17-0698

Haddad, W., Cooper, C. J., Zhang, Z., Brown, J. B., Zhu, Y., Issekutz, A., Fuss, I., Lee, H. O., Kansas, G. S., & Barrett, T. A. (2003). P-selectin and P-selectin glycoprotein ligand 1 are major determinants for Th1 cell recruitment to nonlymphoid effector sites in the intestinal lamina propria. *J Exp Med*, *198*(3), 369-377. https://doi.org/10.1084/jem.20020691

Haghayegh Jahromi, N., Marchetti, L., Moalli, F., Duc, D., Basso, C., Tardent, H., Kaba, E., Deutsch, U., Pot, C., Sallusto, F., Stein, J. V., & Engelhardt, B. (2019). Intercellular Adhesion Molecule-1 (ICAM-1) and ICAM-2 Differentially Contribute to Peripheral Activation and CNS Entry of Autoaggressive Th1 and Th17 Cells in Experimental Autoimmune Encephalomyelitis. *Front Immunol*, *10*, 3056. https://doi.org/10.3389/fimmu.2019.03056

Hanahan, D., & Folkman, J. (1996). Patterns and Emerging Mechanisms of the Angiogenic Switch during Tumorigenesis. *Cell*, *86*(3), 353-364. https://doi.org/10.1016/S0092-8674(00)80108-7

Hänninen, A., Maksimow, M., Alam, C., Morgan, D. J., & Jalkanen, S. (2011). Ly6C supports preferential homing of central memory CD8+ T cells into lymph nodes. *Eur J Immunol*, *41*(3), 634-644. https://doi.org/10.1002/eji.201040760

Harlin, H., Meng, Y., Peterson, A. C., Zha, Y., Tretiakova, M., Slingluff, C., McKee, M., & Gajewski, T. F. (2009). Chemokine expression in melanoma metastases associated with CD8+ T-cell recruitment. *Cancer Res*, *69*(7), 3077-3085. https://doi.org/10.1158/0008-5472.Can-08-2281

Hayward, N. K., Wilmott, J. S., Waddell, N., Johansson, P. A., Field, M. A., Nones, K., Patch, A.-M., Kakavand, H., Alexandrov, L. B., Burke, H., Jakrot, V., Kazakoff, S., Holmes, O., Leonard, C., Sabarinathan, R., Mularoni, L., Wood, S., Xu, Q., Waddell, N., Tembe, V., Pupo, G. M., De Paoli-Iseppi, R., Vilain, R. E., Shang, P., Lau, L. M. S., Dagg, R. A., Schramm, S.-J., Pritchard, A., Dutton-Regester, K., Newell, F., Fitzgerald, A., Shang, C. A., Grimmond, S. M., Pickett, H. A., Yang, J. Y., Stretch, J. R., Behren, A., Kefford, R. F., Hersey, P., Long, G. V., Cebon, J., Shackleton, M., Spillane, A. J., Saw, R. P. M., López-Bigas, N., Pearson, J. V., Thompson, J. F., Scolyer, R. A., & Mann, G. J. (2017). Whole-genome landscapes of major melanoma subtypes. *Nature*, *545*(7653), 175-180. https://doi.org/10.1038/nature22071

Herisson, F., Frodermann, V., Courties, G., Rohde, D., Sun, Y., Vandoorne, K., Wojtkiewicz, G. R., Masson, G. S., Vinegoni, C., Kim, J., Kim, D.-E., Weissleder, R., Swirski, F. K., Moskowitz, M. A., & Nahrendorf, M. (2018). Direct vascular channels connect skull bone marrow and the brain surface enabling myeloid cell migration. *Nature Neuroscience*, *21*(9), 1209-1217. https://doi.org/10.1038/s41593-018-0213-2

Holth, J. K., Fritschi, S. K., Wang, C., Pedersen, N. P., Cirrito, J. R., Mahan, T. E., Finn, M. B., Manis, M., Geerling, J. C., Fuller, P. M., Lucey, B. P., & Holtzman, D. M. (2019). The sleep-wake cycle

regulates brain interstitial fluid tau in mice and CSF tau in humans. *Science*, *363*(6429), 880-884. https://doi.org/10.1126/science.aav2546

Huber, V., Vallacchi, V., Fleming, V., Hu, X., Cova, A., Dugo, M., Shahaj, E., Sulsenti, R., Vergani, E., Filipazzi, P., De Laurentiis, A., Lalli, L., Di Guardo, L., Patuzzo, R., Vergani, B., Casiraghi, E., Cossa, M., Gualeni, A., Bollati, V., Arienti, F., De Braud, F., Mariani, L., Villa, A., Altevogt, P., Umansky, V., Rodolfo, M., & Rivoltini, L. (2018). Tumor-derived microRNAs induce myeloid suppressor cells and predict immunotherapy resistance in melanoma. *J Clin Invest*, *128*(12), 5505-5516. https://doi.org/10.1172/jci98060

Hugues, S., Fetler, L., Bonifaz, L., Helft, J., Amblard, F., & Amigorena, S. (2004). Distinct T cell dynamics in lymph nodes during the induction of tolerance and immunity. *Nature Immunology*, *5*(12), 1235-1242. https://doi.org/10.1038/ni1134

Iliff, J. J., Wang, M., Liao, Y., Plogg, B. A., Peng, W., Gundersen, G. A., Benveniste, H., Vates, G. E., Deane, R., Goldman, S. A., Nagelhus, E. A., & Nedergaard, M. (2012). A paravascular pathway facilitates CSF flow through the brain parenchyma and the clearance of interstitial solutes, including amyloid β. *Science Translational Medicine*, *4*(147), Article 147ra111. https://doi.org/10.1126/scitranslmed.3003748

Iozumi, K., Hoganson, G. E., Pennella, R., Everett, M. A., & Fuller, B. B. (1993). Role of Tyrosinase as the Determinant of Pigmentation in Cultured Human Melanocytes. *Journal of Investigative Dermatology*, *100*(6), 806-811. https://doi.org/https://doi.org/10.1111/1523-1747.ep12476630

Jacob, L., de Brito Neto, J., Lenck, S., Corcy, C., Benbelkacem, F., Geraldo, L. H., Xu, Y., Thomas, J.-M., El Kamouh, M.-R., Spajer, M., Potier, M.-C., Haik, S., Kalamarides, M., Stankoff, B., Lehericy, S., Eichmann, A., & Thomas, J.-L. (2022). Conserved meningeal lymphatic drainage circuits in mice and humans. *Journal of Experimental Medicine*, *219*(8), e20220035. https://doi.org/10.1084/jem.20220035

Jacquemin, G., Benavente-Diaz, M., Djaber, S., Bore, A., Dangles-Marie, V., Surdez, D., Tajbakhsh, S., Fre, S., & Lloyd-Lewis, B. (2021). Longitudinal high-resolution imaging through a flexible intravital imaging window. *Sci Adv*, *7*(25). https://doi.org/10.1126/sciadv.abg7663

Jain, R. K. (2005). Normalization of tumor vasculature: an emerging concept in antiangiogenic therapy. *Science*, *307*(5706), 58-62. https://doi.org/10.1126/science.1104819

Jain, R. K., di Tomaso, E., Duda, D. G., Loeffler, J. S., Sorensen, A. G., & Batchelor, T. T. (2007). Angiogenesis in brain tumours. *Nature Reviews Neuroscience*, *8*(8), 610-622. https://doi.org/10.1038/nrn2175

Jhunjhunwala, S., Hammer, C., & Delamarre, L. (2021). Antigen presentation in cancer: insights into tumour immunogenicity and immune evasion. *Nature Reviews Cancer*, *21*(5), 298-312. https://doi.org/10.1038/s41568-021-00339-z

Jiang, X., Campbell James, J., & Kupper Thomas, S. (2010). Embryonic trafficking of γδ T cells to skin is dependent on E/P selectin ligands and CCR4. *Proceedings of the National Academy of Sciences*, *107*(16), 7443-7448. https://doi.org/10.1073/pnas.0912943107

Kalaora, S., Nagler, A., Wargo, J. A., & Samuels, Y. (2022). Mechanisms of immune activation and regulation: lessons from melanoma. *Nature Reviews Cancer*, *22*(4), 195-207. https://doi.org/10.1038/s41568-022-00442-9

References

Kameyama, K., Takemura, T., Hamada, Y., Sakai, C., Kondoh, S., Nishiyama, S., Urabe, K., & Hearing, V. J. (1993). Pigment Production in Murine Melanoma Cells Is Regulated by Tyrosinase, Tyrosinase-Related Protein 1 (TRP1), DOPAchrome Tautomerase (TRP2), and a Melanogenic Inhibitor. *Journal of Investigative Dermatology*, *100*(2), 126-131. https://doi.org/https://doi.org/10.1111/1523-1747.ep12462778

Kanda, Y., Okazaki, T., & Katakai, T. (2021). Motility Dynamics of T Cells in Tumor-Draining Lymph Nodes: A Rational Indicator of Antitumor Response and Immune Checkpoint Blockade. *Cancers*, *13*(18), 4616. https://www.mdpi.com/2072-6694/13/18/4616

Kang, K., Xie, F., Mao, J., Bai, Y., & Wang, X. (2020). Significance of Tumor Mutation Burden in Immune Infiltration and Prognosis in Cutaneous Melanoma [Original Research]. *Frontiers in Oncology*, *10*. https://doi.org/10.3389/fonc.2020.573141

Karpathiou, G., Camy, F., Dumollard, J. M., & Peoc'h, M. (2021). Immunohistochemical analysis of L1 cell adhesion molecule and high endothelial venules in breast cancer brain metastasis. *Pathol Res Pract*, *223*, 153484. https://doi.org/10.1016/j.prp.2021.153484

Karreman, M. A. (2021). Intravital microscopy. In *Imaging Modalities for Biological and Preclinical Research: A Compendium, Volume 2* (pp. II.1-1-II.1-11). IOP Publishing. https://doi.org/10.1088/978-0-7503-3747-2ch1

Kawakami, N., Nägerl, U. V., Odoardi, F., Bonhoeffer, T., Wekerle, H., & Flügel, A. (2005). Live imaging of effector cell trafficking and autoantigen recognition within the unfolding autoimmune encephalomyelitis lesion. *J Exp Med*, *201*(11), 1805-1814. https://doi.org/10.1084/jem.20050011

Kayatz, P., Thumann, G., Luther, T. T., Jordan, J. F., Bartz–Schmidt, K. U., Esser, P. J., & Schraermeyer, U. (2001). Oxidation Causes Melanin Fluorescence. *Investigative Ophthalmology & Visual Science*, *42*(1), 241-246.

Kedrin, D., Gligorijevic, B., Wyckoff, J., Verkhusha, V. V., Condeelis, J., Segall, J. E., & van Rheenen, J. (2008). Intravital imaging of metastatic behavior through a mammary imaging window. *Nat Methods*, *5*(12), 1019-1021. https://doi.org/10.1038/nmeth.1269

Keller, P. J., Schmidt, A. D., Wittbrodt, J., & Stelzer, E. H. (2008). Reconstruction of zebrafish early embryonic development by scanned light sheet microscopy. *Science*, *322*(5904), 1065-1069. https://doi.org/10.1126/science.1162493

Kelly, T. A., Jeanfavre, D. D., McNeil, D. W., Woska, J. R., Jr., Reilly, P. L., Mainolfi, E. A., Kishimoto, K. M., Nabozny, G. H., Zinter, R., Bormann, B. J., & Rothlein, R. (1999). Cutting edge: a small molecule antagonist of LFA-1-mediated cell adhesion. *J Immunol*, *163*(10), 5173-5177.

Kerfoot, S. M., & Kubes, P. (2002). Overlapping Roles of P-Selectin and α₄ Integrin to Recruit Leukocytes to the Central Nervous System in Experimental Autoimmune Encephalomyelitis. *The Journal of Immunology*, *169*(2), 1000-1006. https://doi.org/10.4049/jimmunol.169.2.1000

Kienast, Y., von Baumgarten, L., Fuhrmann, M., Klinkert, W. E. F., Goldbrunner, R., Herms, J., & Winkler, F. (2010). Real-time imaging reveals the single steps of brain metastasis formation. *Nature Medicine*, *16*(1), 116-122. https://doi.org/10.1038/nm.2072

Kim-Schulze, S., Scotto, L., Vlad, G., Piazza, F., Lin, H., Liu, Z., Cortesini, R., & Suciu-Foca, N. (2006). Recombinant Ig-like transcript 3-Fc modulates T cell responses via induction of Th anergy and differentiation of CD8+ T suppressor cells. *J Immunol*, *176*(5), 2790-2798. https://doi.org/10.4049/jimmunol.176.5.2790

Kim, M., Laramy, J. K., Mohammad, A. S., Talele, S., Fisher, J., Sarkaria, J. N., & Elmquist, W. F. (2019). Brain Distribution of a Panel of Epidermal Growth Factor Receptor Inhibitors Using Cassette Dosing in Wild-Type and Abcb1/Abcg2-Deficient Mice. *Drug metabolism and disposition: the biological fate of chemicals*, *47*(4), 393-404. https://doi.org/10.1124/dmd.118.084210

Kim, T. N., Goodwill, P. W., Chen, Y., Conolly, S. M., Schaffer, C. B., Liepmann, D., & Wang, R. A. (2012). Line-scanning particle image velocimetry: an optical approach for quantifying a wide range of blood flow speeds in live animals. *PloS one*, *7*(6), e38590-e38590. https://doi.org/10.1371/journal.pone.0038590

Kimura, H., Braun, R. D., Ong, E. T., Hsu, R., Secomb, T. W., Papahadjopoulos, D., Hong, K., & Dewhirst, M. W. (1996). Fluctuations in red cell flux in tumor microvessels can lead to transient hypoxia and reoxygenation in tumor parenchyma. *Cancer Res*, *56*(23), 5522-5528.

Kivisäkk, P., Mahad, D. J., Callahan, M. K., Trebst, C., Tucky, B., Wei, T., Wu, L., Baekkevold, E. S., Lassmann, H., Staugaitis, S. M., Campbell, J. J., & Ransohoff, R. M. (2003). Human cerebrospinal fluid central memory CD4+ T cells: evidence for trafficking through choroid plexus and meninges via P-selectin. *Proc Natl Acad Sci U S A*, *100*(14), 8389-8394. https://doi.org/10.1073/pnas.1433000100

Kobayashi, M., Kobayashi, H., Pollard, R. B., & Suzuki, F. (1998). A Pathogenic Role of Th2 Cells and Their Cytokine Products on the Pulmonary Metastasis of Murine B16 Melanoma. *The Journal of Immunology*, *160*(12), 5869-5873. https://www.jimmunol.org/content/jimmunol/160/12/5869.full.pdf

Kohli, K., Pillarisetty, V. G., & Kim, T. S. (2022). Key chemokines direct migration of immune cells in solid tumors. *Cancer Gene Therapy*, *29*(1), 10-21. https://doi.org/10.1038/s41417-021-00303-x

Korn, E. L., Liu, P. Y., Lee, S. J., Chapman, J. A., Niedzwiecki, D., Suman, V. J., Moon, J., Sondak, V. K., Atkins, M. B., Eisenhauer, E. A., Parulekar, W., Markovic, S. N., Saxman, S., & Kirkwood, J. M. (2008). Meta-analysis of phase II cooperative group trials in metastatic stage IV melanoma to determine progression-free and overall survival benchmarks for future phase II trials. *J Clin Oncol*, *26*(4), 527-534. https://doi.org/10.1200/jco.2007.12.7837

Kovacs, Z. I., Kim, S., Jikaria, N., Qureshi, F., Milo, B., Lewis, B. K., Bresler, M., Burks, S. R., & Frank, J. A. (2017). Disrupting the blood-brain barrier by focused ultrasound induces sterile inflammation. *Proc Natl Acad Sci U S A*, *114*(1), E75-e84. https://doi.org/10.1073/pnas.1614777114

Kuczynski, E. A., Vermeulen, P. B., Pezzella, F., Kerbel, R. S., & Reynolds, A. R. (2019). Vessel co-option in cancer. *Nature Reviews Clinical Oncology*, *16*(8), 469-493. https://doi.org/10.1038/s41571-019-0181-9

Larkin, J., Chiarion-Sileni, V., Gonzalez, R., Grob, J.-J., Rutkowski, P., Lao, C. D., Cowey, C. L., Schadendorf, D., Wagstaff, J., Dummer, R., Ferrucci, P. F., Smylie, M., Hogg, D., Hill, A., Márquez-Rodas, I., Haanen, J., Guidoboni, M., Maio, M., Schöffski, P., Carlino, M. S., Lebbé, C., McArthur, G., Ascierto, P. A., Daniels, G. A., Long, G. V., Bastholt, L., Rizzo, J. I., Balogh, A., Moshyk, A., Hodi, F. S., & Wolchok, J. D. (2019). Five-Year Survival with Combined Nivolumab

and Ipilimumab in Advanced Melanoma. *New England Journal of Medicine*, *381*(16), 1535-1546. https://doi.org/10.1056/NEJMoa1910836

Larkin, J., Chiarion-Sileni, V., Gonzalez, R., Grob, J. J., Cowey, C. L., Lao, C. D., Schadendorf, D., Dummer, R., Smylie, M., Rutkowski, P., Ferrucci, P. F., Hill, A., Wagstaff, J., Carlino, M. S., Haanen, J. B., Maio, M., Marquez-Rodas, I., McArthur, G. A., Ascierto, P. A., Long, G. V., Callahan, M. K., Postow, M. A., Grossmann, K., Sznol, M., Dreno, B., Bastholt, L., Yang, A., Rollin, L. M., Horak, C., Hodi, F. S., & Wolchok, J. D. (2015). Combined Nivolumab and Ipilimumab or Monotherapy in Untreated Melanoma. *N Engl J Med*, *373*(1), 23-34. https://doi.org/10.1056/NEJMoa1504030

Larson, A. M. (2011). Multiphoton microscopy. *Nature Photonics*, *5*(1), 1-1. https://doi.org/10.1038/nphoton.an.2010.2

Lau, D., Garçon, F., Chandra, A., Lechermann, L. M., Aloj, L., Chilvers, E. R., Corrie, P. G., Okkenhaug, K., & Gallagher, F. A. (2020). Intravital Imaging of Adoptive T-Cell Morphology, Mobility and Trafficking Following Immune Checkpoint Inhibition in a Mouse Melanoma Model [Methods]. *Frontiers in Immunology*, *11*(1514). https://doi.org/10.3389/fimmu.2020.01514

Lawrence, M. S., Stojanov, P., Polak, P., Kryukov, G. V., Cibulskis, K., Sivachenko, A., Carter, S. L., Stewart, C., Mermel, C. H., Roberts, S. A., Kiezun, A., Hammerman, P. S., McKenna, A., Drier, Y., Zou, L., Ramos, A. H., Pugh, T. J., Stransky, N., Helman, E., Kim, J., Sougnez, C., Ambrogio, L., Nickerson, E., Shefler, E., Cortés, M. L., Auclair, D., Saksena, G., Voet, D., Noble, M., DiCara, D., Lin, P., Lichtenstein, L., Heiman, D. I., Fennell, T., Imielinski, M., Hernandez, B., Hodis, E., Baca, S., Dulak, A. M., Lohr, J., Landau, D.-A., Wu, C. J., Melendez-Zajgla, J., Hidalgo-Miranda, A., Koren, A., McCarroll, S. A., Mora, J., Lee, R. S., Crompton, B., Onofrio, R., Parkin, M., Winckler, W., Ardlie, K., Gabriel, S. B., Roberts, C. W. M., Biegel, J. A., Stegmaier, K., Bass, A. J., Garraway, L. A., Meyerson, M., Golub, T. R., Gordenin, D. A., Sunyaev, S., Lander, E. S., & Getz, G. (2013). Mutational heterogeneity in cancer and the search for new cancer-associated genes. *Nature*, *499*(7457), 214-218. https://doi.org/10.1038/nature12213

Lee, J. H., Torisu-Itakara, H., Cochran, A. J., Kadison, A., Huynh, Y., Morton, D. L., & Essner, R. (2005). Quantitative analysis of melanoma-induced cytokine-mediated immunosuppression in melanoma sentinel nodes. *Clin Cancer Res*, *11*(1), 107-112.

Ley, K., & Kansas, G. S. (2004). Selectins in T-cell recruitment to non-lymphoid tissues and sites of inflammation. *Nature Reviews Immunology*, *4*(5), 325-336. https://doi.org/10.1038/nri1351

Li, Q., & Barres, B. A. (2018). Microglia and macrophages in brain homeostasis and disease. *Nat Rev Immunol*, *18*(4), 225-242. https://doi.org/10.1038/nri.2017.125

Lockman, P. R., Mittapalli, R. K., Taskar, K. S., Rudraraju, V., Gril, B., Bohn, K. A., Adkins, C. E., Roberts, A., Thorsheim, H. R., Gaasch, J. A., Huang, S., Palmieri, D., Steeg, P. S., & Smith, Q. R. (2010). Heterogeneous blood-tumor barrier permeability determines drug efficacy in experimental brain metastases of breast cancer. *Clin Cancer Res*, *16*(23), 5664-5678. https://doi.org/10.1158/1078-0432.Ccr-10-1564

Lodygin, D., Hermann, M., Schweingruber, N., Flügel-Koch, C., Watanabe, T., Schlosser, C., Merlini, A., Körner, H., Chang, H. F., Fischer, H. J., Reichardt, H. M., Zagrebelsky, M., Mollenhauer, B., Kügler, S., Fitzner, D., Frahm, J., Stadelmann, C., Haberl, M., Odoardi, F., & Flügel, A. (2019). β-Synuclein-reactive T cells induce autoimmune CNS grey matter degeneration. *Nature*, *566*(7745), 503-508. https://doi.org/10.1038/s41586-019-0964-2

Long, G. V., Atkinson, V., Lo, S., Sandhu, S., Guminski, A. D., Brown, M. P., Wilmott, J. S., Edwards, J., Gonzalez, M., Scolyer, R. A., Menzies, A. M., & McArthur, G. A. (2018). Combination nivolumab and ipilimumab or nivolumab alone in melanoma brain metastases: a multicentre randomised phase 2 study. *Lancet Oncol*, *19*(5), 672-681. https://doi.org/10.1016/s1470-2045(18)30139-6

Louveau, A., Herz, J., Alme, M. N., Salvador, A. F., Dong, M. Q., Viar, K. E., Herod, S. G., Knopp, J., Setliff, J. C., Lupi, A. L., Da Mesquita, S., Frost, E. L., Gaultier, A., Harris, T. H., Cao, R., Hu, S., Lukens, J. R., Smirnov, I., Overall, C. C., Oliver, G., & Kipnis, J. (2018). CNS lymphatic drainage and neuroinflammation are regulated by meningeal lymphatic vasculature. *Nat Neurosci*, *21*(10), 1380-1391. https://doi.org/10.1038/s41593-018-0227-9

Louveau, A., Smirnov, I., Keyes, T. J., Eccles, J. D., Rouhani, S. J., Peske, J. D., Derecki, N. C., Castle, D., Mandell, J. W., Lee, K. S., Harris, T. H., & Kipnis, J. (2015). Structural and functional features of central nervous system lymphatic vessels. *Nature*, *523*(7560), 337-341. https://doi.org/10.1038/nature14432

Lowe, M. M., Boothby, I., Clancy, S., Ahn, R. S., Liao, W., Nguyen, D. N., Schumann, K., Marson, A., Mahuron, K. M., Kingsbury, G. A., Liu, Z., Munoz Sandoval, P., Rodriguez, R. S., Pauli, M. L., Taravati, K., Arron, S. T., Neuhaus, I. M., Harris, H. W., Kim, E. A., Shin, U. S., Krummel, M. F., Daud, A., Scharschmidt, T. C., & Rosenblum, M. D. (2019). Regulatory T cells use arginase 2 to enhance their metabolic fitness in tissues. *JCI insight*, *4*(24). https://doi.org/10.1172/jci.insight.129756

Łuksza, M., Sethna, Z. M., Rojas, L. A., Lihm, J., Bravi, B., Elhanati, Y., Soares, K., Amisaki, M., Dobrin, A., Hoyos, D., Guasp, P., Zebboudj, A., Yu, R., Chandra, A. K., Waters, T., Odgerel, Z., Leung, J., Kappagantula, R., Makohon-Moore, A., Johns, A., Gill, A., Gigoux, M., Wolchok, J., Merghoub, T., Sadelain, M., Patterson, E., Monasson, R., Mora, T., Walczak, A. M., Cocco, S., Iacobuzio-Donahue, C., Greenbaum, B. D., & Balachandran, V. P. (2022). Neoantigen quality predicts immunoediting in survivors of pancreatic cancer. *Nature*, *606*(7913), 389-395. https://doi.org/10.1038/s41586-022-04735-9

Lyck, R., Reiss, Y., Gerwin, N., Greenwood, J., Adamson, P., & Engelhardt, B. (2003). T-cell interaction with ICAM-1/ICAM-2 double-deficient brain endothelium in vitro: the cytoplasmic tail of endothelial ICAM-1 is necessary for transendothelial migration of T cells. *Blood*, *102*(10), 3675-3683. https://doi.org/10.1182/blood-2003-02-0358

Lyle, L. T., Lockman, P. R., Adkins, C. E., Mohammad, A. S., Sechrest, E., Hua, E., Palmieri, D., Liewehr, D. J., Steinberg, S. M., Kloc, W., Izycka-Swieszewska, E., Duchnowska, R., Nayyar, N., Brastianos, P. K., Steeg, P. S., & Gril, B. (2016). Alterations in Pericyte Subpopulations Are Associated with Elevated Blood–Tumor Barrier Permeability in Experimental Brain Metastasis of Breast Cancer. *Clinical Cancer Research*, *22*(21), 5287-5299. https://doi.org/10.1158/1078-0432.Ccr-15-1836

Ma, W., Wang, Y., Zhang, R., Yang, F., Zhang, D., Huang, M., Zhang, L., Dorsey, J. F., Binder, Z. A., O'Rourke, D. M., Fraietta, J. A., Gong, Y., & Fan, Y. (2021). Targeting PAK4 to reprogram the vascular microenvironment and improve CAR-T immunotherapy for glioblastoma. *Nature Cancer*, *2*(1), 83-97. https://doi.org/10.1038/s43018-020-00147-8

Malik, B. T., Byrne, K. T., Vella, J. L., Zhang, P., Shabaneh, T. B., Steinberg, S. M., Molodtsov, A. K., Bowers, J. S., Angeles, C. V., Paulos, C. M., Huang, Y. H., & Turk, M. J. (2017). Resident memory T cells in the skin mediate durable immunity to melanoma. *Science Immunology*, *2*(10), eaam6346. https://doi.org/doi:10.1126/sciimmunol.aam6346

References

Maniotis, A. J., Folberg, R., Hess, A., Seftor, E. A., Gardner, L. M., Pe'er, J., Trent, J. M., Meltzer, P. S., & Hendrix, M. J. (1999). Vascular channel formation by human melanoma cells in vivo and in vitro: vasculogenic mimicry. *Am J Pathol*, *155*(3), 739-752. https://doi.org/10.1016/s0002-9440(10)65173-5

Mapunda, J. A., Tibar, H., Regragui, W., & Engelhardt, B. (2022). How Does the Immune System Enter the Brain? [Review]. *Frontiers in Immunology*, *13*. https://doi.org/10.3389/fimmu.2022.805657

Martins, F., Sofiya, L., Sykiotis, G. P., Lamine, F., Maillard, M., Fraga, M., Shabafrouz, K., Ribi, C., Cairoli, A., Guex-Crosier, Y., Kuntzer, T., Michielin, O., Peters, S., Coukos, G., Spertini, F., Thompson, J. A., & Obeid, M. (2019). Adverse effects of immune-checkpoint inhibitors: epidemiology, management and surveillance. *Nature Reviews Clinical Oncology*, *16*(9), 563-580. https://doi.org/10.1038/s41571-019-0218-0

Mason, D. W., Charlton, H. M., Jones, A. J., Lavy, C. B., Puklavec, M., & Simmonds, S. J. (1986). The fate of allogeneic and xenogeneic neuronal tissue transplanted into the third ventricle of rodents. *Neuroscience*, *19*(3), 685-694. https://doi.org/10.1016/0306-4522(86)90292-7

Masopust, D., & Schenkel, J. M. (2013). The integration of T cell migration, differentiation and function. *Nature Reviews Immunology*, *13*(5), 309-320. https://doi.org/10.1038/nri3442

Mathiisen, T. M., Lehre, K. P., Danbolt, N. C., & Ottersen, O. P. (2010). The perivascular astroglial sheath provides a complete covering of the brain microvessels: An electron microscopic 3D reconstruction. *Glia*, *58*(9), 1094-1103. https://doi.org/https://doi.org/10.1002/glia.20990

McGranahan, N., & Swanton, C. (2019). Neoantigen quality, not quantity. *Science Translational Medicine*, *11*(506), eaax7918. https://doi.org/doi:10.1126/scitranslmed.aax7918

Medawar, P. B. (1948). Immunity to homologous grafted skin; the fate of skin homografts transplanted to the brain, to subcutaneous tissue, and to the anterior chamber of the eye. *Br J Exp Pathol*, *29*(1), 58-69.

Mempel, T. R., Henrickson, S. E., & von Andrian, U. H. (2004). T-cell priming by dendritic cells in lymph nodes occurs in three distinct phases. *Nature*, *427*(6970), 154-159. https://doi.org/10.1038/nature02238

Mestre, H., Hablitz, L. M., Xavier, A. L., Feng, W., Zou, W., Pu, T., Monai, H., Murlidharan, G., Castellanos Rivera, R. M., Simon, M. J., Pike, M. M., Plá, V., Du, T., Kress, B. T., Wang, X., Plog, B. A., Thrane, A. S., Lundgaard, I., Abe, Y., Yasui, M., Thomas, J. H., Xiao, M., Hirase, H., Asokan, A., Iliff, J. J., & Nedergaard, M. (2018). Aquaporin-4-dependent glymphatic solute transport in the rodent brain. *eLife*, *7*. https://doi.org/10.7554/eLife.40070

Mestre, H., Mori, Y., & Nedergaard, M. (2020). The Brain’s Glymphatic System: Current Controversies. *Trends in Neurosciences*, *43*(7), 458-466. https://doi.org/10.1016/j.tins.2020.04.003

Mestre, H., Tithof, J., Du, T., Song, W., Peng, W., Sweeney, A. M., Olveda, G., Thomas, J. H., Nedergaard, M., & Kelley, D. H. (2018). Flow of cerebrospinal fluid is driven by arterial pulsations and is reduced in hypertension. *Nature Communications*, *9*(1), 4878. https://doi.org/10.1038/s41467-018-07318-3

Miarka, L., & Valiente, M. (2021). Animal models of brain metastasis. *Neuro-oncology advances*, *3*(Suppl 5), v144-v156. https://doi.org/10.1093/noajnl/vdab115

Miller, M. J., Wei, S. H., Parker, I., & Cahalan, M. D. (2002). Two-photon imaging of lymphocyte motility and antigen response in intact lymph node. *Science*, *296*(5574), 1869-1873. https://doi.org/10.1126/science.1070051

Mitchell, D., Shireman, J., Sierra Potchanant, E. A., Lara-Velazquez, M., & Dey, M. (2021). Neuroinflammation in Autoimmune Disease and Primary Brain Tumors: The Quest for Striking the Right Balance [Review]. *Frontiers in Cellular Neuroscience*, *15*. https://doi.org/10.3389/fncel.2021.716947

Morales, J., Homey, B., Vicari, A. P., Hudak, S., Oldham, E., Hedrick, J., Orozco, R., Copeland, N. G., Jenkins, N. A., McEvoy, L. M., & Zlotnik, A. (1999). CTACK, a skin-associated chemokine that preferentially attracts skin-homing memory T cells. *Proc Natl Acad Sci U S A*, *96*(25), 14470-14475. https://doi.org/10.1073/pnas.96.25.14470

Motz, G. T., & Coukos, G. (2013). Deciphering and reversing tumor immune suppression. *Immunity*, *39*(1), 61-73. https://doi.org/10.1016/j.immuni.2013.07.005

Mrass, P., Kinjyo, I., Ng, L. G., Reiner, S. L., Puré, E., & Weninger, W. (2008). CD44 Mediates Successful Interstitial Navigation by Killer T Cells and Enables Efficient Antitumor Immunity. *Immunity*, *29*(6), 971-985. https://doi.org/https://doi.org/10.1016/j.immuni.2008.10.015

Mrass, P., Takano, H., Ng, L. G., Daxini, S., Lasaro, M. O., Iparraguirre, A., Cavanagh, L. L., von Andrian, U. H., Ertl, H. C., Haydon, P. G., & Weninger, W. (2006). Random migration precedes stable target cell interactions of tumor-infiltrating T cells. *J Exp Med*, *203*(12), 2749-2761. https://doi.org/10.1084/jem.20060710

Mulazzani, M., Fräßle, S. P., von Mücke-Heim, I., Langer, S., Zhou, X., Ishikawa-Ankerhold, H., Leube, J., Zhang, W., Dötsch, S., Svec, M., Rudelius, M., Dreyling, M., von Bergwelt-Baildon, M., Straube, A., Buchholz, V. R., Busch, D. H., & von Baumgarten, L. (2019). Long-term in vivo microscopy of CAR T cell dynamics during eradication of CNS lymphoma in mice. *Proc Natl Acad Sci U S A*, *116*(48), 24275-24284. https://doi.org/10.1073/pnas.1903854116

Muller, W. A. (2011). Mechanisms of Leukocyte Transendothelial Migration. *Annual Review of Pathology: Mechanisms of Disease*, *6*(1), 323-344. https://doi.org/10.1146/annurev-pathol-011110-130224

Natalini, A., Simonetti, S., Favaretto, G., Peruzzi, G., Antonangeli, F., Santoni, A., Muñoz-Ruiz, M., Hayday, A., & Di Rosa, F. (2021). OMIP-079: Cell cycle of CD4+ and CD8+ naïve/memory T cell subsets, and of Treg cells from mouse spleen. *Cytometry Part A*, *99*(12), 1171-1175. https://doi.org/https://doi.org/10.1002/cyto.a.24509

Nguyen, L. T., Saibil, S. D., Sotov, V., Le, M. X., Khoja, L., Ghazarian, D., Bonilla, L., Majeed, H., Hogg, D., Joshua, A. M., Crump, M., Franke, N., Spreafico, A., Hansen, A., Al-Habeeb, A., Leong, W., Easson, A., Reedijk, M., Goldstein, D. P., McCready, D., Yasufuku, K., Waddell, T., Cypel, M., Pierre, A., Zhang, B., Boross-Harmer, S., Cipollone, J., Nelles, M., Scheid, E., Fyrsta, M., Lo, C. S., Nie, J., Yam, J. Y., Yen, P. H., Gray, D., Motta, V., Elford, A. R., DeLuca, S., Wang, L., Effendi, S., Ellenchery, R., Hirano, N., Ohashi, P. S., & Butler, M. O. (2019). Phase II clinical trial of adoptive cell therapy for patients with metastatic melanoma with autologous tumor-infiltrating lymphocytes and low-dose interleukin-2. *Cancer Immunology, Immunotherapy*, *68*(5), 773-785. https://doi.org/10.1007/s00262-019-02307-x

Nimmerjahn, A., Kirchhoff, F., & Helmchen, F. (2005). Resting microglial cells are highly dynamic surveillants of brain parenchyma in vivo. *Science*, *308*(5726), 1314-1318. https://doi.org/10.1126/science.1110647

Nishihara, H., Soldati, S., Mossu, A., Rosito, M., Rudolph, H., Muller, W. A., Latorre, D., Sallusto, F., Sospedra, M., Martin, R., Ishikawa, H., Tenenbaum, T., Schroten, H., Gosselet, F., & Engelhardt, B. (2020). Human CD4+ T cell subsets differ in their abilities to cross endothelial and epithelial brain barriers in vitro. *Fluids and Barriers of the CNS*, *17*(1), 3. https://doi.org/10.1186/s12987-019-0165-2

Nitta, T., Hata, M., Gotoh, S., Seo, Y., Sasaki, H., Hashimoto, N., Furuse, M., & Tsukita, S. (2003). Size-selective loosening of the blood-brain barrier in claudin-5-deficient mice. *J Cell Biol*, *161*(3), 653-660. https://doi.org/10.1083/jcb.200302070

Ohmori, Y., Wyner, L., Narumi, S., Armstrong, D., Stoler, M., & Hamilton, T. A. (1993). Tumor necrosis factor-alpha induces cell type and tissue-specific expression of chemoattractant cytokines in vivo. *Am J Pathol*, *142*(3), 861-870.

Ott, P. A., Hu, Z., Keskin, D. B., Shukla, S. A., Sun, J., Bozym, D. J., Zhang, W., Luoma, A., Giobbie-Hurder, A., Peter, L., Chen, C., Olive, O., Carter, T. A., Li, S., Lieb, D. J., Eisenhaure, T., Gjini, E., Stevens, J., Lane, W. J., Javeri, I., Nellaiappan, K., Salazar, A. M., Daley, H., Seaman, M., Buchbinder, E. I., Yoon, C. H., Harden, M., Lennon, N., Gabriel, S., Rodig, S. J., Barouch, D. H., Aster, J. C., Getz, G., Wucherpfennig, K., Neuberg, D., Ritz, J., Lander, E. S., Fritsch, E. F., Hacohen, N., & Wu, C. J. (2017). An immunogenic personal neoantigen vaccine for patients with melanoma. *Nature*, *547*(7662), 217-221. https://doi.org/10.1038/nature22991

Overwijk, W. W., Theoret, M. R., Finkelstein, S. E., Surman, D. R., de Jong, L. A., Vyth-Dreese, F. A., Dellemijn, T. A., Antony, P. A., Spiess, P. J., Palmer, D. C., Heimann, D. M., Klebanoff, C. A., Yu, Z., Hwang, L. N., Feigenbaum, L., Kruisbeek, A. M., Rosenberg, S. A., & Restifo, N. P. (2003). Tumor regression and autoimmunity after reversal of a functionally tolerant state of self-reactive CD8+ T cells. *J Exp Med*, *198*(4), 569-580. https://doi.org/10.1084/jem.20030590

Overwijk, W. W., Tsung, A., Irvine, K. R., Parkhurst, M. R., Goletz, T. J., Tsung, K., Carroll, M. W., Liu, C., Moss, B., Rosenberg, S. A., & Restifo, N. P. (1998). gp100/pmel 17 Is a Murine Tumor Rejection Antigen: Induction of "Self"-reactive, Tumoricidal T Cells Using High-affinity, Altered Peptide Ligand. *Journal of Experimental Medicine*, *188*(2), 277-286. https://doi.org/10.1084/jem.188.2.277

Owens, T., Bechmann, I., & Engelhardt, B. (2008). Perivascular spaces and the two steps to neuroinflammation. *J Neuropathol Exp Neurol*, *67*(12), 1113-1121. https://doi.org/10.1097/NEN.0b013e31818f9ca8

Pardoll, D. M. (2012). The blockade of immune checkpoints in cancer immunotherapy. *Nature Reviews Cancer*, *12*(4), 252-264. https://doi.org/10.1038/nrc3239

Park, S. L., Buzzai, A., Rautela, J., Hor, J. L., Hochheiser, K., Effern, M., McBain, N., Wagner, T., Edwards, J., McConville, R., Wilmott, J. S., Scolyer, R. A., Tüting, T., Palendira, U., Gyorki, D., Mueller, S. N., Huntington, N. D., Bedoui, S., Hölzel, M., Mackay, L. K., Waithman, J., & Gebhardt, T. (2019). Tissue-resident memory CD8+ T cells promote melanoma–immune equilibrium in skin. *Nature*, *565*(7739), 366-371. https://doi.org/10.1038/s41586-018-0812-9

Peña, L. A., Fuks, Z., & Kolesnick, R. N. (2000). Radiation-induced apoptosis of endothelial cells in the murine central nervous system: Protection by fibroblast growth factor and sphingomyelinase

deficiency. *Cancer Research*, *60*(2), 321-327. https://www.scopus.com/inward/record.uri?eid=2-s2.0-0342545909&partnerID=40&md5=1f636906717a9fe34f0397d6c03817ee

Peña, L. A., Fuks, Z., & Kolesnick, R. N. (2000). Radiation-induced Apoptosis of Endothelial Cells in the Murine Central Nervous System: Protection by Fibroblast Growth Factor and Sphingomyelinase Deficiency1. *Cancer Research*, *60*(2), 321-327.

Pentcheva-Hoang, T., Simpson, T. R., Montalvo-Ortiz, W., & Allison, J. P. (2014). Cytotoxic T lymphocyte antigen-4 blockade enhances antitumor immunity by stimulating melanoma-specific T-cell motility. *Cancer Immunol Res*, *2*(10), 970-980. https://doi.org/10.1158/2326-6066.Cir-14-0104

Peranzoni, E., Lemoine, J., Vimeux, L., Feuillet, V., Barrin, S., Kantari-Mimoun, C., Bercovici, N., Guérin, M., Biton, J., Ouakrim, H., Régnier, F., Lupo, A., Alifano, M., Damotte, D., & Donnadieu, E. (2018). Macrophages impede CD8 T cells from reaching tumor cells and limit the efficacy of anti–PD-1 treatment. *Proceedings of the National Academy of Sciences*, *115*(17), E4041-E4050. https://doi.org/10.1073/pnas.1720948115

Pfeifer, G. P., You, Y.-H., & Besaratinia, A. (2005). Mutations induced by ultraviolet light. *Mutation Research/Fundamental and Molecular Mechanisms of Mutagenesis*, *571*(1), 19-31. https://doi.org/https://doi.org/10.1016/j.mrfmmm.2004.06.057

Phillipson, M., Heit, B., Colarusso, P., Liu, L., Ballantyne, C. M., & Kubes, P. (2006). Intraluminal crawling of neutrophils to emigration sites: a molecularly distinct process from adhesion in the recruitment cascade. *J Exp Med*, *203*(12), 2569-2575. https://doi.org/10.1084/jem.20060925

Picker, L. J., Michie, S. A., Rott, L. S., & Butcher, E. C. (1990). A unique phenotype of skin-associated lymphocytes in humans. Preferential expression of the HECA-452 epitope by benign and malignant T cells at cutaneous sites. *Am J Pathol*, *136*(5), 1053-1068.

Pinto-Teixeira, F., Muzzopappa, M., Swoger, J., Mineo, A., Sharpe, J., & López-Schier, H. (2013). Intravital imaging of hair-cell development and regeneration in the zebrafish. *Frontiers in Neuroanatomy*, *7*, 33-33. https://doi.org/10.3389/fnana.2013.00033

Rakhilin, N., Garrett, A., Eom, C.-Y., Chavez, K. R., Small, D. M., Daniel, A. R., Kaelberer, M. M., Mejooli, M. A., Huang, Q., Ding, S., Kirsch, D. G., Bohórquez, D. V., Nishimura, N., Barth, B. B., & Shen, X. (2019). An intravital window to image the colon in real time. *Nature Communications*, *10*(1), 5647. https://doi.org/10.1038/s41467-019-13699-w

Reboldi, A., Coisne, C., Baumjohann, D., Benvenuto, F., Bottinelli, D., Lira, S., Uccelli, A., Lanzavecchia, A., Engelhardt, B., & Sallusto, F. (2009). C-C chemokine receptor 6-regulated entry of TH-17 cells into the CNS through the choroid plexus is required for the initiation of EAE. *Nat Immunol*, *10*(5), 514-523. https://doi.org/10.1038/ni.1716

Reed, C. M., Cresce, N. D., Mauldin, I. S., Slingluff, C. L., Jr., & Olson, W. C. (2015). Vaccination with Melanoma Helper Peptides Induces Antibody Responses Associated with Improved Overall Survival. *Clinical cancer research : an official journal of the American Association for Cancer Research*, *21*(17), 3879-3887. https://doi.org/10.1158/1078-0432.CCR-15-0233

Reiss, Y., Proudfoot, A. E., Power, C. A., Campbell, J. J., & Butcher, E. C. (2001). CC chemokine receptor (CCR)4 and the CCR10 ligand cutaneous T cell-attracting chemokine (CTACK) in lymphocyte trafficking to inflamed skin. *J Exp Med*, *194*(10), 1541-1547. https://doi.org/10.1084/jem.194.10.1541

Ren, X., Akiyoshi, K., Vandenbark, A. A., Hurn, P. D., & Offner, H. (2011). Programmed death-1 pathway limits central nervous system inflammation and neurologic deficits in murine experimental stroke. *Stroke*, *42*(9), 2578-2583. https://doi.org/10.1161/strokeaha.111.613182

Restifo, N. P., Marincola, F. M., Kawakami, Y., Taubenberger, J., Yannelli, J. R., & Rosenberg, S. A. (1996). Loss of functional beta 2-microglobulin in metastatic melanomas from five patients receiving immunotherapy. *Journal of the National Cancer Institute*, *88*(2), 100-108. https://doi.org/10.1093/jnci/88.2.100

Ritsma, L., Steller, E. J., Beerling, E., Loomans, C. J., Zomer, A., Gerlach, C., Vrisekoop, N., Seinstra, D., van Gurp, L., Schäfer, R., Raats, D. A., de Graaff, A., Schumacher, T. N., de Koning, E. J., Rinkes, I. H., Kranenburg, O., & van Rheenen, J. (2012). Intravital microscopy through an abdominal imaging window reveals a pre-micrometastasis stage during liver metastasis. *Sci Transl Med*, *4*(158), 158ra145. https://doi.org/10.1126/scitranslmed.3004394

Rizvi, N. A., Hellmann, M. D., Snyder, A., Kvistborg, P., Makarov, V., Havel, J. J., Lee, W., Yuan, J., Wong, P., Ho, T. S., Miller, M. L., Rekhtman, N., Moreira, A. L., Ibrahim, F., Bruggeman, C., Gasmi, B., Zappasodi, R., Maeda, Y., Sander, C., Garon, E. B., Merghoub, T., Wolchok, J. D., Schumacher, T. N., & Chan, T. A. (2015). Cancer immunology. Mutational landscape determines sensitivity to PD-1 blockade in non-small cell lung cancer. *Science*, *348*(6230), 124-128. https://doi.org/10.1126/science.aaa1348

Robert, C., Grob, J. J., Stroyakovskiy, D., Karaszewska, B., Hauschild, A., Levchenko, E., Chiarion Sileni, V., Schachter, J., Garbe, C., Bondarenko, I., Gogas, H., Mandalá, M., Haanen, J., Lebbé, C., Mackiewicz, A., Rutkowski, P., Nathan, P. D., Ribas, A., Davies, M. A., Flaherty, K. T., Burgess, P., Tan, M., Gasal, E., Voi, M., Schadendorf, D., & Long, G. V. (2019). Five-Year Outcomes with Dabrafenib plus Trametinib in Metastatic Melanoma. *N Engl J Med*, *381*(7), 626-636. https://doi.org/10.1056/NEJMoa1904059

Rosenberg, S. A., & Restifo, N. P. (2015). Adoptive cell transfer as personalized immunotherapy for human cancer. *Science*, *348*(6230), 62-68. https://doi.org/doi:10.1126/science.aaa4967

Rosenberg, S. A., Yang, J. C., Sherry, R. M., Kammula, U. S., Hughes, M. S., Phan, G. Q., Citrin, D. E., Restifo, N. P., Robbins, P. F., Wunderlich, J. R., Morton, K. E., Laurencot, C. M., Steinberg, S. M., White, D. E., & Dudley, M. E. (2011). Durable Complete Responses in Heavily Pretreated Patients with Metastatic Melanoma Using T-Cell Transfer Immunotherapy. *Clinical Cancer Research*, *17*(13), 4550-4557. https://doi.org/10.1158/1078-0432.CCR-11-0116

Rudd, C. E. (2008). The reverse stop-signal model for CTLA4 function. *Nature Reviews Immunology*, *8*(2), 153-160. https://doi.org/10.1038/nri2253

Rustenhoven, J., Drieu, A., Mamuladze, T., de Lima, K. A., Dykstra, T., Wall, M., Papadopoulos, Z., Kanamori, M., Salvador, A. F., Baker, W., Lemieux, M., Da Mesquita, S., Cugurra, A., Fitzpatrick, J., Sviben, S., Kossina, R., Bayguinov, P., Townsend, R. R., Zhang, Q., Erdmann-Gilmore, P., Smirnov, I., Lopes, M.-B., Herz, J., & Kipnis, J. (2021). Functional characterization of the dural sinuses as a neuroimmune interface. *Cell*, *184*(4), 1000-1016.e1027. https://doi.org/https://doi.org/10.1016/j.cell.2020.12.040

Sage, P. T., & Carman, C. V. (2009). Settings and mechanisms for trans-cellular diapedesis. *Frontiers in bioscience (Landmark edition)*, *14*(13), 5066-5083. https://doi.org/10.2741/3587

Sahin, U., Derhovanessian, E., Miller, M., Kloke, B.-P., Simon, P., Löwer, M., Bukur, V., Tadmor, A. D., Luxemburger, U., Schrörs, B., Omokoko, T., Vormehr, M., Albrecht, C., Paruzynski, A., Kuhn, A.

N., Buck, J., Heesch, S., Schreeb, K. H., Müller, F., Ortseifer, I., Vogler, I., Godehardt, E., Attig, S., Rae, R., Breitkreuz, A., Tolliver, C., Suchan, M., Martic, G., Hohberger, A., Sorn, P., Diekmann, J., Ciesla, J., Waksmann, O., Brück, A.-K., Witt, M., Zillgen, M., Rothermel, A., Kasemann, B., Langer, D., Bolte, S., Diken, M., Kreiter, S., Nemecek, R., Gebhardt, C., Grabbe, S., Höller, C., Utikal, J., Huber, C., Loquai, C., & Türeci, Ö. (2017). Personalized RNA mutanome vaccines mobilize poly-specific therapeutic immunity against cancer. *Nature*, *547*(7662), 222-226. https://doi.org/10.1038/nature23003

Sampson, J. H., Carter, J. H., Jr., Friedman, A. H., & Seigler, H. F. (1998). Demographics, prognosis, and therapy in 702 patients with brain metastases from malignant melanoma. *J Neurosurg*, *88*(1), 11-20. https://doi.org/10.3171/jns.1998.88.1.0011

Sampson, J. H., Gunn, M. D., Fecci, P. E., & Ashley, D. M. (2020). Brain immunology and immunotherapy in brain tumours. *Nature Reviews Cancer*, *20*(1), 12-25. https://doi.org/10.1038/s41568-019-0224-7

Sanchez, J. N., Wang, T., & Cohen, M. S. (2018). BRAF and MEK Inhibitors: Use and Resistance in BRAF-Mutated Cancers. *Drugs*, *78*(5), 549-566. https://doi.org/10.1007/s40265-018-0884-8

Schenkel, A. R., Mamdouh, Z., & Muller, W. A. (2004). Locomotion of monocytes on endothelium is a critical step during extravasation. *Nat Immunol*, *5*(4), 393-400. https://doi.org/10.1038/ni1051

Scherz, P. J., Huisken, J., Sahai-Hernandez, P., & Stainier, D. Y. (2008). High-speed imaging of developing heart valves reveals interplay of morphogenesis and function. *Development*, *135*(6), 1179-1187. https://doi.org/10.1242/dev.010694

Schetters, S. T. T., Gomez-Nicola, D., Garcia-Vallejo, J. J., & Van Kooyk, Y. (2018). Neuroinflammation: Microglia and T Cells Get Ready to Tango [Hypothesis and Theory]. *Frontiers in Immunology*, *8*. https://doi.org/10.3389/fimmu.2017.01905

Schindelin, J., Arganda-Carreras, I., Frise, E., Kaynig, V., Longair, M., Pietzsch, T., Preibisch, S., Rueden, C., Saalfeld, S., Schmid, B., Tinevez, J.-Y., White, D. J., Hartenstein, V., Eliceiri, K., Tomancak, P., & Cardona, A. (2012). Fiji: an open-source platform for biological-image analysis. *Nature Methods*, *9*(7), 676-682. https://doi.org/10.1038/nmeth.2019

Schmitt, C., Strazielle, N., & Ghersi-Egea, J. F. (2012). Brain leukocyte infiltration initiated by peripheral inflammation or experimental autoimmune encephalomyelitis occurs through pathways connected to the CSF-filled compartments of the forebrain and midbrain. *J Neuroinflammation*, *9*, 187. https://doi.org/10.1186/1742-2094-9-187

Schneider, H., Downey, J., Smith, A., Zinselmeyer, B. H., Rush, C., Brewer, J. M., Wei, B., Hogg, N., Garside, P., & Rudd, C. E. (2006). Reversal of the TCR Stop Signal by CTLA-4. *Science*, *313*(5795), 1972-1975. https://doi.org/doi:10.1126/science.1131078

Schneider, H., Smith, X., Liu, H., Bismuth, G., & Rudd, C. E. (2008). CTLA-4 disrupts ZAP70 microcluster formation with reduced T cell/APC dwell times and calcium mobilization. *Eur J Immunol*, *38*(1), 40-47. https://doi.org/10.1002/eji.200737423

Schreiter, J., Meyer, S., Schmidt, C., Schulz, R. M., & Langer, S. (2017). Dorsal skinfold chamber models in mice. *GMS Interdiscip Plast Reconstr Surg DGPW*, *6*, Doc10. https://doi.org/10.3205/iprs000112

References

Shah, V. B., Huang, Y., Keshwara, R., Ozment-Skelton, T., Williams, D. L., & Keshvara, L. (2008). Beta-glucan activates microglia without inducing cytokine production in Dectin-1-dependent manner. *J Immunol*, *180*(5), 2777-2785. https://doi.org/10.4049/jimmunol.180.5.2777

Shipley, F. B., Dani, N., Xu, H., Deister, C., Cui, J., Head, J. P., Sadegh, C., Fame, R. M., Shannon, M. L., Flores, V. I., Kishkovich, T., Jang, E., Klein, E. M., Goldey, G. J., He, K., Zhang, Y., Holtzman, M. J., Kirchhausen, T., Wyart, C., Moore, C. I., Andermann, M. L., & Lehtinen, M. K. (2020). Tracking Calcium Dynamics and Immune Surveillance at the Choroid Plexus Blood-Cerebrospinal Fluid Interface. *Neuron*, *108*(4), 623-639.e610. https://doi.org/10.1016/j.neuron.2020.08.024

Skelton, D., Satake, N., & Kohn, D. B. (2001). The enhanced green fluorescent protein (eGFP) is minimally immunogenic in C57BL/6 mice. *Gene Therapy*, *8*(23), 1813-1814. https://doi.org/10.1038/sj.gt.3301586

Song, E., Mao, T., Dong, H., Boisserand, L. S. B., Antila, S., Bosenberg, M., Alitalo, K., Thomas, J.-L., & Iwasaki, A. (2020). VEGF-C-driven lymphatic drainage enables immunosurveillance of brain tumours. *Nature*, *577*(7792), 689-694. https://doi.org/10.1038/s41586-019-1912-x

Song, J., Wu, C., Korpos, E., Zhang, X., Agrawal, Smriti M., Wang, Y., Faber, C., Schäfers, M., Körner, H., Opdenakker, G., Hallmann, R., & Sorokin, L. (2015). Focal MMP-2 and MMP-9 Activity at the Blood-Brain Barrier Promotes Chemokine-Induced Leukocyte Migration. *Cell Reports*, *10*(7), 1040-1054. https://doi.org/https://doi.org/10.1016/j.celrep.2015.01.037

Sorensen, E. W., Lian, J., Ozga, A. J., Miyabe, Y., Ji, S. W., Bromley, S. K., Mempel, T. R., & Luster, A. D. (2018). CXCL10 stabilizes T cell–brain endothelial cell adhesion leading to the induction of cerebral malaria. *JCI insight*, *3*(8). https://doi.org/10.1172/jci.insight.98911

Sprowls, S. A., Arsiwala, T. A., Bumgarner, J. R., Shah, N., Lateef, S. S., Kielkowski, B. N., & Lockman, P. R. (2019). Improving CNS Delivery to Brain Metastases by Blood–Tumor Barrier Disruption. *Trends in Cancer*, *5*(8), 495-505. https://doi.org/10.1016/j.trecan.2019.06.003

Staunton, D. E., Marlin, S. D., Stratowa, C., Dustin, M. L., & Springer, T. A. (1988). Primary structure of ICAM-1 demonstrates interaction between members of the immunoglobulin and integrin supergene families. *Cell*, *52*(6), 925-933. https://doi.org/10.1016/0092-8674(88)90434-5

Stegmayr, C., Oliveira, D., Niemietz, N., Willuweit, A., Lohmann, P., Galldiks, N., Shah, N. J., Ermert, J., & Langen, K. J. (2017). Influence of Bevacizumab on Blood-Brain Barrier Permeability and O-(2-(18)F-Fluoroethyl)-l-Tyrosine Uptake in Rat Gliomas. *J Nucl Med*, *58*(5), 700-705. https://doi.org/10.2967/jnumed.116.187047

Stein, J. V., Rot, A., Luo, Y., Narasimhaswamy, M., Nakano, H., Gunn, M. D., Matsuzawa, A., Quackenbush, E. J., Dorf, M. E., & von Andrian, U. H. (2000). The Cc Chemokine Thymus-Derived Chemotactic Agent 4 (Tca-4, Secondary Lymphoid Tissue Chemokine, 6ckine, Exodus-2) Triggers Lymphocyte Function–Associated Antigen 1–Mediated Arrest of Rolling T Lymphocytes in Peripheral Lymph Node High Endothelial Venules. *Journal of Experimental Medicine*, *191*(1), 61-76. https://doi.org/10.1084/jem.191.1.61

Steinbach, K., Vincenti, I., Kreutzfeldt, M., Page, N., Muschaweckh, A., Wagner, I., Drexler, I., Pinschewer, D., Korn, T., & Merkler, D. (2016). Brain-resident memory T cells represent an autonomous cytotoxic barrier to viral infection. *J Exp Med*, *213*(8), 1571-1587. https://doi.org/10.1084/jem.20151916

Sucker, A., Zhao, F., Real, B., Heeke, C., Bielefeld, N., Maβen, S., Horn, S., Moll, I., Maltaner, R., Horn, P. A., Schilling, B., Sabbatino, F., Lennerz, V., Kloor, M., Ferrone, S., Schadendorf, D., Falk, C. S., Griewank, K., & Paschen, A. (2014). Genetic evolution of T-cell resistance in the course of melanoma progression. *Clin Cancer Res*, *20*(24), 6593-6604. https://doi.org/10.1158/1078-0432.Ccr-14-0567

Taggart, D., Andreou, T., Scott, K. J., Williams, J., Rippaus, N., Brownlie, R. J., Ilett, E. J., Salmond, R. J., Melcher, A., & Lorger, M. (2018). Anti-PD-1/anti-CTLA-4 efficacy in melanoma brain metastases depends on extracranial disease and augmentation of CD8(+) T cell trafficking. *Proc Natl Acad Sci U S A*, *115*(7), E1540-e1549. https://doi.org/10.1073/pnas.1714089115

Tanda, E. T., Vanni, I., Boutros, A., Andreotti, V., Bruno, W., Ghiorzo, P., & Spagnolo, F. (2020). Current State of Target Treatment in BRAF Mutated Melanoma [Mini Review]. *Frontiers in Molecular Biosciences*, *7*. https://doi.org/10.3389/fmolb.2020.00154

Tawbi, H. A., Forsyth, P. A., Algazi, A., Hamid, O., Hodi, F. S., Moschos, S. J., Khushalani, N. I., Lewis, K., Lao, C. D., Postow, M. A., Atkins, M. B., Ernstoff, M. S., Reardon, D. A., Puzanov, I., Kudchadkar, R. R., Thomas, R. P., Tarhini, A., Pavlick, A. C., Jiang, J., Avila, A., Demelo, S., & Margolin, K. (2018). Combined Nivolumab and Ipilimumab in Melanoma Metastatic to the Brain. *New England Journal of Medicine*, *379*(8), 722-730. https://doi.org/10.1056/NEJMoa1805453

Thurston, G., Baluk, P., & McDonald, D. M. (2000). Determinants of endothelial cell phenotype in venules. *Microcirculation*, *7*(1), 67-80.

Tivol, E. A., Borriello, F., Schweitzer, A. N., Lynch, W. P., Bluestone, J. A., & Sharpe, A. H. (1995). Loss of CTLA-4 leads to massive lymphoproliferation and fatal multiorgan tissue destruction, revealing a critical negative regulatory role of CTLA-4. *Immunity*, *3*(5), 541-547. https://doi.org/10.1016/1074-7613(95)90125-6

Tiwary, S., Morales, J. E., Kwiatkowski, S. C., Lang, F. F., Rao, G., & McCarty, J. H. (2018). Metastatic Brain Tumors Disrupt the Blood-Brain Barrier and Alter Lipid Metabolism by Inhibiting Expression of the Endothelial Cell Fatty Acid Transporter Mfsd2a. *Scientific Reports*, *8*(1), 8267. https://doi.org/10.1038/s41598-018-26636-6

Ueno, M., Fujita, Y., Tanaka, T., Nakamura, Y., Kikuta, J., Ishii, M., & Yamashita, T. (2013). Layer V cortical neurons require microglial support for survival during postnatal development. *Nat Neurosci*, *16*(5), 543-551. https://doi.org/10.1038/nn.3358

Umansky, V., Sevko, A., Gebhardt, C., & Utikal, J. (2014). Myeloid-derived suppressor cells in malignant melanoma. *J Dtsch Dermatol Ges*, *12*(11), 1021-1027. https://doi.org/10.1111/ddg.12411

Unger, M. S., Schernthaner, P., Marschallinger, J., Mrowetz, H., & Aigner, L. (2018). Microglia prevent peripheral immune cell invasion and promote an anti-inflammatory environment in the brain of APP-PS1 transgenic mice. *J Neuroinflammation*, *15*(1), 274. https://doi.org/10.1186/s12974-018-1304-4

Urban, S. L., Jensen, I. J., Shan, Q., Pewe, L. L., Xue, H. H., Badovinac, V. P., & Harty, J. T. (2020). Peripherally induced brain tissue-resident memory CD8(+) T cells mediate protection against CNS infection. *Nat Immunol*, *21*(8), 938-949. https://doi.org/10.1038/s41590-020-0711-8

Valiente, M., Ahluwalia, M. S., Boire, A., Brastianos, P. K., Goldberg, S. B., Lee, E. Q., Le Rhun, E., Preusser, M., Winkler, F., & Soffietti, R. (2018). The Evolving Landscape of Brain Metastasis. *Trends in Cancer*, *4*(3), 176-196. https://doi.org/https://doi.org/10.1016/j.trecan.2018.01.003

References

Valiente, M., Van Swearingen, A. E. D., Anders, C. K., Bairoch, A., Boire, A., Bos, P. D., Cittelly, D. M., Erez, N., Ferraro, G. B., Fukumura, D., Gril, B., Herlyn, M., Holmen, S. L., Jain, R. K., Joyce, J. A., Lorger, M., Massague, J., Neman, J., Sibson, N. R., Steeg, P. S., Thorsen, F., Young, L. S., Varešlija, D., Vultur, A., Weis-Garcia, F., & Winkler, F. (2020). Brain Metastasis Cell Lines Panel: A Public Resource of Organotropic Cell Lines. *Cancer Res*, *80*(20), 4314-4323. https://doi.org/10.1158/0008-5472.Can-20-0291

Valiente, M., Van Swearingen, A. E. D., Anders, C. K., Bairoch, A., Boire, A., Bos, P. D., Cittelly, D. M., Erez, N., Ferraro, G. B., Fukumura, D., Gril, B., Herlyn, M., Holmen, S. L., Jain, R. K., Joyce, J. A., Lorger, M., Massague, J., Neman, J., Sibson, N. R., Steeg, P. S., Thorsen, F., Young, L. S., Varešlija, D., Vultur, A., Weis-Garcia, F., & Winkler, F. (2020). Brain Metastasis Cell Lines Panel: A Public Resource of Organotropic Cell Lines. *Cancer Research*, *80*(20), 4314-4323. https://doi.org/10.1158/0008-5472.CAN-20-0291

van der Woude, L. L., Gorris, M. A. J., Halilovic, A., Figdor, C. G., & de Vries, I. J. M. (2017). Migrating into the Tumor: a Roadmap for T Cells. *Trends in Cancer*, *3*(11), 797-808. https://doi.org/10.1016/j.trecan.2017.09.006

Vestweber, D. (2015). How leukocytes cross the vascular endothelium. *Nature Reviews Immunology*, *15*(11), 692-704. https://doi.org/10.1038/nri3908

Vogelstein, B., Papadopoulos, N., Velculescu, V. E., Zhou, S., Diaz, L. A., Jr., & Kinzler, K. W. (2013). Cancer genome landscapes. *Science*, *339*(6127), 1546-1558. https://doi.org/10.1126/science.1235122

von Andrian, U. H., & Mackay, C. R. (2000). T-Cell Function and Migration — Two Sides of the Same Coin. *New England Journal of Medicine*, *343*(14), 1020-1034. https://doi.org/10.1056/nejm200010053431407

Vorbrodt, A. W., & Dobrogowska, D. H. (2003). Molecular anatomy of intercellular junctions in brain endothelial and epithelial barriers: electron microscopist's view. *Brain Res Brain Res Rev*, *42*(3), 221-242. https://doi.org/10.1016/s0165-0173(03)00177-2

Vosoughi, E., Lee, J. M., Miller, J. R., Nosrati, M., Minor, D. R., Abendroth, R., Lee, J. W., Andrews, B. T., Leng, L. Z., Wu, M., Leong, S. P., Kashani-Sabet, M., & Kim, K. B. (2018). Survival and clinical outcomes of patients with melanoma brain metastasis in the era of checkpoint inhibitors and targeted therapies. *BMC Cancer*, *18*(1), 490. https://doi.org/10.1186/s12885-018-4374-x

Waldman, A. D., Fritz, J. M., & Lenardo, M. J. (2020). A guide to cancer immunotherapy: from T cell basic science to clinical practice. *Nature Reviews Immunology*, *20*(11), 651-668. https://doi.org/10.1038/s41577-020-0306-5

Wang, R., Chadalavada, K., Wilshire, J., Kowalik, U., Hovinga, K. E., Geber, A., Fligelman, B., Leversha, M., Brennan, C., & Tabar, V. (2010). Glioblastoma stem-like cells give rise to tumour endothelium. *Nature*, *468*(7325), 829-833. https://doi.org/10.1038/nature09624

Wang, Y., Cella, M., Mallinson, K., Ulrich, J. D., Young, K. L., Robinette, M. L., Gilfillan, S., Krishnan, G. M., Sudhakar, S., Zinselmeyer, B. H., Holtzman, D. M., Cirrito, J. R., & Colonna, M. (2015). TREM2 lipid sensing sustains the microglial response in an Alzheimer's disease model. *Cell*, *160*(6), 1061-1071. https://doi.org/10.1016/j.cell.2015.01.049

Waterhouse, P., Penninger, J. M., Timms, E., Wakeham, A., Shahinian, A., Lee, K. P., Thompson, C. B., Griesser, H., & Mak, T. W. (1995). Lymphoproliferative disorders with early lethality in mice

deficient in Ctla-4. *Science*, *270*(5238), 985-988. https://doi.org/10.1126/science.270.5238.985

Weidner, N., Semple, J. P., Welch, W. R., & Folkman, J. (1991). Tumor angiogenesis and metastasis--correlation in invasive breast carcinoma. *N Engl J Med*, *324*(1), 1-8. https://doi.org/10.1056/nejm199101033240101

Winkler, F., Kozin, S. V., Tong, R. T., Chae, S. S., Booth, M. F., Garkavtsev, I., Xu, L., Hicklin, D. J., Fukumura, D., di Tomaso, E., Munn, L. L., & Jain, R. K. (2004). Kinetics of vascular normalization by VEGFR2 blockade governs brain tumor response to radiation: role of oxygenation, angiopoietin-1, and matrix metalloproteinases. *Cancer Cell*, *6*(6), 553-563. https://doi.org/10.1016/j.ccr.2004.10.011

Xie, L., Kang, H., Xu, Q., Chen, M. J., Liao, Y., Thiyagarajan, M., O'Donnell, J., Christensen, D. J., Nicholson, C., Iliff, J. J., Takano, T., Deane, R., & Nedergaard, M. (2013). Sleep drives metabolite clearance from the adult brain. *Science*, *342*(6156), 373-377. https://doi.org/10.1126/science.1241224

Xu, H.-T., Pan, F., Yang, G., & Gan, W.-B. (2007). Choice of cranial window type for in vivo imaging affects dendritic spine turnover in the cortex. *Nature Neuroscience*, *10*(5), 549-551. https://doi.org/10.1038/nn1883

Yaguchi, T., Goto, Y., Kido, K., Mochimaru, H., Sakurai, T., Tsukamoto, N., Kudo-Saito, C., Fujita, T., Sumimoto, H., & Kawakami, Y. (2012). Immune suppression and resistance mediated by constitutive activation of Wnt/β-catenin signaling in human melanoma cells. *J Immunol*, *189*(5), 2110-2117. https://doi.org/10.4049/jimmunol.1102282

Yao, H., Price, T. T., Cantelli, G., Ngo, B., Warner, M. J., Olivere, L., Ridge, S. M., Jablonski, E. M., Therrien, J., Tannheimer, S., McCall, C. M., Chenn, A., & Sipkins, D. A. (2018). Leukaemia hijacks a neural mechanism to invade the central nervous system. *Nature*, *560*(7716), 55-60. https://doi.org/10.1038/s41586-018-0342-5

You, R., Artichoker, J., Fries, A., Edwards, A. W., Combes, A. J., Reeder, G. C., Samad, B., & Krummel, M. F. (2021). Active surveillance characterizes human intratumoral T cell exhaustion. *The Journal of Clinical Investigation*, *131*(18). https://doi.org/10.1172/JCI144353

Yuan, F., Salehi, H. A., Boucher, Y., Vasthare, U. S., Tuma, R. F., & Jain, R. K. (1994). Vascular permeability and microcirculation of gliomas and mammary carcinomas transplanted in rat and mouse cranial windows. *Cancer Res*, *54*(17), 4564-4568.

Yuan, H., Gaber, M. W., McColgan, T., Naimark, M. D., Kiani, M. F., & Merchant, T. E. (2003). Radiation-induced permeability and leukocyte adhesion in the rat blood-brain barrier: modulation with anti-ICAM-1 antibodies. *Brain Res*, *969*(1-2), 59-69. https://doi.org/10.1016/s0006-8993(03)02278-9

Yuan, W., Li, G., Zeng, M., & Fu, B. M. (2010). Modulation of the blood–brain barrier permeability by plasma glycoprotein orosomucoid. *Microvascular Research*, *80*(1), 148-157. https://doi.org/https://doi.org/10.1016/j.mvr.2010.03.011

Zhang, R. D., Price, J. E., Fujimaki, T., Bucana, C. D., & Fidler, I. J. (1992). Differential permeability of the blood-brain barrier in experimental brain metastases produced by human neoplasms implanted into nude mice. *Am J Pathol*, *141*(5), 1115-1124.

References

Zhang, W., Karschnia, P., von Mücke-Heim, I. A., Mulazzani, M., Zhou, X., Blobner, J., Mueller, N., Teske, N., Dede, S., Xu, T., Thon, N., Ishikawa-Ankerhold, H., Straube, A., Tonn, J. C., & von Baumgarten, L. (2021). In vivo two-photon characterization of tumor-associated macrophages and microglia (TAM/M) and CX3CR1 during different steps of brain metastasis formation from lung cancer. *Neoplasia (New York, N.Y.)*, *23*(11), 1089-1100. https://doi.org/10.1016/j.neo.2021.09.001

Zhang, X.-W., Huck, K., Jähne, K., Cichon, F., Sonner, J. K., Ufer, F., Bauer, S., Woo, M. S., Green, E., Lu, K., Kilian, M., Friese, M. A., Platten, M., & Sahm, K. (2021). Activity-regulated cytoskeleton-associated protein/activity-regulated gene 3.1 (Arc/Arg3.1) enhances dendritic cell vaccination in experimental melanoma. *Oncoimmunology*, *10*(1), 1920739-1920739. https://doi.org/10.1080/2162402X.2021.1920739

Zhao, B., Chen, Y., Liu, J., Zhang, L., Wang, J., Yang, Y., Lv, Q., & Xie, M. (2018). Blood-brain barrier disruption induced by diagnostic ultrasound combined with microbubbles in mice. *Oncotarget*, *9*(4), 4897-4914. https://doi.org/10.18632/oncotarget.23527

Zhao, Z., Zhang, C., Zhou, L., Dong, P., & Shi, L. (2021). Immune Checkpoint Inhibitors and Neurotoxicity. *Current neuropharmacology*, *19*(8), 1246-1263. https://doi.org/10.2174/1570159X19666201230151224

Zomer, A., Croci, D., Kowal, J., van Gurp, L., & Joyce, J. A. (2022). Multimodal imaging of the dynamic brain tumor microenvironment during glioblastoma progression and in response to treatment. *iScience*, *25*(7). https://doi.org/10.1016/j.isci.2022.104570

Zou, W., & Chen, L. (2008). Inhibitory B7-family molecules in the tumour microenvironment. *Nature Reviews Immunology*, *8*(6), 467-477. https://doi.org/10.1038/nri2326